Metabolic and transcriptional rewiring required for regeneration in *Xenopus tropicalis*

Jeet Hiteshkumar Patel

A dissertation

submitted in partial fulfillment of the

requirements for the degree of

Doctor of Philosophy

University of Washington

2022

Reading Committee:

Andrea Wills, Chair

David Raible

Dana Miller

Program Authorized to Offer Degree:

Molecular and Cellular Biology

University of Washington

Abstract

Metabolic and transcriptional rewiring required for regeneration in *Xenopus tropicalis*

Jeet H Patel

Chair of the Supervisory Committee:
Professor Andrea Wills, PhD
Biochemistry

Regeneration requires access to and mobilization of resources to build new tissues, which must then be patterned in order to restore the form and function of lost structures. This process begins at the time of injury, when a number of injury-induced signals initiate regeneration. Articulating how regeneration competent animals respond to injury to create a regeneration permissive environment, as well as instruct growth and patterning, is an important step in understanding the biology of complex tissue formation and in the advancement of regenerative medicine. I sought to identify post-wounding checkpoints using *Xenopus tropicalis* tadpoles, which are able to regenerate their tails following severe truncation. First, I define a regenerative refractory period that occurs during normal tadpole development in which regeneration is temporarily restricted. By

showing that nutrient surplus at the time of injury dictates regenerative outcome, I identify nutrient sensing as a checkpoint in wound healing outcomes. I then examine how nutrients are mobilized to rapidly generate new tissue via glucose metabolism, characterizing a metabolic prioritization of the pentose phosphate pathway required for full regeneration. Finally, I explore how new tissues are properly patterned downstream of injury induced stressors by demonstrating a requirement for Hif1α in re-establishment of posterior patterning genes in tandem with Wnt signaling. This body of work delineates 3 key checkpoints (nutrient availability, metabolic prioritization, and stress-mediated transcriptional responses) which must be properly activated to allow regeneration and presents mechanisms for how each of these factors contributes to the regrowth of a tail.

TABLE OF CONTENTS

LIST OF FIGURES

LIST OF TABLES

ACKNOWLEDGEMENTS

One of my favorite quotes comes from John of Salisbury: "…we see more and farther than our predecessors, not because we have keener vision or greater height, but because we are lifted up and borne aloft on their gigantic stature." I would be remiss to not acknowledge the decades of work which have guided how I think about biology and the many scholars whose work formed the basis of my own. I would like to acknowledge the Coast Salish Peoples of this land which touches the shared waters of all tribes and bands within the Suquamish, Tulalip, and Muckleshoot nations, upon whose land this work has been undertaken.

I am thankful for the incredible research community at the University of Washington. The MCB Program has provided me with peers with a wide range of interest whom I have been fortunate to learn from. Maia Low and Denise Barnes, in particular, thank you for your logistical and emotional support throughout my time here. The Biochemistry Department, which I ended up in with roughly 0 training in biochemistry, has been a fantastic department to explore out of my comfort zone. Notably, I would like to specifically thank Celia Bisbach, Arianne Caudal, Daniel Hass, and Young Kwon, who were generous with their time in teaching me about metabolism and without whom I don't know if Chapter 3 of this work would have been possible. To the Dub Club (Jilliane Perkins, Marcella Cline, and Courtnee Clough), thank for constant coffee and support throughout grad school. Special thanks to Courtnee for navigating teaching our first course together, it was a blast to design and implement with you! And thanks to the rest of my MCB cohort for all of the memories we have made, I look forward to seeing what we all do next. Extra love to Samantha Schuster and Alexandre

Germanos for being great roommates who dealt with my constant stress and made sure I was always having fun outside of lab. Thanks finally to my committee – Cecilia Moens, Dana Miller, David Raible, Timothy Cherry – for their guidance and ideas throughout my thesis work. Your influence has shaped my approach to science and many of the ideas presented in the following chapters.

To my new friends in Seattle, thank you for getting me out of lab and helping me become a well-rounded person. My Dungeons and Dragons campaigns, bouldering companions, trivia teammates, and foodie friends have made my time in Seattle all the more memorable. I'm also like to note here my Samily, the PNW contingent of my family and our friends Sam and Jenna (who are also family), who have been a stable source of fun and support throughout my time in grad school. I have done nothing more regularly than watch Star Trek and, now, eat Oreos, in my entire life.

I also want to acknowledge the support networks that have stuck with me from before starting this journey. Thank you to the Nerd Herd for always making time to reconnect during my short and often last-minute trips back to NC and for the ease of falling into our old rhythms. To Danielle, Abby, and Jina (Wondergrads 2.0™), thank you for being a phone call away and providing perspective and unconditional support at all time. Steve and Savannah, it's been a pleasure to lose "who will become a doctor first;" thank you for fun discussion and a fully removed perspective on my work and the bubble that research can sometimes fall into. Finally, thank you to my amazing scientific mentors from UNC – Scott Williams, Blaire Steinwand, Frank Conlon, and Kevin Byrd – who shaped me so many ways and gave me a strong foundation in research, communication, and education.

Huge thanks to my mentor Andrea Wills. Your energy and passion for development have really carried me through the sloggiest of experiments and your mentorship, patience, and support have really meant the world to me. I have learned so much in the lab and I hope that I can channel your compassion and excitement in my own leadership role someday. Also, thank you for assembling a team of scientists who have been amazing resources and also have become some of my closest friends. Hannah Arbach, Anneke Kakebeen, Alex Chitsazan, Lauren Loh, and Madison Williams, thank you for welcoming me into the group and teaching me everything about frogs, statistics, and regeneration. Hannah and Anneke, I really can't imagine doing this without the two of you. Huge thanks to the many undergraduate students who have helped with my thesis work (Evan Takayoshi, Preston Schattinger, Peter Thomas, Daniel Ong, Kaycie Opiyo, and Morgan McCartney) for teaching me about your interests and giving me the opportunity to teach you. Thanks Avery Angell Swearer and Claire Williams for being the basis of the new era of the lab and for bringing new background and perspectives, I can't want to see what you do next!

And finally, I want to thank my incredible family. My extended family has been supportive and helped me to really disconnect from the lab when we get together. Thanks to my brother for his sometimes unreasonably long phone calls that have helped inspire distractions like anime binges or new video games to play. Extra special thanks to my parents, who are really the giants that I have built my entire life around. I appreciate all the things that you had to give up so I could have the opportunity to do this work and for so much else that I have today.

DEDICATION

This work is dedicated to my grandfathers, Hiruprasad Jashbhai Patel and Arvindbhai Kantilal Patel, who inspired and indulged my curiosity throughout my life.

Chapter 1. INTRODUCTION

Developing from a single cell into an organism with multiple tissue types that properly pattern and functionally integrate involves a highly orchestrated series of events. Numerous signaling pathways must be activated in exactly the right places in proper temporal order to specify the major axes of the body and then to generate functional structures and organs. For instance, in *Xenopus*, establishment of the dorsal organizer prior to gastrulation is required to generate a gradient of BMP signaling which establishes the dorsoventral axis and facilitates specification of the anteroposterior axis (Carron & Shi, 2016; Jansen et al., 2007). This single, yet vital, specification event occurs when the embryo is relatively simple, with only a few thousand cells. Development becomes increasingly complex as new cell types, tissues, and organ systems are established. Once developed, however, organisms are prone to injury and tissue damage which can necessitate replacement of structures previously only formed in development. So how, in a new, complex environment, are organisms able to replicate developmental outcomes to regenerate lost organisms or structures? Are developmental mechanisms re-employed in adult organisms or are the mechanisms of forming new tissues fundamentally different?

To start, the ability to regenerate is highly variable across animals and even across tissues and developmental stages within the same animal. Following injury, there are 2 major wounding outcomes: regeneration and scar formation. Scar tissue is characterized by increased fibroblast and collagen deposition at the wound site and is usually considered the more rapid, but short term, consequence of injury (Erickson &

Echeverri, 2018; Finnson et al., 2013; Kakebeen & Wills, 2019). Regeneration is a restoration of the lost tissue, replacing most of the lost cell types and patterning them in a functional new structure. The decision to implement scar formation vs regeneration is made early, with injury-induced signals instructing which wound outcome is achieved. In my thesis work, I set out to identify steps in wound response that enable a regenerative outcome in complex appendage injury from the perspectives of nutrient sufficiency, metabolic prioritization, and transcriptional regulation of cell fate.

1.1 *XENOPUS AS A MODEL SYSTEM FOR APPENDAGE REGENERATION*

Many organisms are capable of regenerating following severe injury, including planarian worms, *Hydra*, zebrafish, salamanders, and axolotls. However, these species retain this ability throughout their entire lives (Li et al., 2015). In contrast, *Xenopus* are stage-specific regenerators, meaning that they are highly regenerative as juveniles but gradually lose this potential as they undergo metamorphosis (Beck, 2012). *Xenopus* tadpoles, as such, has been extensively used to study the requirements for developmental signaling pathways (including Wnt, BMP, Notch, TGFß, and FGF) in appendage regeneration, both in the developing limb buds as well as the tail (Beck et al., 2001; Ho & Whitman, 2008; Slack et al., 2008). The *Xenopus* tail is a powerful model for interrogating regenerative potential as it is a complex appendage containing distinct structures such as the spinal cord, notochord, somites, vasculature, and epidermis, all of which are regenerated within days of injury (Beck, 2012) (Figure 1-1).

Because tails can be amputated within 3 days of fertilization and regeneration assays can be performed in petri dishes over the course of 3-7 days, the use of

molecular techniques such as morpholinos and pharmacological perturbation is relatively simple (Figure 1-1). These tools have been leveraged to identify several injury-induced stresses that are required for full tail regeneration. Further, at least in *Xenopus laevis*, there is a period of development known as the refractory period, which is defined as a 3-4 day window during normal development when tadpoles transiently lose regenerative potential (Beck et al., 2003; Slack et al., 2004). This has been a powerful tool in identifying signals and processes which are not only required for regeneration, but also sufficient to rescue the phenotype in a largely similar biological context (Barker & Beck, 2009; Fukazawa et al., 2009).

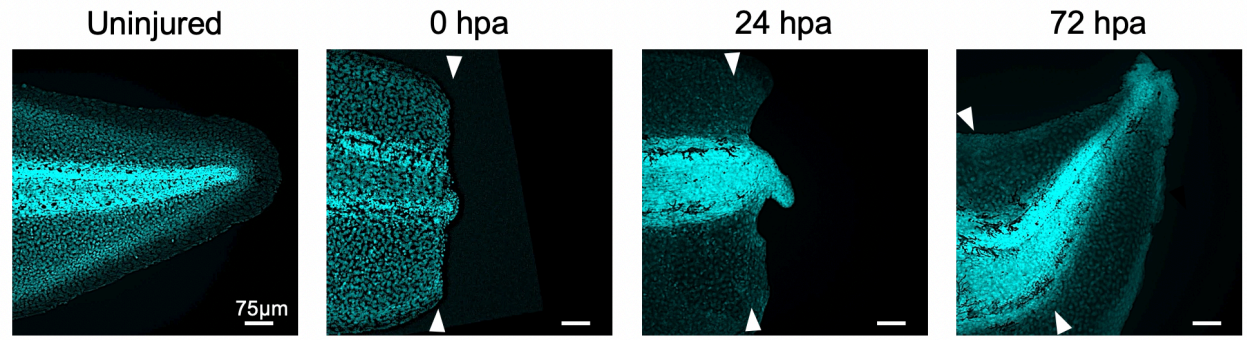

Figure 1-1: **Timecourse of *Xenopus tropicalis* tail regeneration**

DAPI counterstained tails depicting the first 72 hours post amputation (hpa) of tail regeneration. White arrowheads indicate amputation plane, scale bars are 75 µm.

As *Xenopus* have a fully sequenced genome, genomic and transcriptomic studies have been leveraged and datasets are now available to interrogate factors that are induced during whole tissue regeneration (Chang et al., 2017; N. R. Love et al., 2011) and in specific tissues such as the spinal cord (Kakebeen et al., 2020; Pelzer et al., 2021). More recently, RNA-sequencing studies have been carried out under regenerative and non-regenerative conditions, highlighting key differences between

injury response in these contexts. For instance, in the spinal cord, neural progenitor cells have been shown to first differentiate and then undergo significant proliferation during normal regeneration, but fail to undergo either process in the refractory period (Kakebeen et al., 2020; Pelzer et al., 2021). Furthermore, use of scRNA-sequencing to contrast regenerative and non-regenerative stages has allowed the identification of "regeneration organizing cells," or ROCs, in *Xenopus laevis*, which are required for tail regeneration (Aztekin et al., 2019). scRNA-seq has also been leveraged to contrast *Xenopus laevis* limb regeneration during non-regenerative stages to that of life-long regenerators, axolotls, identifying differences in differentiation programs that could contribute to varied regeneration outcomes (T.-Y. Lin et al., 2021). These datasets are not only valuable in their initial use, but also provide useful tools for hypothesis generation and testing in future studies.

Xenopus tail regeneration has also been fruitful in establishing injury-induced stressors which are critical in regeneration, due to the ease of live imaging as tails are relatively flat and transparent. Bioelectrical signaling, reactive oxygen species (ROS) accumulation, oxygen metabolism, and immune cell migration have all been shown to be iniitated by injury in *Xenopus* and are required for complete tail regeneration (Adams et al., 2007; Aztekin et al., 2020; Ferreira et al., 2018; N. R. Love et al., 2013). As these signals propagate from the wound, they are interesting candidates for factors that dictate if an injury will result in scar formation or regeneration. For instance, in *Xenopus*, it has been found that there are 2 classes of myeloid cells which migrate to the wound site, reparative macrophages that drive regeneration and inflammatory macrophages that are recruited during the refractory period (Aztekin et al., 2020). This differential

capacity for immune cell infiltration has been seen in other regenenerative models including the African spiny mouse, suggesting that the resident immune landscape may be a break in the wound healing decision tree.

These findings beg the question: what makes for a pro-regenerative tissue environment? To review the above points, we find that specific injury stresses must be activated, and the lack of any of these stress signals results in reduced or failed regeneration. These signals must then be interpreted to activate developmental signaling pathways which allow for differentiation and patterning. This order of operations becomes apparent when factoring in that activation of developmental pathways in non-regenerative settings, when injury stresses fail to activate, is sufficent to induce regeneration. While many injury-induced stresses likely remain to be identified, understanding how these cues are coupled to downstream regenerative processes will provide insight into how tissues deliniate between a scarring or regenerative wound outcome. Further, this framework will be improved by determining pre-requesites, or requirements for the tissue at the time of injury, that dictate if the wounded tissue is compentent to pro-regeneratve signals at all.

1.2 A PHYSIOLOGICAL PERSPECTIVE ON REGENERATION

The above framework is however, somewhat biased towards a transcription centric view of regeneration: injury cues must activate transcriptional cascades which drive regeneration. However, in the early 20th century, a group of scholars was driven by a more physiological perspective on regeneration. The same stressors as above may well activate transcriptional responses, but as first described by Charles Manning Child and his contemporaries, perhaps injury changes the physiological state of nearby cells

and these changes govern regenerative outcomes, namely patterning. While a modern lens tells us that transcriptional and physiological changes are inextricably coupled, in the next section I will highlight the contributions of Charles Manning Child to my own view of regeneration and several recent advances in the abiltiy to study and knowledge of how physiological gradients influence regeneration.

NOTE: the remainder of this sub-section is adapted with minimal modification from sections 3-7 of:

Patel J.H., Wills A.E., 2022. Gradient expectations: revisiting Charles Manning Child's theory of metabolic regionalization in developmental patterning and regeneration. *Wound Repair and Regeneration*. PMID: 35142418 [link]

1.2.1 *Susceptibility: early identification of metabolic gradients*

Child's work on metabolic gradients began in earnest in 1915. He made use of a general paradigm, which he termed susceptibility, in which he would first inhibit a metabolic activity and then assess how quickly tissues succumbed to necrosis after that inhibition (Child, 1913). Tissues which died more rapidly after treatment with the inhibitor were considered to be more dependent on the underlying process, and therefore to have more of that activity. By observing a single tissue or organism over time, regional differences in activity could be deduced (Figure 1-2). In one specific series of experiments, Child would take whole organisms, or remove segments of tissue from different axial positions, and place them in a solution of potassium cyanide, which was known at that time to be an inhibitor of oxidative cellular respiration. Child and his colleagues found that the susceptibility of tissues to cyanide existed as a gradient that correlated with its axial position. The most susceptible axial positions were at the

anterior and posterior poles, gradually declining towards the mid-region (Figure 1-2) (Parker, 1929). Further, some tissues such as the heart and eyes were much more susceptible to cyanide toxicity, suggesting they were more oxidatively active, as has been confirmed by recent studies in retinal pigment epithelium and cardiomyocytes, proving how mechanistically fruitful this early assay was (Hyman, 1921, 1927b; Martínez et al., 2017; Rajala, 2020).

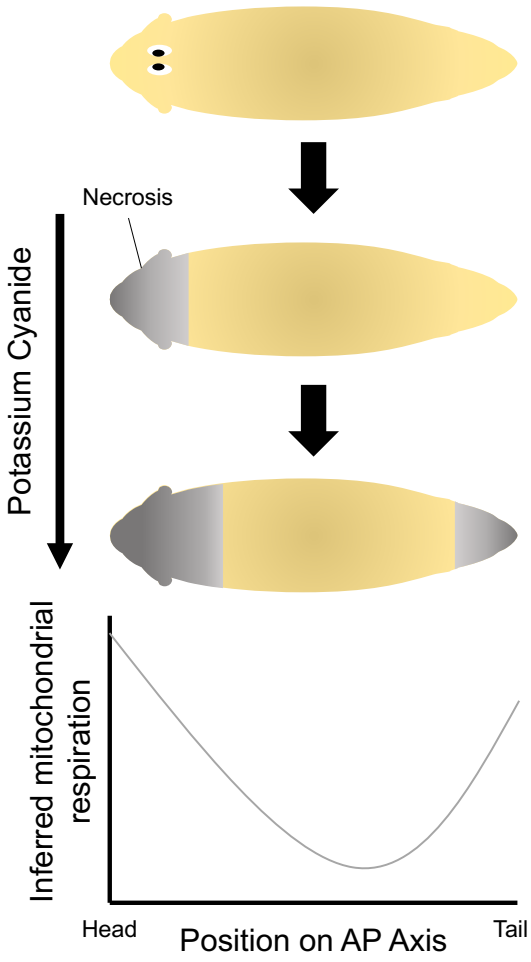

Figure 1-2: **Model of gradient identification via susceptibility**

A target animal or tissue, such as a planaria, is exposed to a targeted inhibitor. Here, potassium cyanide, which inhibits mitochondrial respiration, is schematized. Necrosis is assayed periodically. Tissues which die early (gray) are considered to have greater activity of the targeted process. In planaria, inhibition of respiration first leads to death of anterior structures and, after more time has passed, posterior structures. This allows the

conclusion that there are 2 gradients for mitochondrial respiration, a stronger anterior based gradient and a weaker posterior based one.

1.2.2 *Oxygen availability impacts differentiation and cell fate specification*

Due to the availability of mitochondrial toxins, most of the gradient studies in Child's era focused on oxygen gradients, identifying primarily anterior biased gradients as well as weaker secondary posterior gradients of activity in embryos (Hyman, 1921, 1927a). Initial studies by Child showing the importance of oxygen gradients were largely restricted to embryos that develop externally due to the nature of his experimental toolkit. Today, the use of dyes such as EF5 and pimonidazole, which form adducts with thiol groups specifically in hypoxic cells, now allow identification of regional differences in oxygen availability in tissues and enable us to define oxygen gradients in organisms that develop *in utero* (De Bock et al., 2013; Koch, 2008). In placental mammals, embryos develop in a naturally hypoxic environment; that is, cells in the embryo have graded oxygen availability up to less than half the amount of oxygen in adult tissues (E. Y. Chen et al., 1999; Iyer et al., 1998). *in vitro* culture of rat embryos under varying oxygen conditions has shown that hypoxic conditions induce microcephaly and overall reduction in growth. The reduction in head size observed suggests that normal anterior development requires oxygen, in line with Child's finding that there are anterior requirements for oxidative metabolism in invertebrates and Hyman's similar observations in teleosts, while a reduced overall size of the embryo may suggest other regional requirements for oxygen, but these have not been thoroughly classified thus far (E. Y. Chen et al., 1999; Hyman, 1921). Hyperoxic conditions result in failure to close the neural tube and form somites, indicating that regulation of oxygen availability is

crucial for developmental organization across multiple cell lineages and developmental axes (E. Y. Chen et al., 1999). These tools for visualization of oxygen levels have greatly improved our understanding of oxygen availability in healthy embryonic tissues and are critical to interpreting perturbations to oxygen homeostasis in development.

The importance of oxygen availability to differentiation has also been extensively studied in the context of cell culture of numerous cell lines. Embryonic stem cells (ESCs) remain quiescent when incubated under hypoxic conditions but begin to proliferate as oxygen availability increases (Millman et al., 2009). Varying oxygen levels also has dramatic effects on cell fate even along a single trajectory. ESCs cultured in hypoxia are less likely to adopt the neural stem cell (NSC) lineage, though further differentiation of NSCs to neurons is actually promoted under low oxygen conditions (Davies et al., 2016; Mondragon-Teran et al., 2009). Because the partial pressure of oxygen varies across tissues, it is difficult to generalize principles of oxygen availability on differentiation, though modulation of oxygen concentration has become a useful experimental variable for manipulating progenitor differentiation and proliferation (Mas-Bargues et al., 2019; Millman et al., 2009). The use of cell culture allows more regulated control of oxygen availability in cellular monolayers and has provided unique insight into regulation of cell fates by local oxygen signals which could translate to better understanding of differentiation *in vivo*.

1.2.3 *Physiological gradients in vertebrates are required for development and regeneration*

Metabolic pathways have also recently re-emerged as developmental regulators. One major advancement in this vein is the identification of posterior biased glycolytic

gradients, which have been described in both mammalian and chick embryogenesis (Bulusu et al., 2017; Oginuma et al., 2017). The central observation of this work is that transcriptional gradients for glycolytic enzymes exist in the presomitic mesoderm (PSM). Notably, rate-regulating enzymes for glycolysis, such as *phosphofructokinase* (*pfkp*) and *pyruvate kinase* (*pkm*), are enriched in the posterior extreme of mouse and chick embryos and gradually decline in expression in the anterior PSM and somites (Bulusu et al., 2017; Oginuma et al., 2017). To characterize the function of these transcriptional gradients, mass spectrometry and pharmacological perturbations were leveraged. In mice, ^{13}C-isotope tracing found that the posterior PSM was indeed heavily glycolytic relative to the anterior PSM as evidenced by increase in labeled glycolytic intermediates (Bulusu et al., 2017). Unlabeled mass spectrometry comparing somites to anterior and posterior PSM also revealed a greater amount of glycolytic intermediates in the posterior PSM, in line with transcript based readouts (Oginuma et al., 2017). In both systems, the posterior region was shown to have significant increases in lactate production, indicative of a Warburg-like metabolic state favoring aerobic glycolysis. Upon addition of 2-deoxyglucose, a non-hydrolysable glucose mimic, or substitution of glucose for its downstream metabolic pyruvate, somitogenesis and elongation of the primary axis were disrupted (Bulusu et al., 2017; Oginuma et al., 2017). These studies were able to show that the early reactions of glycolysis are required for PSM elongation and segmentation.

More recently, carbon metabolism has been explored in the context of regeneration using zebrafish larval tails as a model. Quickly after injury, the regenerating tail blastema takes up a large degree of glucose and the mitochondria in

this structure exhibit a fragmented phenotype, indicating that the cells in this structure are undergoing aerobic glycolysis (Sinclair et al., 2021). This injury-induced metabolic shift is required for proper activation of TGFβ signaling and blastema formation, highlighting a critical role in signal transduction and regeneration. This causal relationship between metabolic flux and developmental growth and patterning is a logical progression of Child's initial theories, merging advances in transcriptomic, pharmacological, and metabolic analysis from the last century to test the importance of various physiological gradients in development and regeneration.

1.2.4 *Oxygen regulation is critical for regeneration*

Not only have metabolic pathways been shown to be critical in regeneration, but so too have the oxidative gradients initially described by Child. A major interest in tissue regeneration has been the role of injury induced reactive oxygen signals (ROS) in facilitating wound response (Ferreira et al., 2018; Godwin et al., 2013; N. R. Love et al., 2013; Pirotte et al., 2015; M. M. G. Romero et al., 2018; Simkin et al., 2017). In most of these regenerative contexts, failure to induce ROS leads to reduced or failed regeneration and can increase scar tissue formation. As more attention has been paid to transcriptional regulation in regeneration, we now have more insight into how oxygen metabolism in the form of ROS facilitate regeneration. Much as Child's early work in planaria showed increased activity of mitochondrial oxidative phosphorylation following injury, Pirotte and colleagues found that ROS accumulate at wound sites and that this ROS accumulation in required for proper regeneration of both anterior and posterior aspects of planaria (Pirotte et al., 2015). Specifically, these injury-induced ROS are required for activation of differentiation programs in neoblasts and activation of neuronal

gene signatures, suggesting that ROS are important for initiating transcriptional programs in regeneration. Similarly, in *Xenopus* ROS have been shown to be upstream of FGF signaling and in zebrafish they are required upstream of Hedgehog signaling, both pathways well-established regulators of cell fate and patterning (N. R. Love et al., 2013; M. M. G. Romero et al., 2018). This body of work is actively growing and not only indicates that activation of physiological gradients is required for responding to injury stresses but suggests that these gradients could facilitate tissue patterning in regeneration as they do in development.

Recent technological advances in oxygen recording have enabled more careful observation of oxygen flux following injury. A study by Ferreira et al. using *Xenopus laevis* tadpoles, which are capable of whole tail regeneration, adapted an optrode system to measure changes in oxygen flux during regeneration (Ferreira et al., 2018). Following injury, there is a large influx of oxygen into the freshly amputated tissue and this influx is sustained even following wound epidermis formation, or closure of the open wound. Prior studies looking in the hours immediately following injury had also shown an increase in ROS at the wound site, highlighting the critical role of O_2 metabolism in regeneration (N. R. Love et al., 2013). This study further identified a critical hypoxic microenvironment, generated by the ROS produced by increased oxygen flux, in regenerative animals but not in non-regenerative developmental stages, suggesting that this regionalized hypoxia is instructive in regeneration. While the local hypoxic niche is non-intuitively a result of increased oxygen flux into the regenerating tail, these results are in direct agreement with Child's findings that regenerating tissues have increased oxygen demand based on increased susceptibility to mitochondrial toxins.

1.2.5 *Conclusion*

While Child's work has become something of a historical footnote, recent work has highlighted previously understudied intersections between metabolic and transcriptional perspectives on biology that make his early insights into redox signaling newly relevant. As our understanding of and ability to study gene regulation deepens, it becomes clear that cell environment and behavior are critical components of transcriptional output. For developing and regenerating tissues, this reinforces that physiological contexts, including access to oxygen or availability of metabolites, are as important inputs to the establishment and maintenance of cell identity as the inherited genome.

The proliferation of new tools to query oxygen tension, redox state, and glycolytic activity make it an exciting time to pursue these variables in the development and regeneration of axial structures and specific organs. One could readily imagine directly revisiting Child's gradient theory with these tools to address questions he was not able to fully resolve. Would we find, for example, that the highly oxidative tissues at the axial termini of tubularia are less glycolytic, due to their reliance on oxidative phosphorylation, thus representing a counterpoint to the highly glycolytic PSM of amniotes? Or would we find that these regions are just highly metabolically active in general, with elevated levels of both glycolysis and oxygen consumption? Similarly, now that we have learned that ROS are important signals to initiate regeneration in planaria and vertebrates, does the intensity and functional requirement for these signals parallel the axial gradients of oxidative activity that Child's susceptibility hypothesis proposed (N. R. Love et al., 2013; Pirotte et al., 2015; M. M. G. Romero et al., 2018)? The experimental tractability of

multiple models in which embryogenesis, regeneration, and homeostatic modulation of tissue identity can all be queried put present day researchers in the enviable position of being able to articulate conserved principles for these processes as well as those that are unique to particular organisms (Erickson & Echeverri, 2018; Ivankovic et al., 2019; Kakebeen & Wills, 2019; Marques et al., 2019). As regional and tissue specific differences in these factors become easier to study, we are eager to learn how Child's early theories of axial gradients integrate with our current understanding of developmental and regenerative patterning.

1.2.6 *Acknowledgments*

We thank members of the Wills, Miller, and Hoppins Lab for helpful discussion contributing to this manuscript.

1.2.7 *Funding*

This work was supported by the National Science Foundation Graduate Research Fellowship under Grant No. DGE-1762114 to J.H. Patel and NIH grant NS099124 and an award from the University of Washington Research Royalty Fund to A.E. Wills.

1.3 A ROADMAP TO REGENERATION: STEPS TOWARD MAKING NEW APPENDAGES

Thus far I have highlighted valuable insights into appendage regeneration that have been gleaned from research in *Xenopus*, including the identification of processes which seem to diverge in regenerative vs non-regenerative settings. I have also explored some wound-healing paradigms in other systems, with a particular emphasis

on studies that highlight physiological mechanisms in addition to more traditional transcriptionally focused studies. These prior studies inform the framework that I will explore in this work, specifically the idea that regeneration is enabled by a series of checkpoints which must be met in order for a lost appendage to grow and properly reform. In Chapter 2, I will leverage the unique capacity for *Xenopus tropicalis* tadpoles to regenerate at a life stage where they are not able to consume nutrients and address if there is a checkpoint at the time of injury asking “are there sufficient available resources to attempt regeneration?” In Chapter 3, I follow-up on this question by asking how nutrients are mobilized to drive rapid growth of new tissue and identify metabolic changes that are required for tissue regeneration. Finally, in Chapter 4, I examine the injury responsive transcription factor, Hif1α, and dissect a mechanism by which injury-induced stressors are able to re-establish positional information to direct regeneration of the correct tissues. Simplified, these chapters address means by which regenerating tissue evaluates if it can/should regenerate, how it will support this process, and how it determines what structures to make. This work fills vital gaps in our understanding of the bifurcation of regenerative vs non-regenerative healing and highlights processes which could be exploited to modulate regenerative competency in other systems.

Chapter 2. NUTRIENT AVAILABILITY CONTRIBTURES TO A GRADED REFRACTORY PERIOD FOR REGENERATION IN *XENOPUS TROPICALIS*

Chapter 2 is adapted with minimal modification from

Williams, M.C.*, Patel, J.H.*, Kakebeen, A.D. and Wills, A.E., 2021. Nutrient availability contributes to a graded refractory period for regeneration in *Xenopus tropicalis*. *Developmental Biology*, *473*, pp.59-70. PMID: 33484704 [link]

*These authors contributed equally to this work.

2.1 ABSTRACT

Xenopus tadpoles are a unique model for regeneration in that they exhibit two distinct phases of age-specific regenerative competence. In *Xenopus laevis*, young tadpoles fully regenerate following major injuries such as tail transection, then transiently lose regenerative competence during the “refractory period” from stages 45-47. Regenerative competence is then regained in older tadpoles before being permanently lost during metamorphosis. Here we show that a similar refractory period exists in *X. tropicalis*. Notably, tadpoles lose regenerative competence gradually in *X. tropicalis*, with full regenerative competence lost at stage 47. We find that the refractory period coincides closely with depletion of maternal yolk stores and the onset of independent feeding, and so we hypothesized that it might be caused in part by nutrient stress. In support of this hypothesis, we find that cell proliferation declines throughout the tail as the refractory period approaches. When we block nutrient mobilization by

inhibiting mTOR inhibitor signaling, we find that tadpole growth and regeneration are reduced, while yolk stores persist. Finally, we are able to restore regenerative competence and cell proliferation during the refractory period by abundantly feeding tadpoles. Our study argues that nutrient stress contributes to lack of regenerative competence and introduces the *X. tropicalis* refractory period as a valuable new model for interrogating how metabolic constraints inform regeneration.

2.2 INTRODUCTION

Animals have variable responses to large-scale injuries. Some are able to fully restore lost structures through regeneration, while others only complete wound closure followed by scarring. Organisms such as axolotls and zebrafish have robust regenerative potential and are able to restore limbs and organs throughout their lives (Erickson & Echeverri, 2018; Marques et al., 2019; Tanaka, 2016). Most mammals have relatively limited regenerative potential. *Xenopus* provides an ideal model to study variations in regenerative competency, as frogs of this genus are capable of regenerating their limbs and tail during the tadpole stage but gradually lose this potential during metamorphosis (Filoni & Bosco, 1981; Slack et al., 2008). This allows one to directly compare injury response between pro- and non-regenerative phases in a single model to understand how cellular and genetic contexts impact regeneration.

A notable phase of *Xenopus laevis* development is the refractory period, a window of development in which regenerative potential is transiently lost between Nieuwkoop and Faber stages 45 and 47 (Beck et al., 2003; Slack et al., 2004). While several factors have been identified that can ameliorate the refractory period and

restore regeneration, the fundamental mechanisms underlying this reversible loss of regeneration are not understood. The refractory period coincides with peak utilization of maternal yolk stores in tadpoles around stage 45 (Selman & Pawsey, 1965). Further, feeding begins at stage 45 of development, following perforation of the buccopharyngeal membrane and opening of the mouth at stage 40-41 (Dickinson & Sive, 2006; McNamara et al., 2018; Tabler et al., 2014). The temporal correlation of this nutritional transition and the loss of regenerative competence raises the possibility that nutrient stress could contribute to the refractory period. Nutrient stress has been shown to restrict proliferation of neural progenitors and to cause developmental delays in *Xenopus laevis* (N. K. Love et al., 2014; McKeown et al., 2017; McKeown & Cline, 2019). In the case of neural progenitors, starvation-induced G2 cell cycle arrest was shown to be at least partially regulated by the mammalian target of rapamycin (mTOR) pathway and was mimicked by treatment with the mTOR inhibitor rapamycin (McKeown & Cline, 2019). The mTOR signaling pathway is known to link nutrient availability, proliferation, and tissue growth in organisms ranging from yeast to mammals (Sabatini, 2017). In states of nutrient sufficiency, mTOR promotes growth in response to molecular signals of nutrient surplus such as leptin and insulin (Chantranupong et al., 2015; Yuan et al., 2013).

Nutrient sensing pathways are also known to play key roles in regeneration. Leptin signaling in particular has been shown to be necessary for regeneration in zebrafish retina and mouse liver models, and promotes wound healing of the epidermis by promoting dermal proliferation (Leclercq et al., 2003; Tadokoro et al., 2015; Zhao et al., 2014). Work in *Xenopus* and zebrafish has implicated nutrient sensing and response

pathways, specifically *leptin*, in appendage regeneration, although its functional role remains unclear. Expression of *leptin* and its receptor are highly upregulated after tail amputation, and the *lepb* enhancer is a reliable marker of regeneration in multiple zebrafish tissues (Aztekin et al., 2019; Kakebeen et al., 2020; Kang et al., 2016; N. R. Love et al., 2011). A role for carbohydrate metabolism, specifically glycolysis and the production of biosynthetic intermediates via the pentose phosphate pathway, has also been suggested but not yet rigorously tested in appendage regeneration (N. R. Love et al., 2014). mTOR signaling has been established as a regulator of regeneration in numerous models. Treatment with rapamycin to block mTOR inhibits proliferation during liver regeneration, and also curtails expansion of satellite cells that direct skeletal muscle regeneration (Espeillac et al., 2011; Ge et al., 2009). Further, ectopic activation of mTOR stimulates epidermal wound closure in mice and epidermal regeneration in *Drosophila* larvae, suggesting that this signal drives wound healing responses in these contexts (Kakanj et al., 2016; Squarize et al., 2010). By contrast, regeneration remains robust during starvation in planaria, which undergo morphallactic regeneration, and in this animal mTOR may have an antagonistic effect (Galliot & Ghila, 2010; González-Estévez, Felix, Rodríguez-Esteban, et al., 2012; González-Estévez, Felix, Smith, et al., 2012; R. Romero & Baguñà, 1991). Thus, while nutrient sensing and response pathways are implicated in regeneration, nutrient stress as a regenerative constraint has not been well characterized.

Here we address the link between nutrient availability and regeneration by first establishing the timeline of a regenerative refractory period in *Xenopus tropicalis* tadpoles. *X. tropicalis* are a valuable complementary model organism to *X. laevis*, due

to their diploid genome and more rapid maturation (Harland & Grainger, 2011; Kakebeen & Wills, 2019). We find that *X. tropicalis* tadpoles are highly regenerative at stage 41, have reduced regeneration between stages 43 and 46, and minimal regenerative capacity at stage 47. We show that this loss of regenerative competency correlates with a decrease in proliferation and changes in distribution of maternally deposited yolk in the unamputated posterior tail. To determine if nutritional stress regulates regenerative competency, we inhibit mTOR signaling using rapamycin or torin and find reduced developmental growth and regeneration length in tadpoles, accompanied by changes in proliferation and yolk distribution. Finally, we ask if the refractory period is a result of nutritional scarcity by abundantly feeding tadpoles during this period and find that relieving nutrient stress restores regeneration and proliferation rates in the tail. These findings highlight nutrient availability as a potential contributor to regenerative refractory periods and suggest new connections between nutrient storage and the regulation of tissue growth in a regenerative context.

2.3 RESULTS

2.3.1 *Xenopus tropicalis tadpoles exhibit a graded refractory period for tail regeneration*

Our first goal was to establish whether the timing and degree of a refractory period for regenerative competence in *Xenopus tropicalis* was similar to that of *Xenopus laevis*. To this end, we reared tadpoles at 22ºC to stages 41-47 and assessed their total length, length from the anal opening (vent) to tail tip, regenerated tissue length, and regeneration index (Beck, 2012) at 24 hours post amputation (hpa), 72 hpa, and 7 days

post amputation (dpa). Tadpole stages were assessed by morphological criteria, particularly the extent of gut coiling, abdominal iridophores, and facial morphology with stage 47 reached by 7 dpf at 22 ºC (Figure 2-1, Figure 2-2). We find that at stage 41, the length of the uninjured tadpole is an average of 3.65+/-0.08 mm (Figure 2-1 A, Y). Following amputation of the distal third of the tail, a strong regenerative response is initiated in which the regenerated tissue makes up more than 30% of the vent-to-tail tip length by 72 hpa, and then increasing slightly in proportion to the growing tadpole by 7 dpa (Figure 2-1 Z, A'). We scored tail regeneration quality as previously described by binning tails into complete, robust, poor, or none groups (Beck, 2012), and find that 100% of tadpoles amputated at stage 41 regenerate either completely or robustly (Figure 2-1 B'). As development progresses, tadpoles increase in length (Figure 2-1 B-E, Y), reaching 6.72+/-0.41 mm in total length by stage 47. Among tadpoles with tails amputated at stages 43-46, we observe reduced regenerated tail tissue at 72 hpa, and a gradual decline in regeneration length as a percentage of vent-to-tail tip length at 7 dpa from stages 43 to 46 (Figure 2-1 Z, A'). Although the regenerate is shorter, we find that quality of regeneration of tails amputated at stage 41-46 is largely complete or robust (Figure 2-1 B'). In tadpoles with tails amputated at stage 47, we see a stronger decrease in regenerate length at 72 hpa and 7 dpa, and most tadpoles only regenerate partially or not at all (Figure 2-1 Y).

We note that at 24 and 72 hpa the regenerative response of tadpoles at stage 41 is qualitatively different than at stages 43-46, with younger tadpoles forming a clear regeneration bud with better epidermal outgrowth of the fin than older tadpoles (Figure 2-1 F-I, K-N). At stage 47, we see a further decrease with tadpoles at this stage

mounting almost no regenerative response by 72 hpa, with the cut tail remaining blunt and the fin epidermis curling at the healed wound edge (Figure 2-1 O). From stage 41 to stage 46, the rate of tadpole growth is slowing, which may partially account for the declining magnitude of regeneration (Figure 2-2 H). In *Xenopus laevis*, the refractory period typically ends by stage 48, the progression to which requires feeding. To determine whether *X. tropicalis* tadpoles also recover their regenerative response, we assayed regeneration at stages 48 and 49, and find that regeneration is greatly improved relative to stage 47 (Figure 2-1 V-X, Figure 2-3). We elected to assay regenerate length and score at stage 49 to avoid any possibility of staging ambiguity with stage 47. We find that regenerate length at 7dpa and regeneration scores are significantly improved at stage 49 relative to stage 47 (Figure 2-1 A', B'). From these data, we conclude that a graded refractory period exists in *X. tropicalis*, in which regeneration is robust at stage 41, declines from stages 43-46 (which we hereafter term reduced regeneration), and is absent at stage 47 (which we hereafter term refractory).

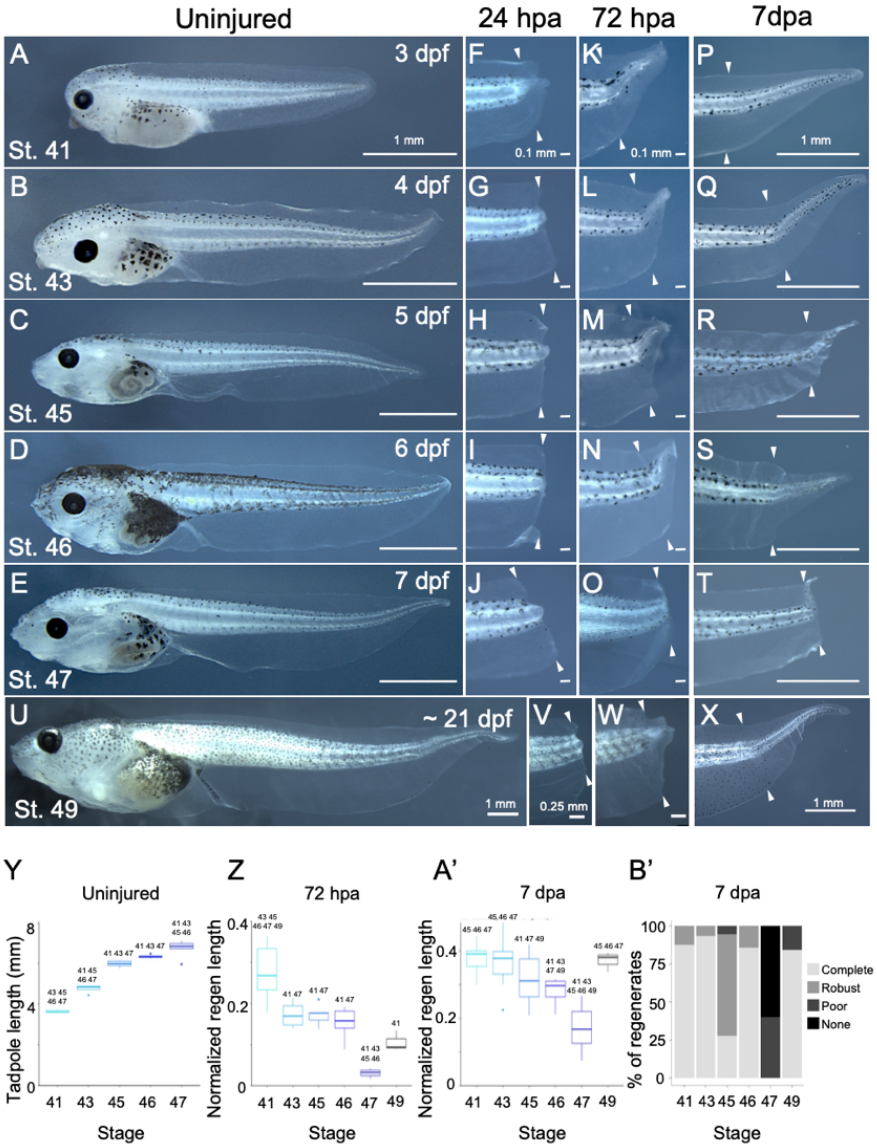

Figure 2-1: **A graded refractory period in *Xenopus tropicalis* shows reduced regenerative capacity at stages 43-46 and lost regenerative capacity at stage 47**

A-E, U) Brightfield images of *X. tropicalis* across a developmental timecourse. Animals were reared at 22ºC. Nieuwkoop and Faber developmental stages as well as days post fertilization (dpf) are indicated. Scale bar is 1 mm. F-J, V) Brightfield images of the regenerating tail at 24 hours post amputation (hpa). Amputations were performed at stage 41 (F), 43 (G), 45 (H), 46 (I), 47 (J), or 49 (V) and removed the distal third of the tail measured from the vent. Scale bar is 0.1 mm. K-O, W) Brightfield images of the regenerating tail at 72 hpa. Amputations were performed at stage 41 (K), 43 (L), 45 (M), 46 (N), 47 (O) or 49 (W). Scale bar is 0.1 mm. P-T, X) Brightfield images of the regenerating tail at 7 days post amputation (dpa). Amputations were performed at stage

41 (P), 43 (Q), 45 (R), 46 (S), 47 (T) or 49 (X). Scale bar is 0.1 mm. Y) Box-and-whisker plot showing the length of the tadpole across a developmental timecourse. Z, A') Box-and-whisker plots showing the length of the regenerated tail at 72 hpa (Z) or 7 dpa (A'), normalized to vent-to-tail tip length of the tadpole at that timepoint. B') Regeneration quality index showing regeneration quality over development at 7 dpa. Regeneration scores are shown as complete, robust, poor, or none. The stage indicated represents the stage at amputation. For (Y-A'), the midline represents the median of all tadpoles measured, box size represents the interquartile range, and the lines represent the range. Outliers are indicated as points. Stage numbers above a condition indicated statistical significance ($p<0.05$) between the given group and those stages as determined by ANOVA ($p=1.59x10^{-13}$) followed by Tukey's post-test. For (Z) n ranges 3 - 10; for (A') n range is 7 - 29; for (B') n ranges 14 - 15. White arrows indicate amputation site.

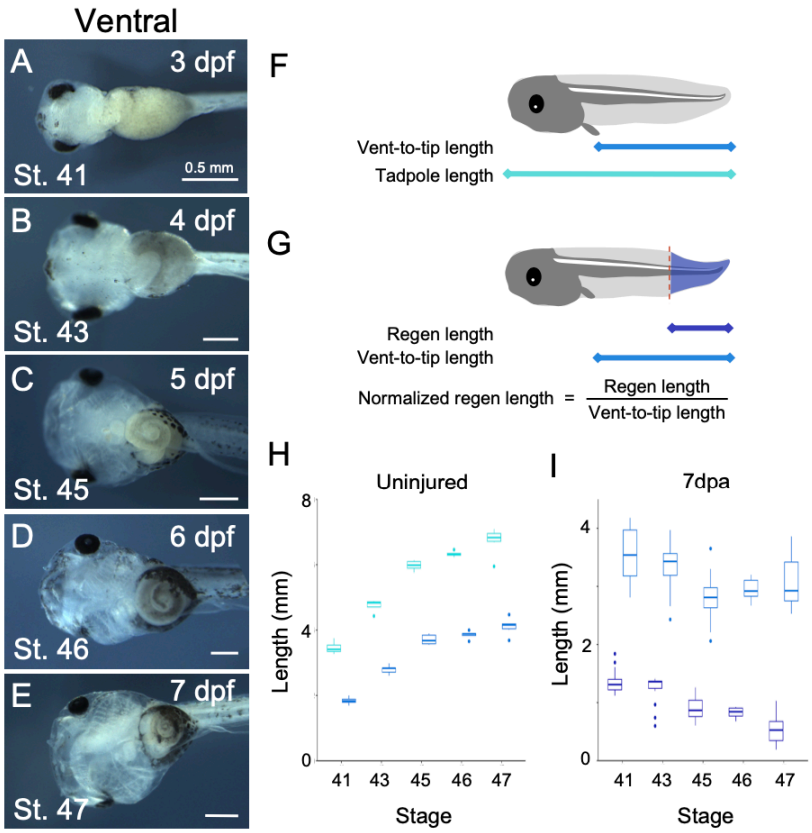

Figure 2-2: ***Xenopus tropicalis* staging series**

A-E) Brightfield, ventral view images of uninjured tadpoles at stages 41 (A), 43 (B), 45 (C), 46 (D), and 47 (E). Scalebar is 0.5 mm. Days post fertilization (dpf) for respective stages is indicated in top right corner of each image. F) Schematic showing length metrics for uninjured tadpoles. G) Schematic showing length metrics for regenerating tadpoles; normalized regeneration length = regeneration length / vent-to-tail tip length. H) Box-and-whisker plot showing tadpole length and vent-to-tail tip lengths of uninjured tadpoles over development. I) Box-and-whisker plot showing the vent-to-tail tip lengths

and regeneration lengths of 7 dpa tadpoles amputated at indicated stages. For (H,I), the midline represents the median of all tadpoles measured, box size represents the interquartile range, and the lines represent the range. Outliers are indicated as points. For (H), n ranges 3 – 10; for (I) n ranges 7 - 29.

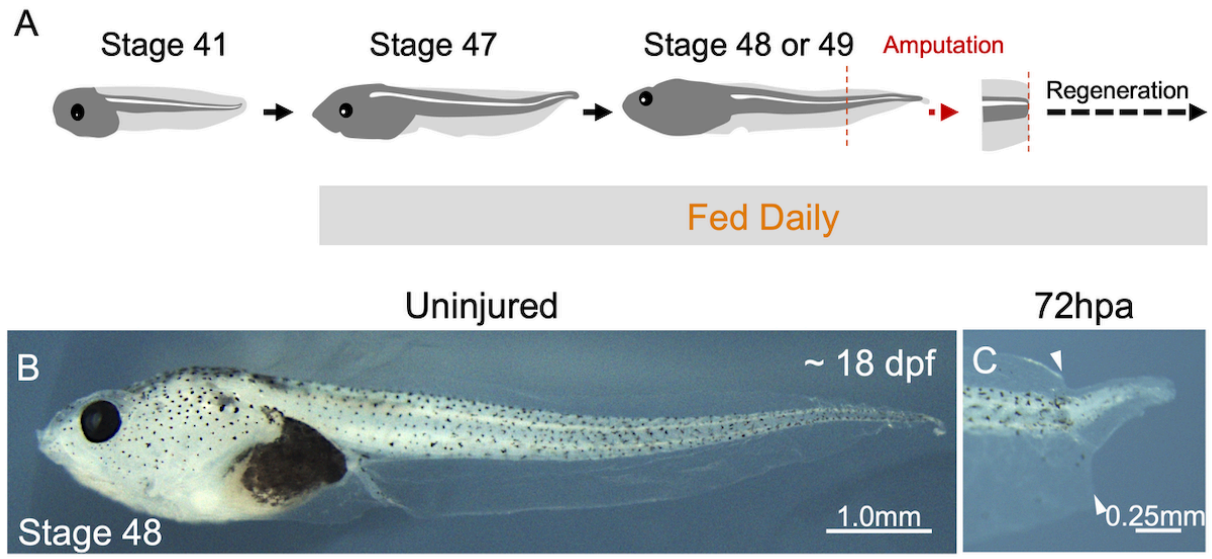

Figure 2-3: **Regeneration is restored after the refractory period at stage 48**

A) Schematic of standard rearing practices. Tadpoles are not fed until stage 47 and then reared until stage 48 or 49 before amputation. B-C) Brightfield images of stage 48 tadpoles before injury (B) and 72 hpa (C). Scale bars are 1 mm (B) or 0.25 mm (C). White arrows indicate amputation site.

2.3.2 *Cell proliferation declines with the refractory period in uninjured tadpoles*

Having established that tail regeneration declines with developmental age, we next interrogated whether cell proliferation in the tail changed over the same developmental timecourse. We hypothesized that cells in the tadpole tail may undergo a decline in their steady-state proliferation rate as tadpoles approach the refractory period. To investigate proliferation in the tail, we used immunofluorescence to stain tadpoles for the mitotic histone variant phospho-histone H3 (pH3) from stage 41 to 47. We found that pH3+ cells are abundant throughout the tail at stage 41, decline at stages

with reduced regeneration (stages 43-46), and are virtually absent at stage 47 (Figure 2-4 A-F). To account for differences in tail size, we normalized the number of divisions to the area of the tail and found that there was a statistically significant decline in the area-normalized number of mitotic cells from stage 41 to stage 43, with a further decline from stage 46 to stage 47 (Figure 2-4 G). We therefore conclude that the decline in regenerative competence from stage 41 to stage 47 is paralleled by a similarly graded decline in cell proliferation throughout the tail.

We then assessed whether proliferation rates change in response to tail amputation by amputating at each stage from 41-47 and staining for pH3+ cells at 24 and 72 hpa (Figure 2-5 A-J). At all stages, there are more pH3+ cells at 72 hpa than 24 hpa. Interestingly, proliferation rates from tadpoles amputated at stage 41 are substantially higher than when amputated at all other stages at both timepoints (Figure 2-5 K,L). When we quantified the density of dividing cells in the regenerated tissue we found that there was not a significant change at 24 hpa and find an increase in pH3 density at 72 hpa (Figure 2-6 A,B). However, it is important to note that the variation in the area of regenerated tail tissue highly influences the resulting density, such that a small number of divisions in a poorly regenerated tail have more weight. Thus, in agreement with the graded refractory period we describe above, we find that overall proliferation declines from stages 43 to 46 when regeneration is reduced and further declines at the stage 47 refractory period, correlating with changes in regeneration outcome.

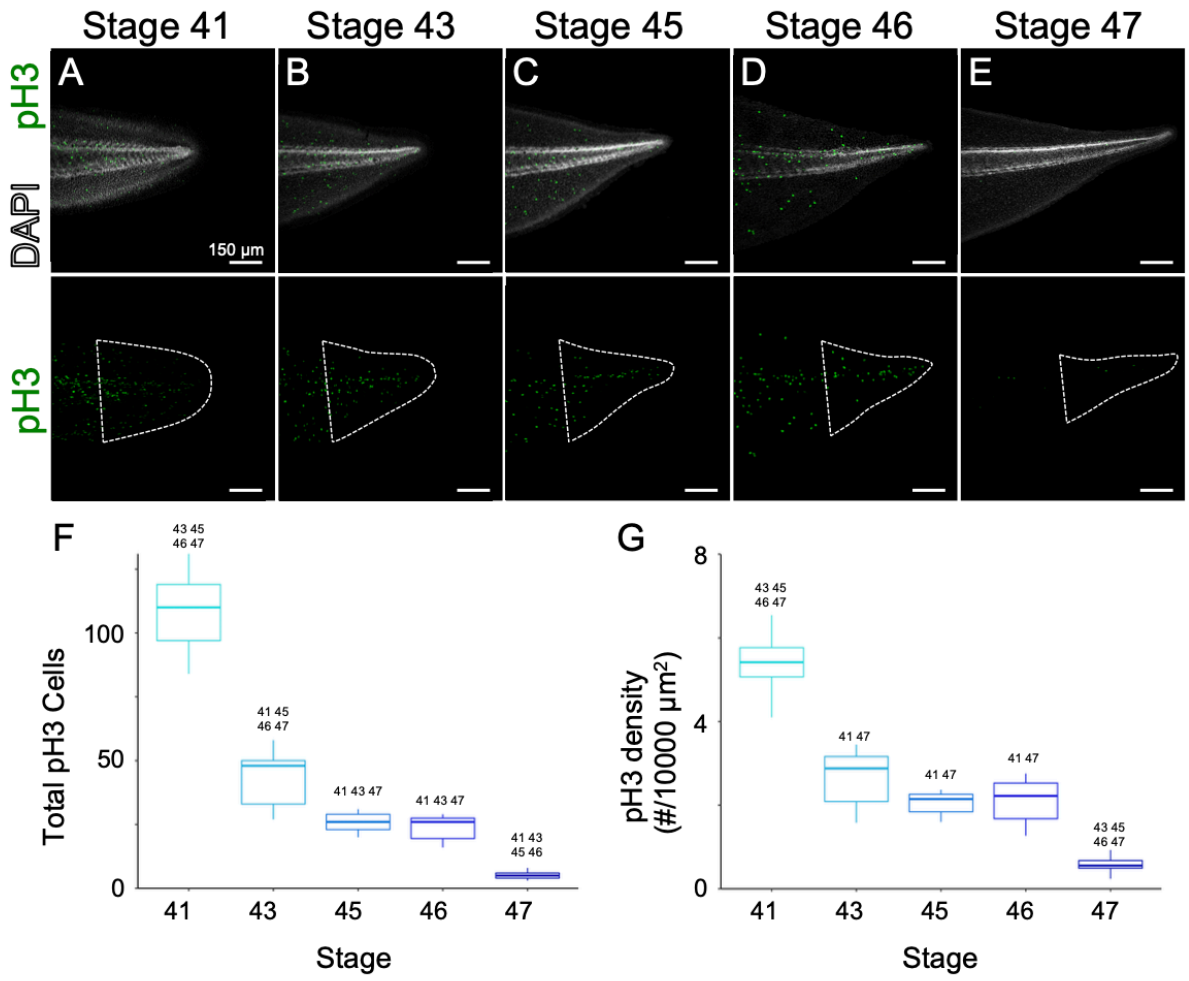

Figure 2-4: **Proliferation in the posterior of the tail declines over development**

A-E) Immunohistochemistry for pH3 in uninjured tails at stage 41 (A), 43 (B), 45 (C), 46 (D), 47 (E) counterstained with DAPI. Scale bar is 150 µm. F,G) Box-and-whisker plots showing total numbers of pH3 positive cells (F) or density of pH3 positive cells per 10,000 μm^2 (G). For (F,G), the midline represents the median of all tadpoles assayed, box size represents the interquartile range, and the lines represent the range. Outliers are indicated as points. n ranges 7 – 9 per group. Stage numbers above a condition indicated statistical significance ($p<0.05$) between the given group and those stages as determined by ANOVA ($p<2x10^{-16}$ for F) and G) followed by Tukey's post-test. Area of quantification is indicated by dashed white outline.

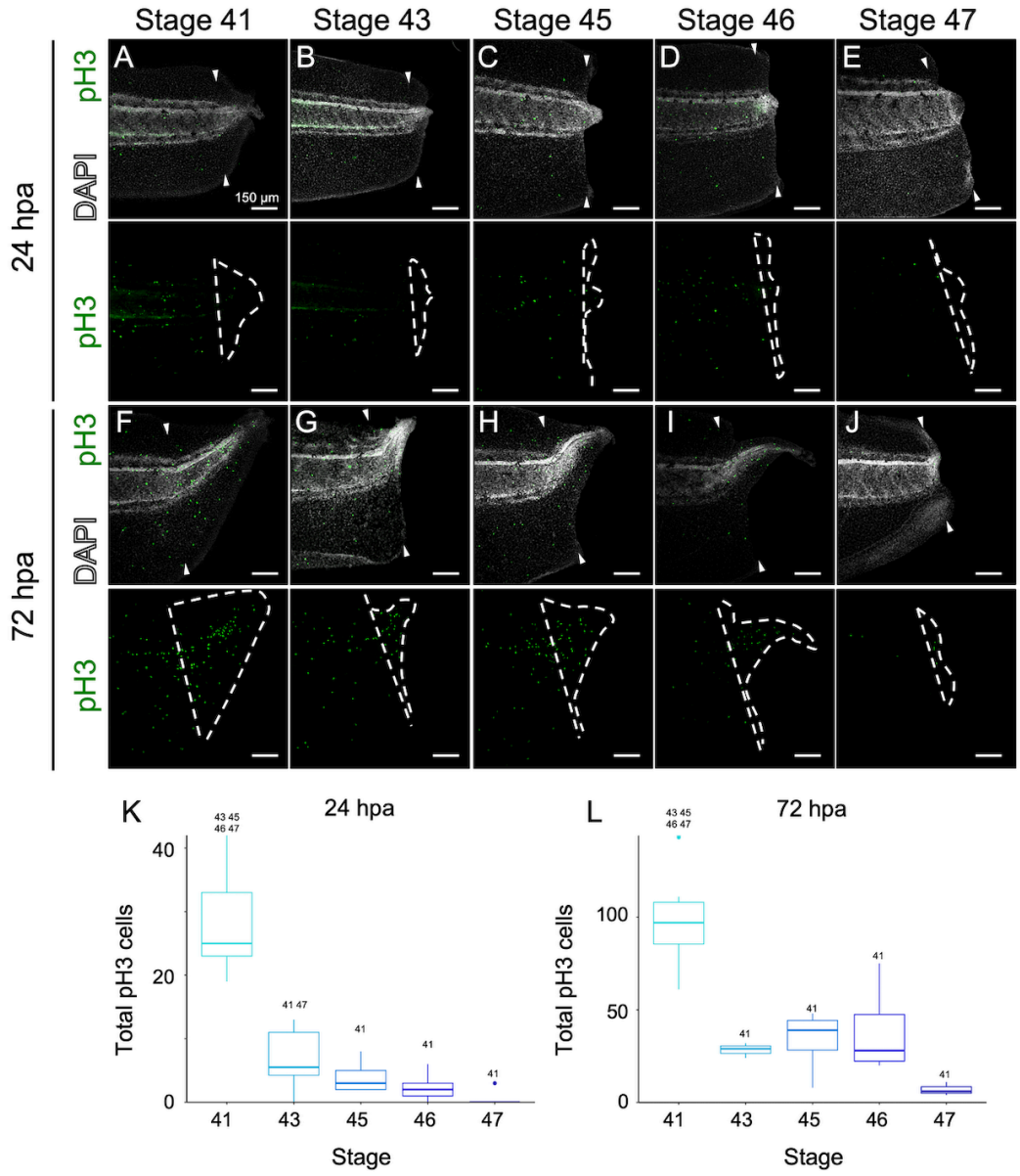

Figure 2-5: **Proliferation following injury declines during refractory period**

A-J) Immunohistochemistry for pH3 in 24 hpa (A-E) and 72 hpa (F-J) tails at stage 41 (A,F), 43 (B,G), 45 (C,H), 46 (D,I), 47 (E,J) counterstained with DAPI. Scale bar is 150 µm. K,L) Box-and-whisker plots showing total numbers of pH3 positive cells at 24 hpa (K) or 72 hpa (L). For (K,L), the midline represents the median of all tadpoles assayed, box size represents the interquartile range, and the lines represent the range. Outliers are indicated as points. Stage numbers above a condition indicate statistical significance ($p<0.05$) between the given group and those stages as determined by ANOVA ($p=4.39x10^{-16}$ for K and $p=1,19x10^{-7}$ for L) followed by Tukey's post-test. For (K) n > 9 per stage; for (L) n ranges 3 - 11 per stage. White arrows indicate amputation site. Area of quantification, the regenerated tissue, is indicated by dashed white outline.

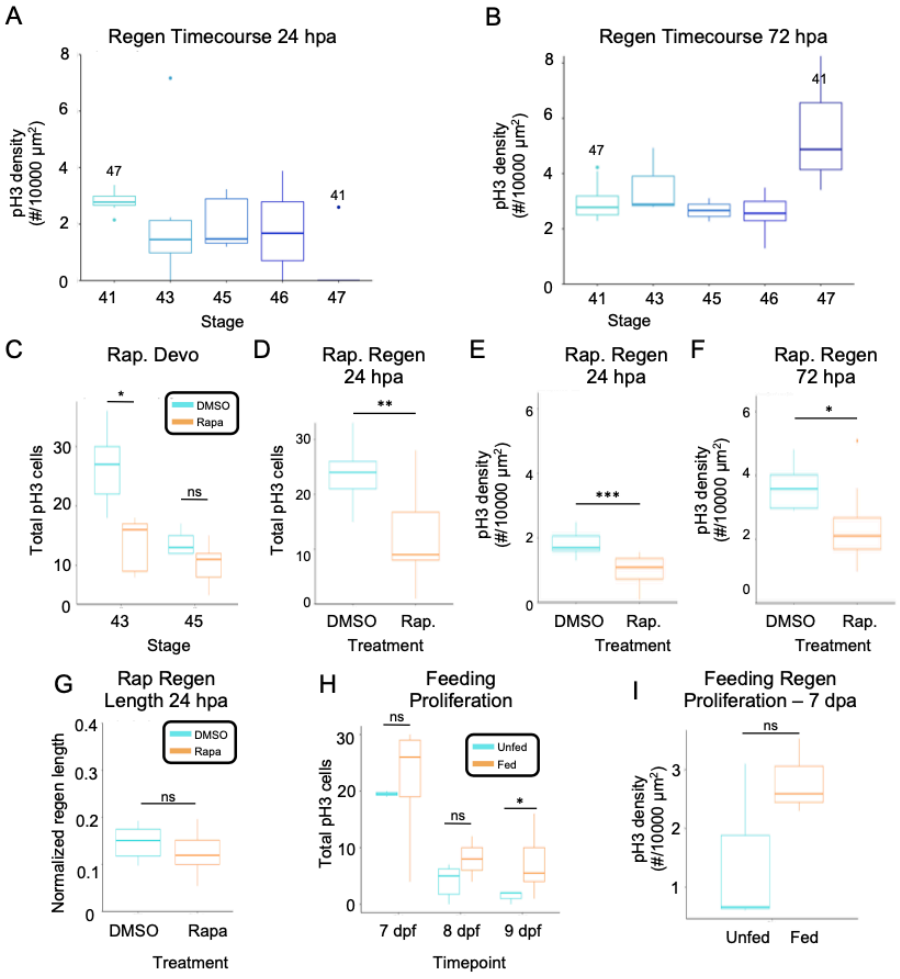

Figure 2-6: **Alternative timepoints and quantification methods for proliferation assays**

A, B) Box-and-whisker plots of pH3 density at 24 hpa (A) or 72 hpa (B) of tadpoles amputated at indicated stages. C-F) Box-and-whisker plots showing either number of pH3+ cells (C, D) or pH3 density (E, F) of DMSO (blue) or Rapamycin (orange) treated regenerates at indicated stages (C) or regeneration time points (D-F). G) Box-and-whisker plot showing the normalized regeneration length of tadples at 24 hpa following either DMSO or Rapamycin treatment. (H, I) Box-and-whisker plot showing number of pH3+ cells (H) or pH3 density (I) at indicated timepoints in unfed (blue) or fed (orange) conditions. For all plots, the midline represents the median of all tadpoles assayed, box size represents the interquartile range, and the lines represent the range. For (A,B) Stage numbers above a condition indicated statistical significance ($p<0.05$) between the given group and those stages as determined by ANOVA ($p=1.59x10^{-13}$) followed by Tukey's post-test. For (C-I), statistical significance between DMSO and Rapamycin, or unfed and fed groups is determined with a two-sided t-test (*$p<0.05$, **$p<0.01$, ***$p<0.001$).

2.3.3 *Maternal yolk stores decline during the refractory period and are redistributed following amputation.*

Having observed that proliferation and regenerative competence both decline from stage 41 to stage 47, we next set out to test the hypothesis that these declines might be linked to nutrient availability. At stage 41, tadpoles are still relying on cell-autonomous stores of maternal yolk for nutrition (Dickinson & Sive, 2006; McNamara et al., 2018). Independent feeding begins at stage 45. We therefore predicted that maternal yolk stores would undergo exhaustion as tadpoles entered the period of reduced regeneration. To test this prediction, we blotted for the yolk protein vitellogenin in tail lysates across a developmental timecourse from stage 41 to 47 and found that yolk is substantially depleted from stages 41 to 43, after which it generally declines in abundance over time (Figure 2-7 A). We then used immunofluorescence to identify where vitellogenin was localized in the tail. At stage 41, we find that vitellogenin is readily detectable throughout the tail, staining all tissues comparably (Figure 2-7 B). From stages 43 to 46, vitellogenin staining in the fin declines revealing stores of vitellogenin in the somites, in agreement with previous reports that muscle cells are strongly labeled with vitellogenin (Figure 2-7 C-E) (Jorgensen et al., 2009). At stage 47, while the overall amount of vitellogenin remains similar to stage 46 in western blot, the distribution of vitellogenin by IF becomes weak and diffuse and is absent from the tail fin (Figure 2-7 F). This graded decline of vitellogenin staining parallels the stepwise loss of regenerative competence and pH3 staining and is consistent with our central hypothesis that nutritive stress may contribute to loss of regenerative competence.

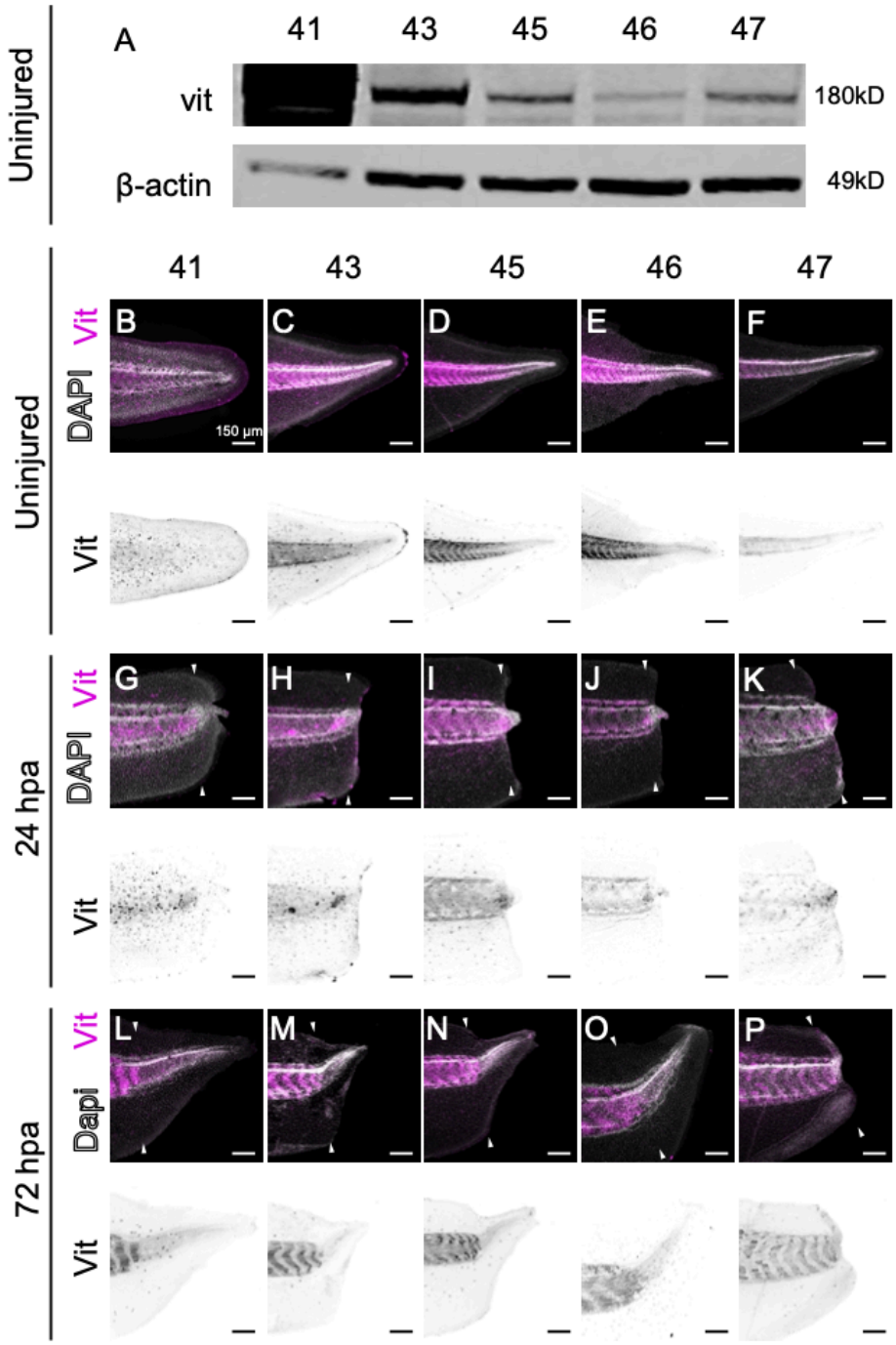

Figure 2-7: **Yolk is redistributed during development and regeneration**

A) Western blot for vitellogenin and β-actin in uninjured tails at stage 41, 43, 45, 46, and 47. Immunohistochemistry for vitellogenin in uninjured tails at stage 41 (B), 43 (C), 45 (D), 46 (E), 47 (F) counterstained with DAPI. In G-O, amputation was performed at stage 41 (G,L), 43 (H,M), 45 (I,N), 46 (J,O), 47 (K,P) and tadpoles were collected at 24 hpa (G-K) or 72 hpa (L-P). White arrows indicate amputation site.

We next set out to test whether the additional stress of amputation altered the depletion of maternal yolk in the tadpole tail. We reasoned that wound healing and regeneration require accelerated cellular biosynthesis and may therefore be accompanied by redistribution or accelerated depletion of maternal yolk stores. Although we did not observe a clear decline in yolk, we found that amputation of the tail at all stages leads to formation of vitellogenin puncta throughout the tail at 24 hpa, but a decline in the background level of vitellogenin staining (Figure 2-7 G-P).

Taken together we conclude that the distribution of maternal yolk is more abundant in the tail fin at stage 41 and declines quickly as regenerative competence is lost. While amputation does not appear to trigger a rapid decline in the overall abundance of maternal yolk, it does lead to a change in yolk distribution in which yolk accumulates in puncta throughout the tail.

2.3.4 *Inhibition of mTOR activity reduces tadpole growth*

Our next goal was to determine if nutrient sensing pathways impact growth and yolk utilization during development. We hypothesize that when nutrients are abundant, mTOR signaling will be active, triggering proliferation and tail growth. Therefore, if mTOR is inhibited we predict a decrease in growth, which may be accompanied by a slower decline in total yolk as these stores are no longer fully mobilized. We inhibited mTOR signaling using rapamycin or torin starting at stage 41 (Figure 2-8 A) and assayed tadpole size, cell proliferation in the tail, and vitellogenin staining at stage 43 and 45 or 46. Compared to control DMSO-treated clutchmates, tadpoles treated with 10

μM rapamycin were shorter at both stage 43 and 46, though we note that the tadpoles were developing through NF stages at the same rate (Figure 2-8 B-E, G). Treatment with rapamycin results in an accumulation of vitellogenin in western blot, suggesting, as expected, that yolk stores are mobilized less efficiently when mTOR is inhibited (Figure 2-8 F). As rapamycin is known to play a role in cellular processes outside of mTOR regulation, we performed these assays in parallel with the ATP-competitive mTOR inhibitor, Torin1 (Chou et al., 2011; Thoreen et al., 2009). We find that treatment with 1 μM Torin1 results in decreased whole body length of tadpoles to a similar degree as rapamycin, suggesting that the effects we observe are due to regulation of mTOR (Figure 2-8 H). Further, rapamycin-treated tadpoles had significantly lower densities of pH3+ cells on average at stage 43 than their DMSO counterparts, though by stage 45 the difference in division rates between groups was no longer significant (Figure 2-8 I-N). The same was true of the total number of pH3+ cells (Figure 2-6). These data suggest that mTOR signaling is required for the full extent of *Xenopus tropicalis* tadpole growth and cell proliferation from stages 41 to 46, and for the consumption of yolk stores during this period.

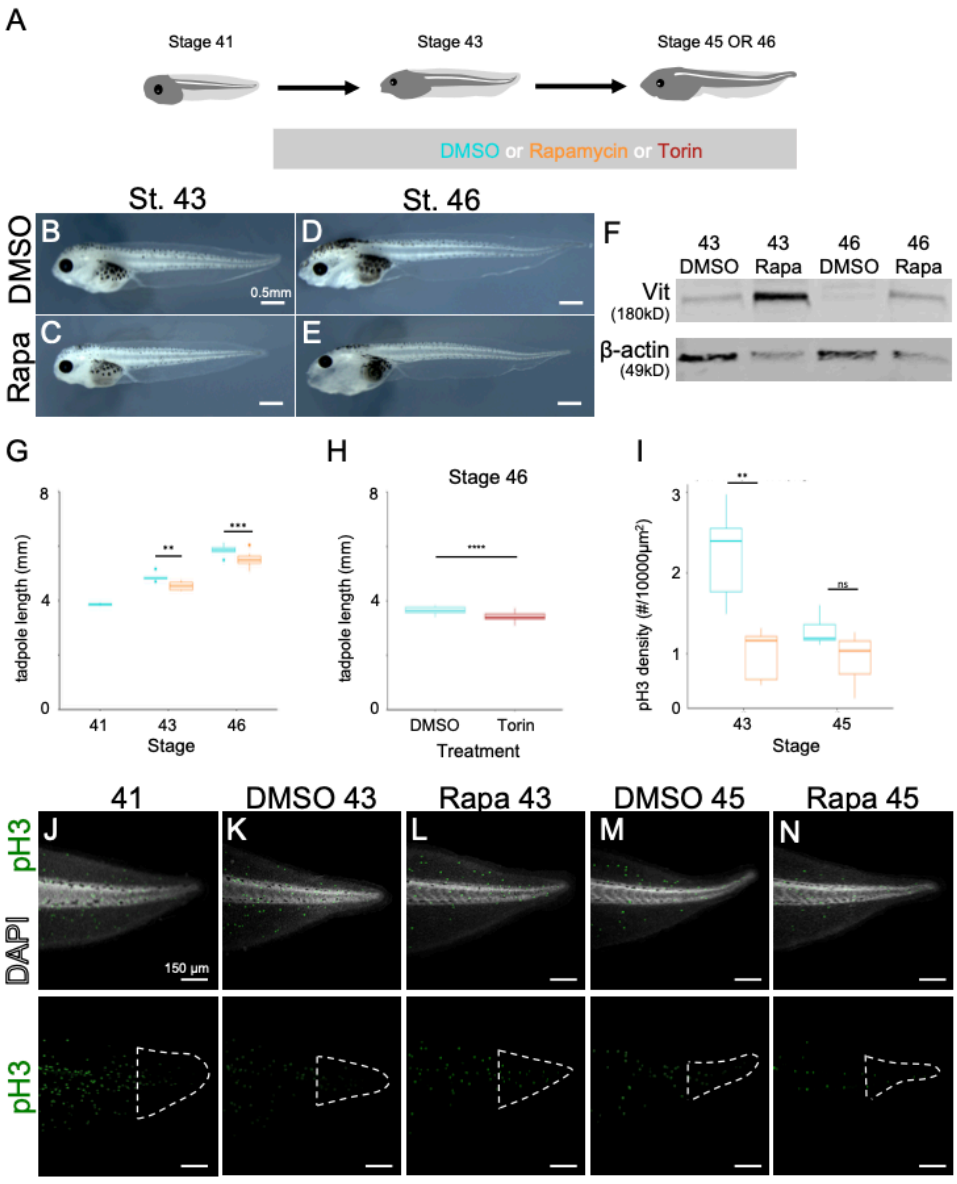

Figure 2-8: **Rapamycin treatment inhibits growth, proliferation, and yolk distribution over development**

A) Schematic of treatment and collection strategy. Tadpoles are treated with either DMSO (B,D,K,M), 10 μM Rapamycin (C,E,L,N) or 1 μM Torin1 before collection at indicted stages. B-E) Brightfield images of tadpoles at stage 43 (C,D) and stage 46 (E,F) following DMSO or Rapamycin treatment. Scale bar is 0.5 mm. F) Western blot for vitellogenin and β-actin at stages 43 and 46, of either DMSO or Rapamycin treated tadpoles. G) Box-and-whisker plot showing the length of tadpoles over development following DMSO or Rapamycin treatment. H) Box-and-whisker plot showing the length of tadpoles at stage 46 following either DMSO or Torin1 treatment. I) Box-and-whisker plot showing the density of pH3+ cells across groups. J-N) Immunohistochemistry for pH3 and vitellogenin in uninjured, untreated stage 41 (J) or treated (K-N) tadpoles at

indicated stages with DAPI counterstain. Scale bar is 150 μm. For (G-I), the midline represents the median of all tadpoles assayed, box size represents the interquartile range, and the lines represent the range. For (G-I), statistical significance between DMSO and Rapamycin or Torin1 groups is determined with a two-sided t-test (*p<0.05, **p<0.01, ***p<0.001). For (G) n ranges 7 - 13 per group; for (H) n ranges 18 – 19 per group: for (I) n ranges 5 - 10 per group.

2.3.5 *Inhibition of mTOR activity reduces tail regeneration*

After finding that mTOR signaling is required for full tadpole growth during development, we asked if it was necessary for tissue growth during regeneration. To this end, we amputated tails at stage 41 and then reared tadpoles in either DMSO, 10 μM rapamycin, or 1 μM Torin1 and assayed regeneration at 24 and 72 hpa (Figure 2-9 A). We find that at 24 hpa there is not a significant difference between the 2 groups, but by 72 hpa mTOR inhibited tails regenerate significantly less tissue than DMSO controls (Figure 2-6 G, Figure 2-9 B,C). The regeneration scores are comparable between DMSO and rapamycin treatments, indicating that while growth is impaired, quality of regeneration is not (Figure 2-9 D). In agreement with a reduced regenerate size, rapamycin-treated tails have significantly fewer dividing cells in the regenerating tissue at 24hpa and 72hpa, suggesting that mTOR is necessary to promote regeneration by activating proliferation (Figure 2-6 D-F, Figure 2-9 E-I). We therefore infer that the decline in proliferation beginning by 24hpa may result in the reduced regenerate length observed by 72hpa. These data indicate that regeneration is reduced when nutrient sensing via mTOR is lost and suggest that the ability to detect sufficient nutrients may be an important part of the tadpole's ability to execute a regenerative response following amputation.

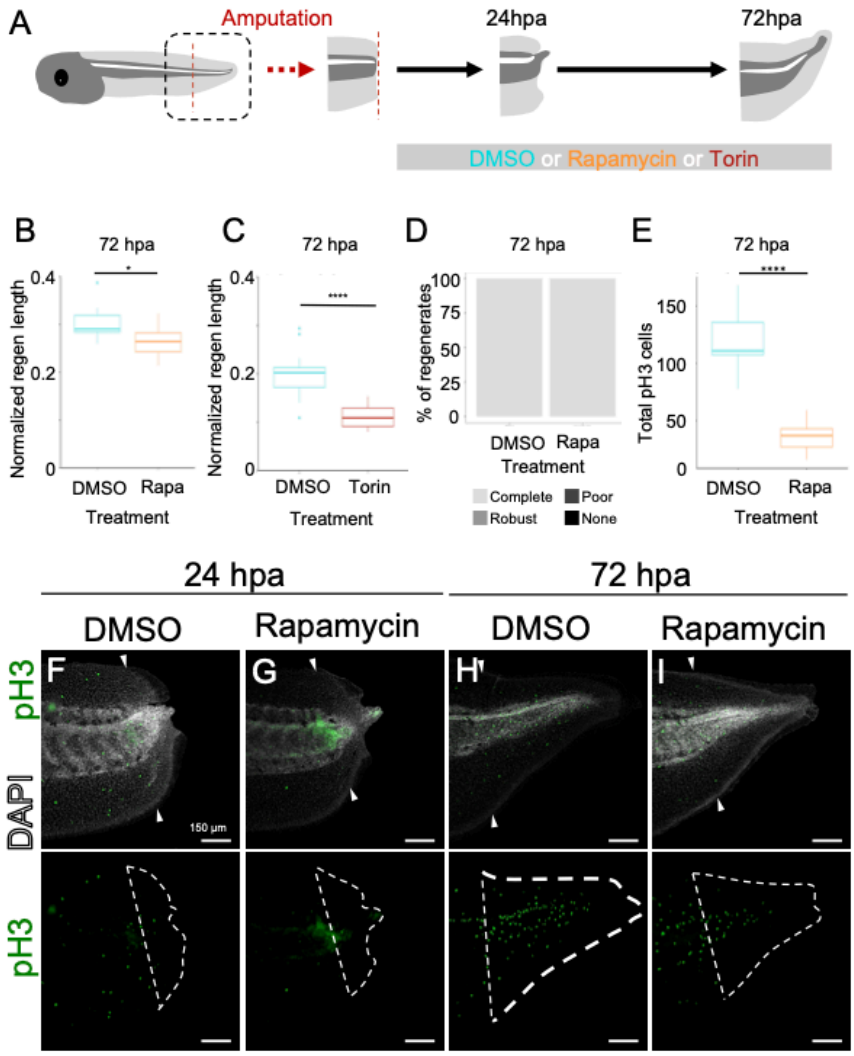

Figure 2-9: **Rapamycin treatment reduces regeneration and proliferation while disrupting regeneration induced yolk mobilization**

A) Schematic of treatment and collection strategy. Tadpoles are amputated then treated with either DMSO (F,H), 10 µM Rapamycin (G,I), or 1 µM Torin1 before collection at indicted timepoints. B) Box-and-whisker plot showing the length of the regenerated tail normalized to vent-to-tail tip length of the tadpole at 72 hpa following DMSO or Rapamycin treatment. C) Box-and-whisker plot showing the length of the regenerated tail normalized to vent-to-tail tip length of the tadpole at 72 hpa following DMSO or Torin1 treatment. D) Regeneration quality index showing regeneration quality of DMSO vs Rapamycin treated tadpoles at 72 hpa. Regeneration scores are shown as complete, robust, poor, or none. E) Box-and-whisker plot showing total numbers of pH3 positive cells at 72 hpa . F-I) Immunohistochemistry for pH3 and vitellogenin at 24 hpa (F,G) or 72 hpa (H,I) after treatment with DMSO or 10 µM Rapamycin with DAPI counterstain. Scale bar is 150 µm. For (B,C, E), the midline represents the median of all tadpoles

assayed, box size represents the interquartile range, and the lines represent the range. For (F-H), statistical significance between DMSO and Rapamycin groups is determined with a two-sided t-test (*p<0.05, **p<0.01,***p<0.001, ****p<0.0001). For (B) n ranges 8 -10; for (C) n ranges 18 – 19; for (D) n ranges 6 – 8; for (E) n ranges 9 - 10. White arrows indicate amputation site. Note autofluorescence of axial tissue in 5G was consistent across samples in this treatment group.

2.3.6 *Proliferation and regeneration are promoted by feeding during the refractory period*

Having observed that yolk stores decline as tadpoles approach the refractory period, we asked if lack of nutrient availability impacts regenerative outcomes. If nutritive stress contributes to the refractory period, then we predict that generously feeding tadpoles could promote regeneration once feeding behaviors begin. To test this, we provided sera micron (SM) to tadpoles starting at stage 46 (Figure 2-10 A). This feeding scheme did not result in substantial changes in overall developmental rate relative to unfed clutchmates at the stages assayed (Figure 2-10 A, C-D, Figure 2-11 A). We compared normalized regeneration length at 7 days post amputation (dpa) and found that fed tadpoles regenerate much more successfully than unfed tadpoles, both in length of tissue as a proportion of vent-to-tail tip length and in regeneration quality (Figure 2-10 B-K). We then examined proliferation rates by quantifying pH3+ cells and found that proliferation rates were increased in the fed condition relative to the unfed in both uninjured and regenerative contexts. In the uninjured context, we found that proliferation rate increased in the fed condition by 9 dpf, 72 hours after the start of feeding (Figure 2-6 H, Figure 2-10 L-Q, T). In the regenerative context, we found that the absolute number of dividing cells in the regenerated tissue of fed tadpoles is higher

than in unfed tadpoles, which have little to no division following injury (Figure 2-10, R,S,U, Figure 2-6 I).

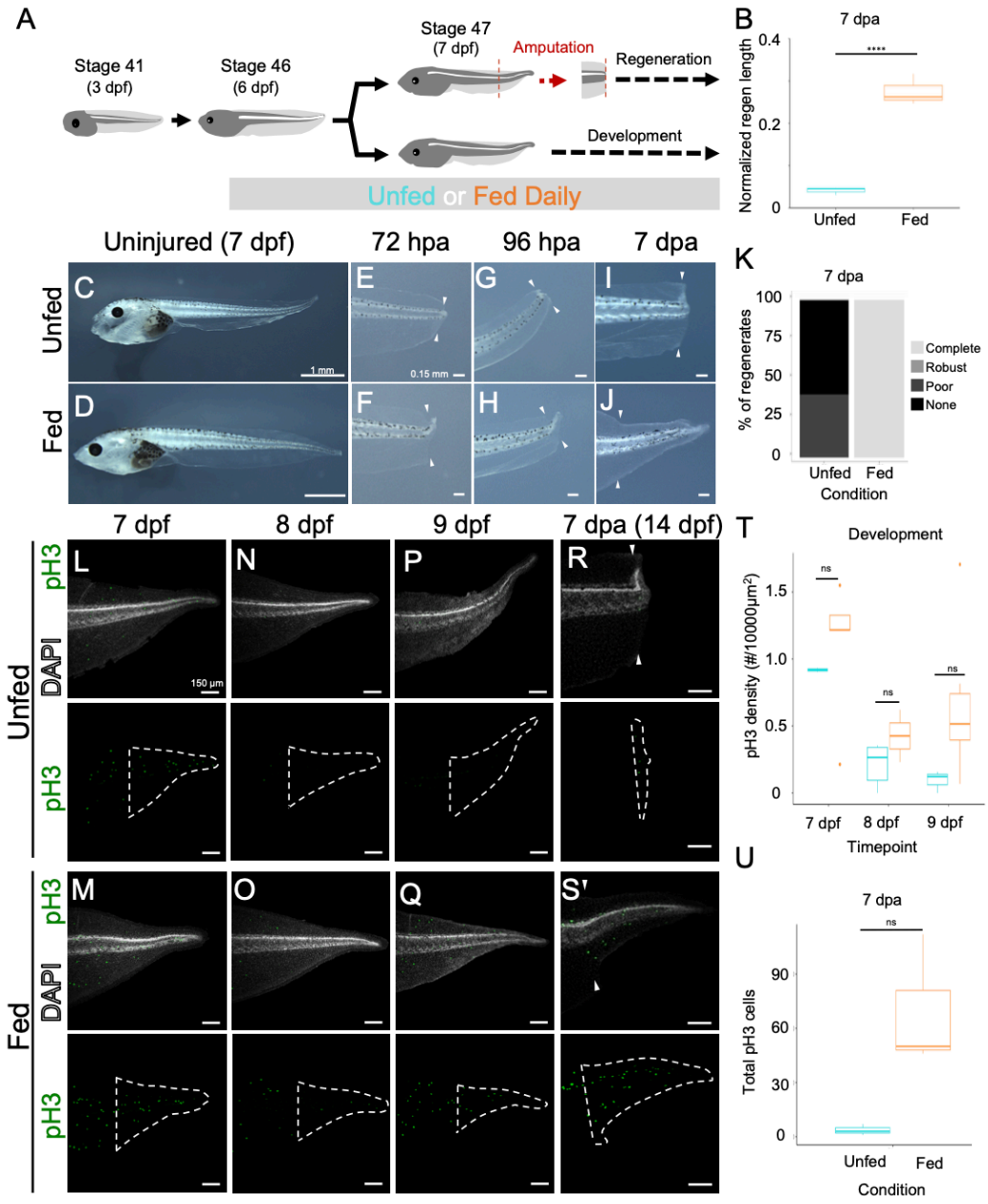

Figure 2-10: **Proliferation and regeneration are promoted by feeding during the refractory period**

A) Schematic of feeding and regeneration assay. Unfed group are provided no food for the duration of the experiment. Fed group are fed daily starting at stage 46 (24 hours before amputation for regeneration assays). B) Box-and-whisker plot showing regeneration length normalized to vent-to-amputation plane length. C-J) Brightfield

images of tadpoles under indicated conditions. For regeneration assays, tadpoles were collected uninjured at stage 47 (C, D), 72 hpa (E,F), 96 hpa (G, H) or 7 dpa (I,J). C-J) Brightfield images of tadpoles under indicated conditions. Scale bars are 1 mm or 0.15 mm. K) Regeneration quality index showing regeneration quality of unfed and fed tadpoles at 7 dpa. Regeneration scores are shown as complete, robust, poor, or none. L-S) Immunohistochemistry for pH3 of uninjured tails at 7 dpf (L,M), 8 dpf (N,O), and 9 dpf (P,Q) under indicated unfed or fed conditions with DAPI counterstain. R,S) Immunohistochemistry for pH3 of 7 dpa tails under unfed (R) or fed (S) conditions with DAPI counterstain. Scale bar is 150 µm. T) Box-and -whisker plot showing density of pH3 positive cells in uninjured tails following feeding protocol at 7, 8, and 9 dpf. U) Box- and -whisker plot showing number of pH3 positive cells 7 dpa. For (B, T- U), statistical significance between unfed and fed groups is determined with a two-sided t-test (*p<0.05, **p<0.01, ns 'not significant'). For (B-K), n ranges 11-12; for (L-T), n ranges 3 – 9; for (U), n is 3 per condition.

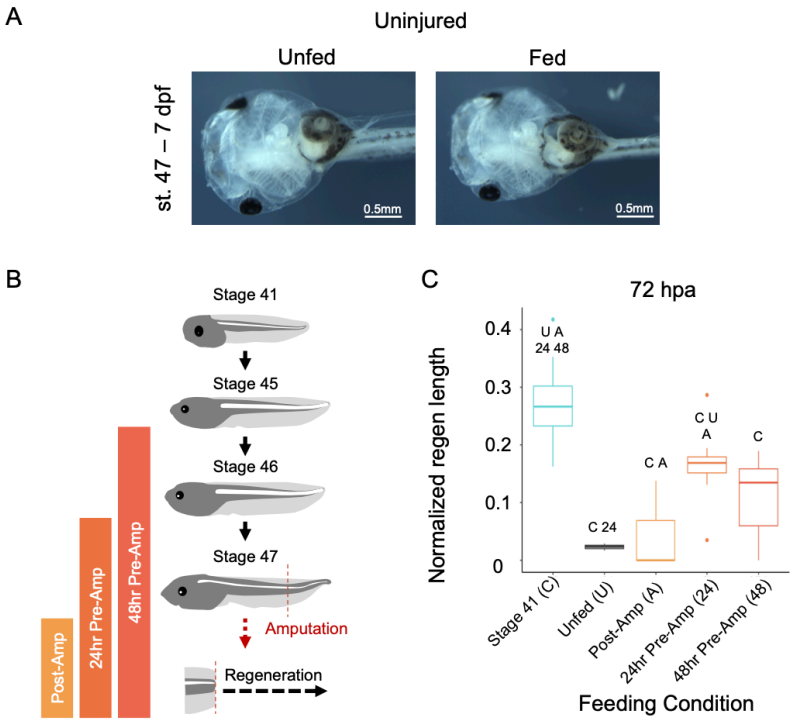

Figure 2-11: **Feeding before amputation does not accelerate development past the refractory period and feeding after amputation is not sufficient to rescue regeneration during the refractory period**

A) Bright field images of 7 dpa tadpoles 24 hours after initiating feeding protocol; both unfed and fed tadpoles are stage 47. Scale bar is 0.5 mm. B) Schematic of various feeding conditions. Tadpoles were fed 48 hours prior to amputation, 24 hours prior to amputation, after amputation, or left unfed. Tadpoles were amputated at stage 47, at 7 dpf. C) Box-and -whisker plot showing regeneration length normalized to vent-to-amputation plane length comparing stage 41 (unfed) and refractory regenerates of

respective feeding schemes. For (C) characters above respective conditions indicate significant difference ($p < 0.05$) between the given group and those conditions as determined by ANOVA ($p=4.39x10^{-16}$ for K and $p=1,19x10^{-7}$ for L) followed by Tukey's post-test. For (C), stage 41 n is 23; for refractory groups, n ranges 3 - 12 per group. C – stage 41; U – Unfed; A – post-amputation; 24 – 24hr pre-amputation; 48 – 48hr pre-amputation.

Our earlier data suggested that nutrient sensing via mTOR is necessary for regeneration, and so we asked if tadpoles needed to be fed prior to amputation or if supplementing food at the time of injury was sufficient to rescue regeneration. Tadpoles that were not fed until amputation did not regenerate, whereas those that were fed 24 or 48 hours before injury regenerated robustly (Figure 2-11 B-C). This suggests surplus nutrient sensing at or prior to the time of injury is critical to regenerative response and that there is a lag between feeding and ability to activate a regenerative program. Collectively, these data show that feeding is sufficient to rescue regeneration and proliferation in the refractory period of *Xenopus tropicalis* and suggest that access to nutrients through feeding can rescue the deficits caused by yolk depletion.

2.4 DISCUSSION

2.4.1 *The refractory period in Xenopus tropicalis is graded*

The mid-tadpole stage refractory period of *X. laevis* has been fruitfully exploited to identify factors that can limit or increase regenerative competence. For example, stimulation of the BMP or Notch signaling pathways has been shown to partially rescue regeneration in the refractory period, suggesting these signals are pro-regenerative (Slack et al., 2004). Immunosuppression with a range of inhibitor-κB kinase inhibitors is also sufficient to rescue regeneration, implicating immune cell activation in this process

(Fukazawa et al., 2009). Stabilization of the stress-induced transcriptional regulator hypoxia inducible factor 1α (Hif1α) by DMOG has also been shown to partially restore tail regeneration, suggesting that proper integration of stress signaling could play a role in regenerative competency (Ferreira et al., 2018). Despite these insights into pro-regenerative cues, relatively little is known about the underlying cause of the refractory period, or whether it is a common feature in anurans. Our findings confirm that a similar refractory period exists in the diploid *X. tropicalis*. However, there are clear differences in the onset and progression of the refractory period between the two species. Whereas in *X. laevis* the refractory period begins abruptly with full loss of regeneration at stage 45 (Beck et al., 2003), in *X. tropicalis* we first observe a decline in regeneration length at stage 43. Modest, but statistically significant loss of regenerative response persists through stage 46, and then becomes much more pronounced at stage 47 with a loss of all axial and fin regeneration. As in *X. laevis*, the refractory period is reversible in *X. tropicalis*, and if tadpoles are fed beginning by stage 47, regenerative capability is fully restored by stage 49.

2.4.2 *Nutrient availability is constrained during the refractory period*

The contribution of nutrition to regeneration has been considered in multiple contexts. Here we find regeneration is reduced beginning at stage 43, which precedes the tadpole's ability to feed independently, and persists through the early stages of independent feeding. During this period, we find that maternal yolk stores decline, reflected in reduced vitellogenin in the tail, and although the tadpole has not fully stopped growing, rates of cell proliferation in the tail decline relative to their stage 41 levels. During this period, the introduction of a major wound such as a tail amputation

would be expected to place an even greater demand on the tadpole's limited nutritive stores, both to replace lost tissue as well as restore homeostasis and maintain overall growth. We find that yolk distribution is altered in response to injury, becoming distributed and punctate. By stage 47, when tails are refractory to regeneration, unfed tadpoles have virtually no cell proliferation in the tail and substantially reduced yolk stores.

The transition to independent feeding is a unique point in the tadpole life cycle, and the relationship between nutritive stress and regenerative competence may well differ during later regenerative stages when independent feeding has been ongoing for days or weeks. Indeed, early experiments by T.H. Morgan in older *Rana* tadpoles suggested that regeneration could proceed even during starvation (Morgan, 1901a). It is striking that feeding has not been previously linked to the refractory period in *X. laevis*. We consider two possibilities for this discrepancy. One is that feeding is simply not sufficient to restore regeneration in *X. laevis*, in contrast to *X. tropicalis*. *X. tropicalis* differ from *X. laevis* in many respects that may impact nutrient availability and mobilization, including their preferred rearing temperature and size (McNamara et al., 2018), and this may be another point of difference. The other is that the amount and timing of feeding must be specific in order to restore regeneration. We find that *X. tropicalis* tadpoles that are not fed until amputation do not regenerate, suggesting that the timing is critical. The possibility that nutrient stress contributes to the refractory period represents an opportunity to consider nutrient sources and their mobilization in other regenerative contexts, as well as in non-regenerative species. It is not yet clear what specific nutrient pathways are required for regeneration. The strong transcriptional

upregulation of *leptin* after injury (Aztekin et al., 2019; Crespi & Denver, 2006; Kakebeen et al., 2020; N. R. Love et al., 2011) suggests that this may be one of the major pathways contributing to nutrient dependence and its interpretation in regeneration, although there is not yet conclusive functional evidence that any specific *leptin* gene product or receptor is required for appendage regeneration.

2.4.3 *The mTOR pathway is required for normal growth and regeneration*

The mTOR kinases serve a multitude of roles in various cells, which include cell growth, proliferation, cell motility, cell survival, autophagy, and regulation of transcription and translation (Giguère, 2018; Sabatini, 2017). Many of these processes must be under active regulation as regeneration proceeds in order for the final size and cell type distribution of the regenerated structure to be restored. It has been shown previously that mTOR is required for several of these processes, including proliferation, in the regeneration of zebrafish caudal fin (Hirose et al., 2014). We find that pharmacological inhibition of mTOR with rapamycin and Torin1 limits tadpole growth and regeneration, but this observation does not discriminate between which of these specific functions is most critical. Similarly, mTOR can be activated by several signaling mechanisms. One mechanism is through leptin signaling, which indicates nutrient abundance, and activates mTOR to permit growth (Haissaguerre et al., 2014; Hu et al., 2016). In mice where growth has been restricted by limited nutrition, endogenous leptin production precedes re-initiation of growth hormone production and tibial length during catch-up growth, effects which can be mimicked by leptin injection (Carro et al., 1997; Gat-Yablonski et al., 2008; Gat-Yablonski & Phillip, 2015). Conversely, inhibition of mTOR by rapamycin treatment mimics nutrient scarcity, restricting growth and proliferation

(Fingar & Blenis, 2004). In regeneration, we predict that mTOR signaling is required for growth and proliferation required to regrow the tail, and inhibition of mTOR cues the tadpole that there are not enough nutrients available for the full execution of this process, similar to the natural nutrient scarcity encountered as the tadpole approaches the refractory period. While we expect that these reductions are due to mTORs role in nutrient sensing, we also must consider that decreased growth and regeneration could result from the changes to the pleiotropic roles of mTOR listed above. Interestingly, our finding that yolk is not fully depleted during the reduced regenerative period of stages 43 - 46 suggests that this cue may not be binary but rather graded to account for available, albeit respectively limited, remaining nutritional stores. As the tadpole begins to rebuild nutrient stores through independent feeding, we hypothesize that this restriction is relieved, and the capacity for regeneration is restored until metamorphosis. Consistent with this, we find that feeding must be initiated prior to tail amputation, and regeneration fails if food is first provided simultaneously with tail amputation, suggesting that nutrient reserves have not recovered enough to enable regeneration.

Our central hypothesis that nutrient levels constrain regenerative competence makes several predictions that remain to be tested. One such prediction is that levels of active mTORC1 will fall as the tadpole enters the refractory period and increase as it exits the refractory period. It will also be interesting to interrogate the functions of nutrient sensing pathways such as leptin, insulin and ghrelin in the tail during regeneration. Exogenous leptin has been shown to increase growth and cell proliferation in the *X. laevis* limb (Crespi & Denver, 2006) and brain (Bender et al., 2017). In zebrafish. the *leptin b* enhancer is a robust reporter of regeneration activation

(Kang et al., 2016), but a functional role for *leptin b* has not been shown. Several other signals, including insulin, can also activate mTOR, and may serve as the instructive signals in regeneration, though it is also possible that these signals regulate nutrient consumption independently. Further inhibition of upstream or parallel nutrient sensing pathways might yield more robust decreases in growth and regenerative potential (Yuan et al., 2013). The precise relationships between nutrient hormone levels, growth, and regenerative potential therefore remain to be articulated.

2.5 Acknowledgements

We thank members of the Wills lab for thoughtful discussion throughout the course of this work. The vitellogenin antibody was a gift from Marc Kirschner's group. We acknowledge Xenbase (www.xenbase.org) for staging and gene expression resources consulted throughout this work. This work was supported by R01NS199024 from NINDS to AEW and National Science Foundation Graduate Research Fellowship under Grant No. DGE-1762114 to JHP.

2.6 Materials and Methods

2.6.1 *X. tropicalis husbandry and use*

Use of *Xenopus tropicalis* was carried out under the approval and oversight of the IACUC committee at UW, an AALAC-accredited institution, under animal protocol 4374-01. Ovulation of adult *X. tropicalis* and generation of embryos by natural matings were performed according to published methods (Khokha et al., 2002; Sive et al., 2000). Embryos were reared as described in (Khokha et al., 2002). Staging was assessed by

the Nieuwkoop and Faber staging series (Nieuwkoop & Faber, 1994). Tadpoles were only fed for experiments in Figure 2-10 or if reared beyond stage 47. For experiments in Figure 2-10, sera micron (SM) was used at 0.5g/mL in 1/9th Modified Ringers solution (MR). 0.39µL SM/tadpole was added directly to 25mL MR daily. 100% of media was cycled daily for both fed and unfed groups. For rearing tadpoles beyond stage 47, we followed standard feeding protocols (McNamara et al., 2018).

2.6.2 *X. tropicalis amputation assay*

Tadpoles were anesthetized with 0.05% ms-222 in 1/9x MR and tested for response to touch prior to amputation surgery. Once fully anesthetized, a sterilized scalpel was used to amputate the posterior third of the tail. Amputated tadpoles were removed from anesthetic media within 10 minutes of amputation into new 1/9x MR. Tadpoles were left to regenerate at a density of no more than 3 tadpoles to 1 mL of media.

2.6.3 *Pharmacological inhibition*

Rapamycin (Sigma-Aldrich R0395) was resuspended to a 10 mM stock in DMSO as a vehicle and Torin1 (Millipore 475991-10MG) was resuspended to a 1 mM stock in DMSO. Uninjured and injured tadpoles were reared with 0.1% DMSO, 10 μM rapamycin, or 1 □M Torin1 diluted in 1/9x MR until collection at 24 or 72 hours following treatment.

2.6.4 *Immunohistochemistry*

X. tropicalis tadpoles were fixed for 1 hour in 1x MEM with 3.7% formaldehyde at room temperature. Tadpoles were permeabilized by washing 3X 20 minutes in PBS + 0.01% Triton x-100 (PBT). Tadpoles were blocked for 1 hour at room temperature in 10% CAS-block (Invitrogen #00-8120) in PBT. Then tadpoles were incubated in primary antibody [1:1000 mouse anti-Histone H3 (phospho S10), Abcam 14955; 1:500 rabbit anti-Vitellogenin (gifted by Marc Kirschner; Jorgensen et al., 2009)] diluted in 100% CAS-block overnight at 4°C. Tadpoles were then washed 3X 10 minutes at room temperature in PBT and blocked for 30 minutes in 10% CAS-block in PBT. Secondary antibody (goat anti-mouse 488, ThermoFisher A11001; goat anti-rabbit 594, Invitrogen A-11012) were diluted 1:500 in 100% CAS-block and incubated for 2 hours at room temperature. Tadpoles were then washed 3X 10 minutes in PBT followed by a 10 minute incubation in 1:2000 DAPI (Sigma D9542) before being washed with 1xPBS for 10 more minutes. Isolated tails were mounted on slides in ProLong Gold (ThermoFisher P36930). Images were acquired using a Leica DM 5500 B microscope using a 10X objective and processed using FIJI image analysis software (Schindelin et al., 2012).

2.6.5 *Western Blotting*

To isolate proteins, 5 tails amputated just posterior to the vent were collected in 100µL of lysis buffer (in 1/9x MR, 50mM Tris pH 7.6, 150mM NaCl, 10mM EDTA, 1% TritonX-100). Samples were homogenized on ice and centrifuged for 20 minutes at 14000 rpm at 4°C to remove insoluble fraction and protein lysate was isolated.

Protein concentration was quantified with a Pierce BCA assay (Thermo Scientific 23227). Samples were denatured at RT for 10 minutes by adding 1/5 volume of 5x cracking buffer (0.3125 M Tris HCl pH 6.8. 12.5% SDS, 25% betamercaptoethanol, and 25% sucrose).Samples were loaded with equal input into a Bolt 4-14% Bis-Tris Gel (Thermo Scientific NW04120BOX) and run in MOPS buffer (prepared according to manufacturer instructions) for 32 minutes at 200V. Transfer to nitrocellulose membrane was performed in transfer buffer (in dH2O, 20% methanol, 25 mM Tris, 192 mM glycine) for 50 minutes at 100V. Membrane was washed 3X 15 minutes in 1xTBST (150 mM NaCl, 10 mM Tris pH 8.0, 0.1% Tween20) then for 1 hour in 4% milk in TBST. Membranes were incubated in primary antibodies (1:1000 rabbit anti-Vitellogenin, 1:10000, mouse anti-b-actin Santa Cruz Biotech sc-47778) were incubated in 4% milk in TBST O/N at 4°C, washed for 3X 10 minutes, then incubated in secondary (1:10000 anti-mouse DyLight 680 Fisher PI35518, 1:10000 anti-rabbit DyLight 800 Fisher PISA510036) for 40 minutes at RT in the dark. After 3X 15 minute washes, membranes were imaged on a LI-COR Imagining System (LI-COR Biosciences).

2.6.6 *Tadpole size and regeneration length measurement*

Stereoscope imaging was performed on a Leica M205 FA with a color camera. Fixed tadpoles were imaged in PBS on a 1% agarose pads and measurements were recorded using the LAS software.

2.6.7 *Cell Proliferation Analysis*

Proliferation was analyzed by quantifying pH3 positive cells in the posterior 500 μm or 750 μm of uninjured tails or in tissue posterior to the amputation place during regeneration using FIJI's Cell Counter plugin. pH3 positive cells were quantified by density (number of cells/10,000 μm^2 of tissue) and by absolute number of pH3 positive cells in the defined tissue region. Size of tissue was determined by tracing the outline of the tail and determining the area with FIJI. pH3 positive cells were counted in the outlined region and density was determined by dividing cell count by the total area.

2.6.8 *Plotting and statistical analysis*

Boxplots were generated using the R package ggplot2 (Wickham, 2009). Length and pH3 measurements between stages and regeneration conditions were compared using ANOVA and post hoc Tukey HSD to identify differences between groups. Pairwise comparisons of DMSO/Rapamycin and feeding experiments were performed using a two-sided t-test. Statistical analysis was performed in R (R Core Team, 2020).

Chapter 3. ELEVATED PENTOSE PHOSPHATE PATHWAY FLUX DRIVES VERTEBRATE REGENERATION

3.1 SUMMARY

A fundamental step in appendage regeneration is rapid growth to replace lost tissue. Cells must generate sufficient lipids, nucleotides, and proteins to fuel rapid cell division. To define the metabolic pathways underlying regenerative growth, we undertook a multimodal investigation of metabolic reprogramming in *Xenopus tropicalis* appendage regeneration. We find that regenerating tissues have increased glucose uptake; however, glycolysis is neither increased nor required for regeneration. Instead, glucose is funneled to the pentose phosphate pathway (PPP), which is essential for full tail regeneration. LC-MS metabolite profiling revealed increased nucleotide and nicotinamide intermediates required for cell division. Using scRNA-Seq, we find that highly proliferative cells have increased transcription of PPP enzymes, and not glycolytic enzymes. We further show that PPP inhibition results in decreased cell division specifically in regenerating tissue. Our results inform a new model wherein regenerating tissues direct glucose towards the PPP, yielding nucleotide precursors to drive regenerative cell proliferation.

3.2 INTRODUCTION

The capacity to replace lost or severely damaged body parts is highly varied across species. Hydra and planaria are capable of regenerating their entire body plans from small, isolated segments (Ivankovic et al., 2019; Reddy et al., 2019). Axolotls and *Xenopus* are able to regrow and pattern entire appendages, though in *Xenopus* this

ability is lost following metamorphosis (Beck et al., 2009; McCusker et al., 2015). Regeneration requires unique injury responses and transcriptional cascades to form the correct structures. Prior to reestablishing patterning and function, regenerating tissues must generate sufficient biomass to support growth, but it is not known how this metabolic demand is met nor what metabolites enable tissue regrowth following injury.

Glucose metabolism is often employed in highly proliferative tissues to meet the biosynthetic demands of growth. In differentiated cells, glucose is primarily metabolized to generate electron donors for oxidative phosphorylation and ATP production (Vander Heiden et al., 2009). However, some cells instead increase glycolysis without oxidative phosphorylation, even under aerobic conditions, in a metabolic paradigm known as the Warburg effect (Vander Heiden et al., 2009). Heavily studied in the retina and cancerous tumors, the Warburg effect is characterized by an increase in glucose consumption coupled to lactate production, and is poised to sustain biosynthesis (Ng et al., 2015). The adaptation of increased glycolysis has been shown to increase proliferation in non-small cell lung cancer, breast cancer, and colorectal cancer, among other tumors (Dai et al., 2020; Lim et al., 2016; T. Liu & Yin, 2017). This metabolic strategy is also implemented in healthy, proliferative cells. Endothelial cells utilize the Warburg effect to drive vessel formation while aerobic glycolysis is necessary for proliferation and differentiation in the developing retina (Agathocleous et al., 2012; De Bock et al., 2013).

Glycolysis is not the only metabolic fate of glucose. The pentose phosphate pathway (PPP) branches from glycolysis at glucose-6-phosphate (G6P) and generates the reducing agent NADPH as well as ribose-5-phosphate (R5P) (Wamelink et al.,

2008). The reducing power of NADPH is important for the reduction of glutathione to regulate redox homeostasis and is also required for the synthesis of fatty acids whereas R5P is a precursor for nucleotide biosynthesis (Wamelink et al., 2008). As these functions suggest, the PPP is a major driver of cell proliferation via lipid and nucleotide biosynthesis. For instance in tumors with TAp73 overexpression, PPP activity is elevated to drive proliferation via increased nucleotide generation (Jiang et al., 2013). The PPP is also necessary for proliferation and survival of mouse and human cardiac progenitor cells (Katare et al., 2013).

Examination of metabolic processes in regeneration has benefited from advances in live metabolic flux measurement as well as genetic and transcriptional techniques (Patel & Wills, 2022). By measuring oxygen and extracellular acidification, Planaria were found to exhibit increased glycolytic activity after injury (Osuma et al., 2018). Larval tail regeneration in zebrafish is characterized by increased glucose uptake; however rather than glycolysis, it is hexosamine biosynthesis which is required for regeneration by enabling blastema formation though TGFß signaling (Sinclair et al., 2021). Transcriptomic studies in *Xenopus tropicalis* have found glucose metabolism genes, including *slc2a3* and *g6pd*, to be increased following injury and proposed requirements for glycolytic and PPP activity during this process (N. R. Love et al., 2011, 2014). While these studies suggest shared elevation of glucose metabolism during regeneration, different branches of glucose breakdown are prioritized in different wounding systems.

Here we tested the hypothesis that regenerating *Xenopus* tails adopt the Warburg effect to drive regeneration. *X. tropicalis* tails have increased glucose uptake in

the regenerating tailbud. However, there is no subsequent increase in nor requirement for glycolytic metabolism in regeneration. Instead, glucose is shunted into the PPP and elevated PPP activity is required for tail regeneration. Via metabolomic profiling of a regeneration timecourse, we find metabolites associated with proliferation and pathways downstream of the PPP to be abundant during regeneration. With single-cell transcriptomics, we show that highly proliferative cells have increased PPP, but not glycolytic, gene expression. Inhibition of the PPP reduces proliferation rates in regenerating tissues, indicating that PPP activity is limiting for proliferation in these cells. Our approach provides a framework for further exploration of metabolic paradigms in regeneration and our results identify a modified Warburg effect that is required for proper growth in regenerating tails.

3.3 RESULTS

3.3.1 *Regenerating X. tropicalis tails increase glucose uptake*

We first sought to determine if regenerating *X. tropicalis* tails have increased glucose demand, as we predict in tissues employing the Warburg effect (Vander Heiden et al., 2009). To this end, we used a fluorescent glucose analog, 2NBDG, to assay glucose uptake by cells (Zou et al., 2005). To ensure systemic delivery, we injected 2NBDG into the ventral tail vein of stage 41 tadpoles and allowed it to circulate for 3 hours until signal could be seen throughout the animal (Figure 3-1 A). Following amputation of the posterior third of the tail, we live imaged at 0, 24, and 72 hours post amputation (hpa). At 0hpa, there was strong signal in the notochord as well as the surrounding axial tissue, but not in the amputated fins (Figure 3-1 B). By 24hpa, when

the regeneration bud has formed, cells in the regenerating tissue showed strong fluorescent signal, indicative of high glucose uptake, while anterior tissues were unchanged from 0hpa (Figure 3-1 B). This trend persisted at 72hpa, with the regenerating tail showing increased glucose uptake (Figure 3-1 B). These data show that cells in the new tissue have increased demand for glucose relative to the wound adjacent tissue.

While 2NBDG uptake can visually identify cells with increased glucose uptake in live tissues, it does not show which transporters are responsible. To complement our 2NBDG uptake assay, we examined previously published RNA-sequencing data to identify changes in glucose transporter transcription between 0 and 24hpa (Patel et al., 2022). We found that the expression of *slc2a1*, *slc2a3*, and *slc2a6* (*glut1*, *glut3*, and *glut6*, respectively) was significantly increased at 24hpa, suggesting that these cells are increasing capacity for glucose uptake (Figure 3-1 C).

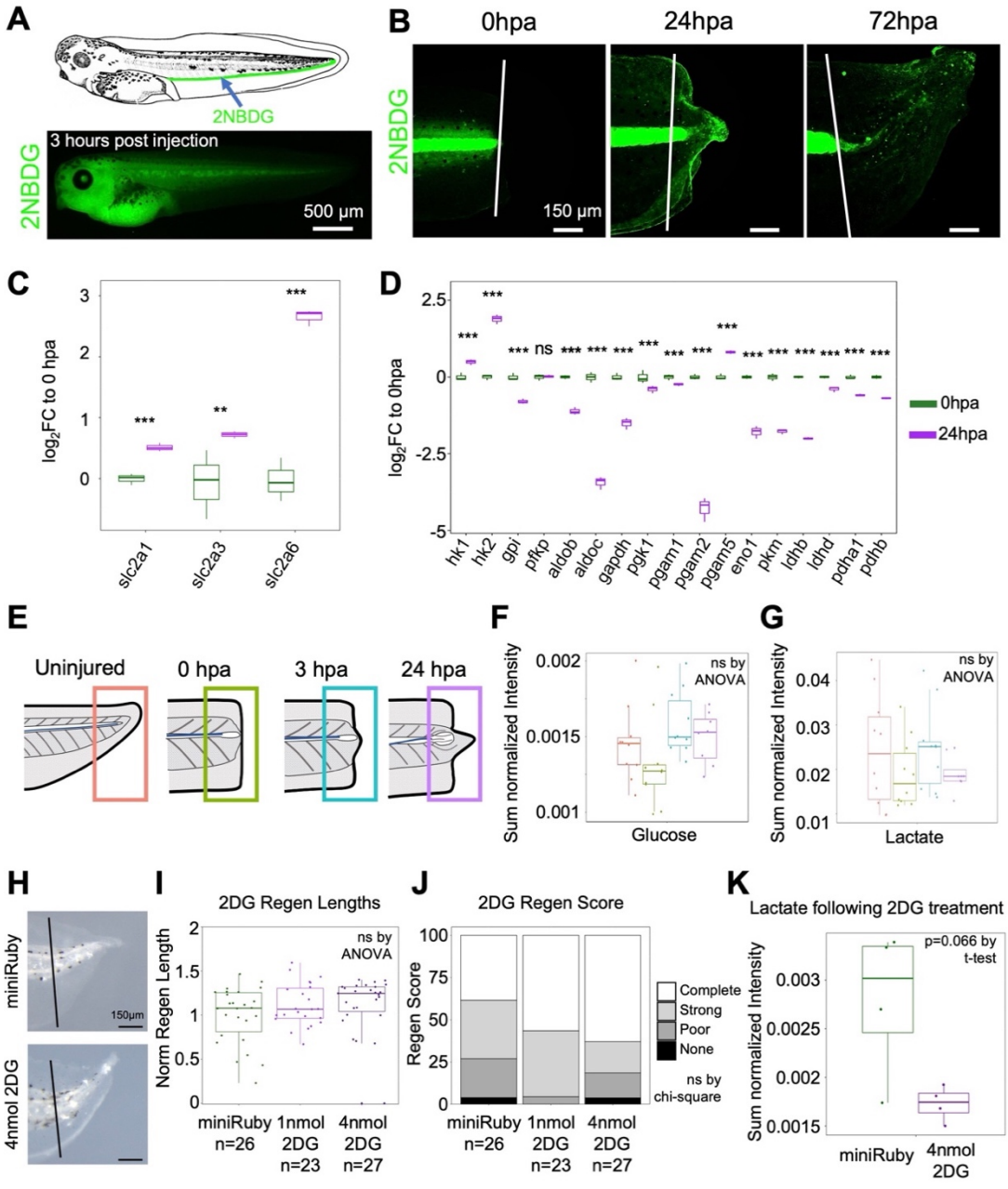

Figure 3-1: **Glucose uptake does not drive increased glycolysis in regeneration**

A) Schematic of tail vein injection (top) and fluorescent image of systemic 2NBDG uptake in stage 41 tadpole 3 hours post injection. B) 2NBDG uptake in regenerating tails at the time of amputation (0hpa), 24, and 72hpa. Signal is saturated to notochord fluorescence, with increased uptake in regenerating tissue visible in the bud at 24hpa and axial tissues by 72hpa. White lines mark amputation. C) Bulk RNA-seq expression of glucose transporters (*slc2a*) which were significantly increased from 0 to 24hpa plotted as log_2FC relative to 0hpa mean. D) Expression of glycolytic genes at 0 and 24hpa plotted as log_2FC relative to 0hpa mean. Statistical significance for C and D was

determined with EdgeR. ** indicates p<0.01; *** indicates p<0.001; ns is not significant. E) Schematic of tissue samples collected for metabolomics. F-G) Plots of sum normalized peak intensities across timecourse, color coded as in E. Glucose (F) trends up at 3 and 24hpa relative to 0hpa while lactate (G) is largely unchanged. H) Representative images of regenerating tails 72hpa following tail-vein injection of miniRuby or 4nmol of 2DG. Black lines mark amputation. I) Quantification of regeneration length and scores for 1 and 4nmol 2DG normalized to miniRuby clutchmates. Statistical significance between groups was evaluated with ANOVA. J) Regeneration scores for experiment in I. The treatments do not have statistically significant differences in phenotype distribution. K) Plot of sum normalized peak intensities for lactate between miniRuby and 2DG injected animals, showing a reduction following inhibition of glycolysis.

3.3.2 *Glycolytic metabolism is not increased or required during regeneration*

Because the regeneration bud had increased glucose uptake, we hypothesized that this tissue would increase glycolytic metabolism to drive lactate production as in the Warburg effect (Vander Heiden et al., 2009). We analyzed the RNA-seq data to determine if expression of glycolytic enzymes increased after injury. Hexokinase, which carries out the first step of glycolysis by converting glucose to G6P, was transcriptionally increased during regeneration (Figure 3-1 D). However, nearly all downstream glycolytic enzymes had lower transcription after injury (Figure 3-1 D). As transcript levels do not always predict enzymatic activity levels, we directly assayed metabolite levels during regeneration. To quantify changes in metabolite abundance, we performed liquid chromatography-mass spectrometry (LC-MS) on tissues across a regeneration timecourse. We collected the posterior 500μm of uninjured tails as a control for the developing tail and 250μm of wound adjacent tissue in addition to regenerating tissue at 0, 3, and 24hpa (Figure 3-1 E, Table 3-1). The 0hpa timepoint allows us to contrast the metabolic state of wound proximal tissue to the same tissue following wound closure by 3hpa or regeneration bud formation by 24hpa (Figure 3-2 A-B). In accord with glucose

uptake experiments, we found a trend towards increased glucose in 24hpa samples over 0hpa samples (Figure 3-1 F). Importantly, we were able to quantify lactate, a metabolite which is obligately enriched when tissues rely on glycolysis. Lactate abundance was unchanged following injury, suggesting that glycolysis is not the sole metabolic fate of glucose in regeneration (Figure 3-1 G). While this does not necessarily indicate a decrease in glycolytic metabolism, it indicates that glycolysis is not upregulated during regeneration either transcriptionally or metabolically.

Because glycolysis was not increased, we asked if glycolysis was critical for regeneration. To functionally test the requirement for glycolysis, we injected tadpoles with a non-hydrolyzable glucose analog, 2-deoxy-glucose (2DG), which is a competitive inhibitor of phosphoglucoisomerase and therefore downstream glycolytic reactions (Wick et al., 1957). By injecting 2DG into the tail vein, we tested if reducing glycolysis resulted in regeneration defects in *Xenopus* as it does in zebrafish (Sinclair et al., 2021). We scored regeneration based on normalized regeneration length and score as described previously (Beck, 2012; Patel et al., 2022). Tadpoles injected with 1 or 4 nmol of 2DG show no change in regeneration length nor quality relative to tracer-injected controls (Figure 3-1 H-J). To confirm a reduction in downstream glycolysis, we performed LC-MS on controls injected with the fluorescent dextran, miniRuby, or 2DG injected, whole tadpoles. We found a reduction in several glycolytic intermediates downstream of 2DG including a strong reduction in lactate and a significant reduction in G1P/F1P/F6P, confirming successful inhibition of glycolysis (Figure 3-1 K, Figure 3-2 C). These data indicate that while regenerating tail tissue increases glucose uptake, increased glycolytic metabolism is not required.

Table 3-1: Differentially abundant metabolites identified via ANOVA with direction of change based on Fisher's LSD

Metabolite	FDR	Change 0 over Tips	Change 3 over Tips	Change 24 over Tips	Change 3 over 0	Change 24 over 0	Change 24 over 3
Hypoxanthine	4.31E-10	Increase	Increase	Increase	Increase	Increase	ns
Choline	4.31E-10	Decrease	Decrease	Decrease	ns	ns	ns
Glutamic acid	1.11E-09	Increase	Increase	Increase	ns	Increase	Increase
2-Aminoadipate	9.98E-09	Increase	Increase	Increase	Increase	ns	Decrease
Inositol	1.26E-08	ns	Increase	Increase	ns	Increase	Increase
Glucoronate	1.21E-07	Decrease	Decrease	ns	ns	Increase	Increase
isoValerylcarnitine	2.02E-07	ns	ns	Increase	ns	Increase	Increase
Acetylcarnitine	9.05E-06	Decrease	Decrease	Decrease	Decrease	Decrease	ns
2'-Deoxycytidine	9.61E-06	Increase	Increase	Increase	ns	Increase	Increase
Glycerophosphocholine	1.29E-05	Decrease	Decrease	Increase	Increase	Increase	Increase
N-Acetylneuraminate	1.30E-05	Increase	Increase	Increase	ns	ns	Increase
7-Methylguanine	1.86E-05	Increase	Increase	Increase	ns	ns	Increase
Dimethylarginine (A/SDMA)	2.72E-05	Increase	Increase	Increase	ns	Increase	ns
Niacinamide	2.80E-05	Increase	Increase	Increase	ns	Increase	Increase
Inosine	3.67E-05	Increase	Increase	Increase	ns	ns	Increase
Hydroxyproline	3.67E-05	Increase	Increase	Increase	ns	ns	ns
Creatine	7.72E-05	Increase	Increase	Increase	ns	ns	ns
Adenine	0.00011676	Decrease	Decrease	Decrease	ns	ns	ns
Guanine	0.00011676	ns	Increase	Increase	Increase	Increase	Increase
1-Methyladenosine	0.00019695	ns	ns	Increase	ns	Increase	Increase
Itaconic Acid	0.00019695	ns	ns	Increase	ns	Increase	Increase
Guanosine	0.00026025	Increase	ns	Increase	ns	Increase	Increase
Alanine	0.00027059	Increase	Increase	Increase	ns	ns	ns
Aspartic Acid	0.00039639	ns	Increase	Increase	ns	Increase	Increase
Tryptophan	0.0010557	Increase	Increase	ns	ns	Decrease	Decrease
5'-Methylthioadenosine	0.0013541	ns	ns	Increase	ns	Increase	Increase
Tyrosine	0.0016582	Increase	Increase	ns	Decrease	Decrease	ns
Phenylalanine	0.0028778	Increase	ns	ns	ns	Decrease	Decrease

DCMP	0.0028778	Increase	Increase	Increase	ns	Increase	ns
Carnitine	0.0030427	ns	Increase	Increase	ns	Increase	ns
N6-Trimethyllysine	0.0045456	Decrease	Decrease	Decrease	ns	ns	ns
Carnosine	0.0058351	Increase	Increase	Increase	ns	ns	ns
Linolenic Acid	0.0067529	ns	ns	Decrease	ns	Decrease	Decrease
UDP-Glucose	0.010138	ns	ns	Increase	ns	Increase	Increase
Cytidine	0.01045	Increase	ns	Increase	ns	ns	Increase
gamma-Aminobutyrate	0.024139	ns	Increase	Increase	ns	Increase	ns
Trigonelline	0.024696	Decrease	Decrease	Decrease	ns	ns	ns
Uridine	0.027047	Increase	ns	Increase	ns	ns	Increase
Reduced Glutathione	0.033447	ns	Increase	Increase	ns	Increase	ns
Lysine	0.038786	Increase	Increase	Increase	ns	ns	ns
DL DOPA	0.043682	Increase	Increase	ns	ns	ns	ns
Pantothenate	0.048911	ns	ns	ns	ns	Decrease	Decrease

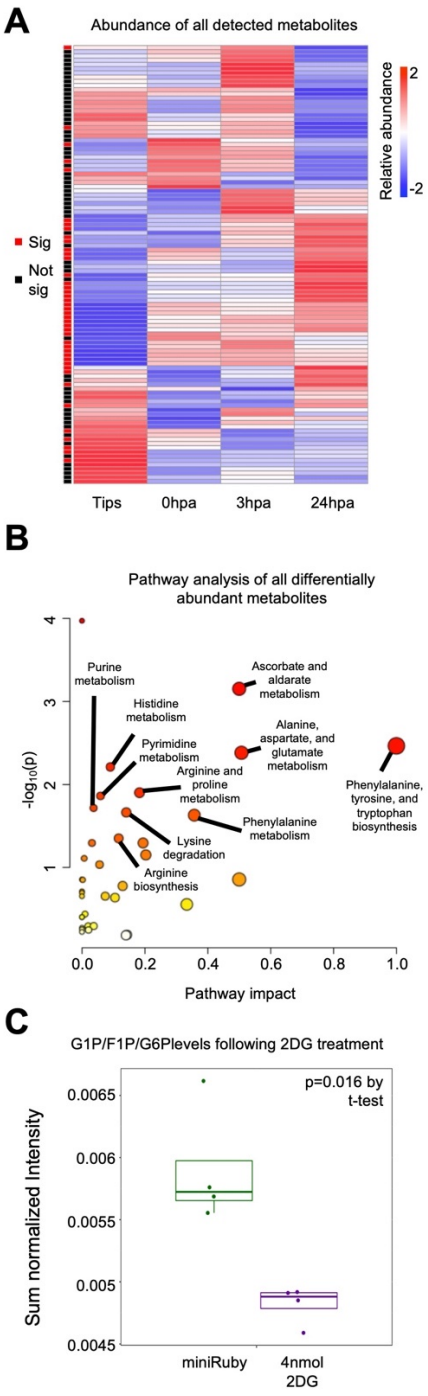

Figure 3-2: **Nucleotide metabolic intermediates are increased at 24hpa**

A) Heatmap of all metabolites detected. Metabolites with significant changes in abundance (as determined by ANOVA, FDR<0.05) are marked with a red box. B) Pathway analysis of differentially abundant metabolites. Processes which have a p value<0.05 and pathway impact>0 are labeled. C) Plot of sum normalized peak intensities across miniRuby and 2DG injected tadpoles. G1P/F1P/G6P are significantly reduced in 2DG treated samples.

3.3.3 *Pentose phosphate pathway activity is elevated in regenerating tissues*

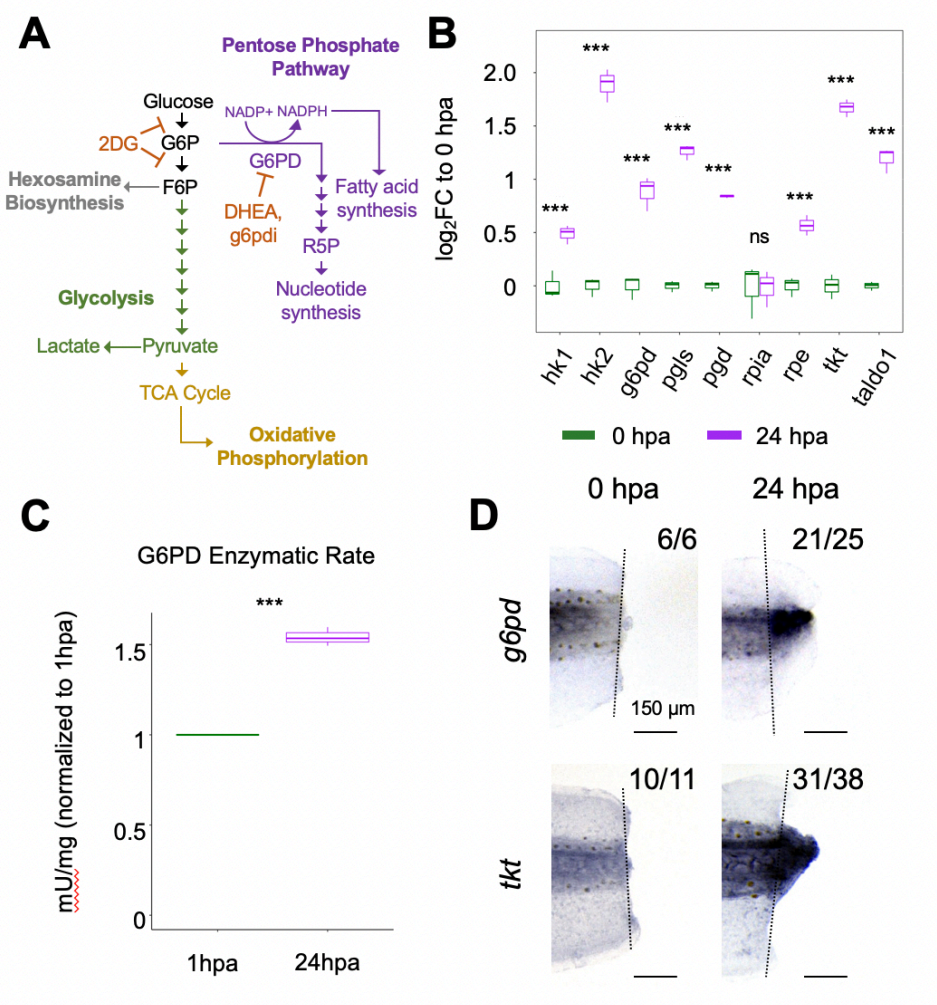

Figure 3-3: **Pentose phosphate flux is increased in regeneration**

A) Schematic of glucose metabolic pathways coded by reactions unique to glycolysis, hexosamine biosynthesis, pentose phosphate pathway, and oxidative phosphorylation. Activity of inhibitors are marked to indicate where they impact glucose metabolism. B) Transcript expression of PPP genes at 0 and 24hpa plotted as log_2FC relative to 0hpa mean. Statistical significance was determined using EdgeR. *** indicates $p<0.001$; ns is not significant. C) Enzymatic activity of G6PD at 1 or 24hpa (normalized to 1hpa) reported in mUnits/mg of isolated protein. Significance was evaluated with a t-test, $p=0.003045$. D) Representative *in situ* hybridization of *g6pd* and *tkt* at 0 and 24hpa. Both transcripts are expressed in axial tissues, with notable increases in the regenerating tissue at 24. For 0hpa, upper right indicates number which look like representative image over number assayed. For 24hpa, upper right indicates number with transcript expression in regenerating tissues over the total number assayed. Dashed black lines mark amputation.

The PPP is an alternative fate for glucose, using G6P as a source of reducing equivalents and carbon to generate NADPH and R5P (Ghanem et al., 2021). NADPH is and R5P are critical precursors of lipids, redox regulators, and nucleotides (Figure 3-3 A). As such, we tested the hypothesis that glucose is directed toward the PPP during regeneration. Transcriptionally, all but one PPP enzyme was upregulated in regeneration (Figure 3-3 B). To test if this increase correlated with changes in PPP activity, we performed an enzymatic rate assay for the PPP rate-limiting enzyme, glucose-6-phosphate dehydrogenase (G6PD). When we compared immediately injured (less than 1hpa) to regenerating 24hpa tissues, there was a significant increase in G6PD activity indicating increased PPP flux (Figure 3-3 C). To determine this increase was specific to regenerating tissue, we performed *in situ* hybridization for *g6pd* and *transketolase* (*tkt*). Both transcripts are expressed throughout the axial tissue at 0hpa and strongly in the regeneration bud at 24hpa (Figure 3-3 D), confirming elevated PPP activity in regenerating tissues.

3.3.4 *G6PD activity is required for tail regeneration*

Having found increased PPP activity following injury, we asked if this pathway was required for regeneration. We employed 2 small molecule antagonists for G6PD, dihydroepiandrosterone (DHEA) and G6PD-inhibitor (g6pdi), for which we performed dose curves to identify non-toxic, effective concentrations (Figure 3-4 A, Figure 3-5) (Ghergurovich et al., 2020; Raineri & Levy, 1970). Treatment of regenerating tadpoles with either inhibitor resulted in tails that were notably smaller with a significant reduction in regeneration length and score compared to DMSO controls, confirming that PPP activity is required for regeneration (Figure 3-4).

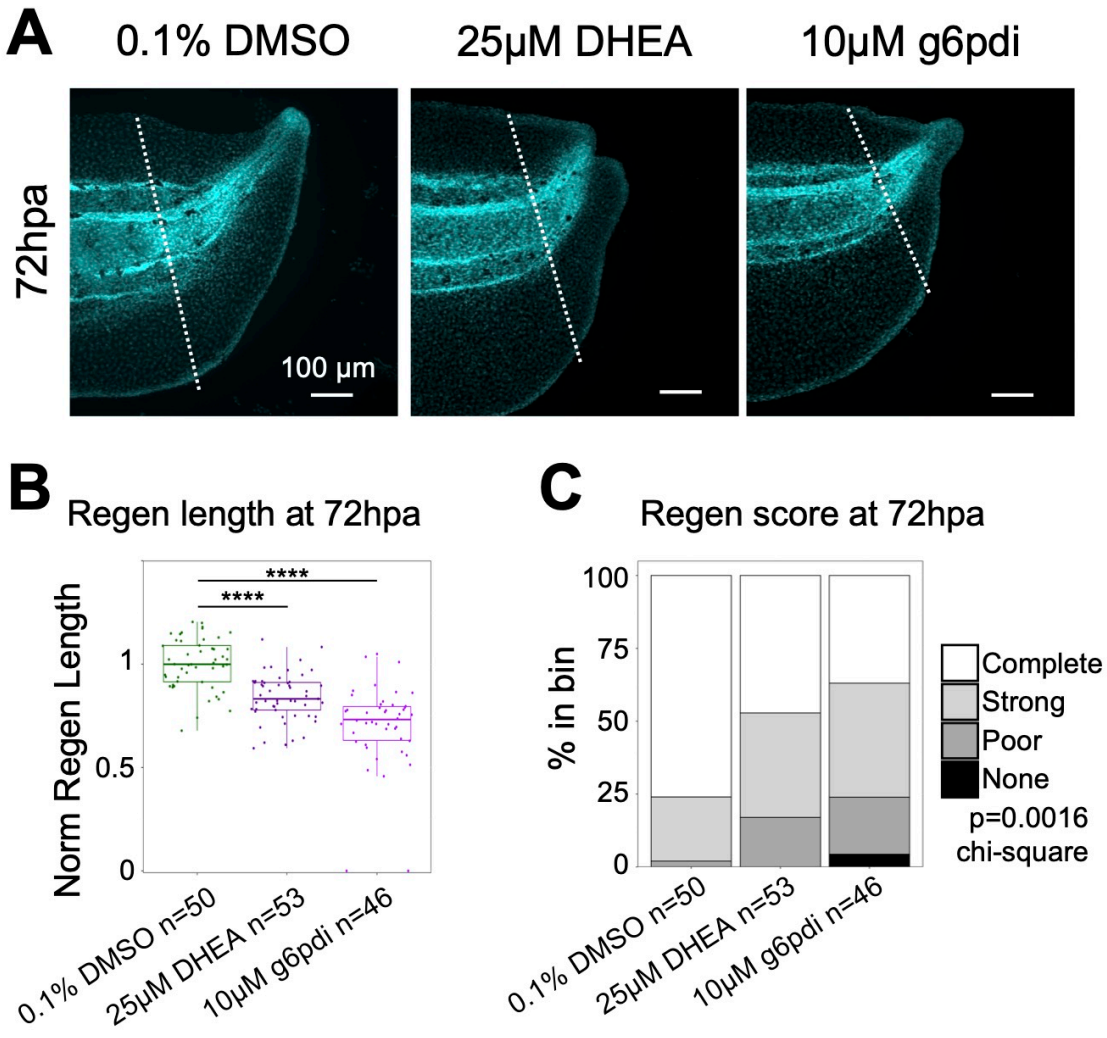

Figure 3-4: **Pentose phosphate flux is required for tail regeneration**

A) Representative DAPI counterstained tails 72hpa treated with either 0.1% DMSO, 25μM DHEA, or 10 μM g6pdi. Dashed white lines mark amputation. B) Quantification of regeneration length normalized to DMSO clutchmates. Statistical significance between groups was determined by ANOVA ($p<2e-16$) followed by Tukey's posttest. **** indicates $p<0.0001$. C) Regeneration scores at 72hpa. The treatments have statistically significant distribution of phenotypes.

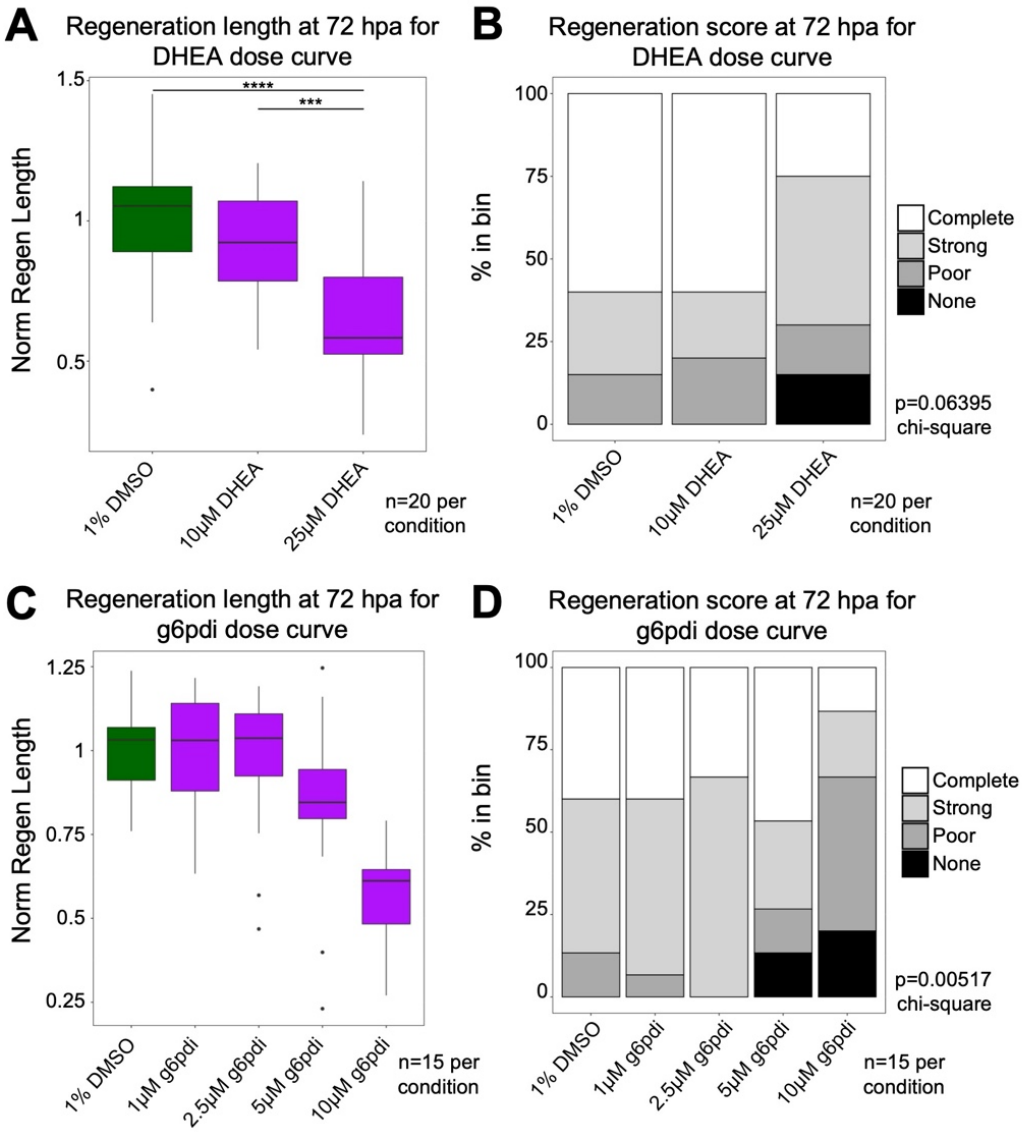

Figure 3-5: **Effective dose determination for G6PD inhibitors**

A,C) Quantification of regeneration length normalized to DMSO clutchmates for DHEA (A) and g6pdi (C) dose curves. B,D) Regeneration scores for the same dose curves binned to complete (full tail regeneration), strong (incomplete fin regeneration), poor (very little regeneration), or none. For C, 10μM is significantly different from all other conditions ($p<0.01$). For A and C, significance was determined by ANOVA followed by Tukey's posttest.

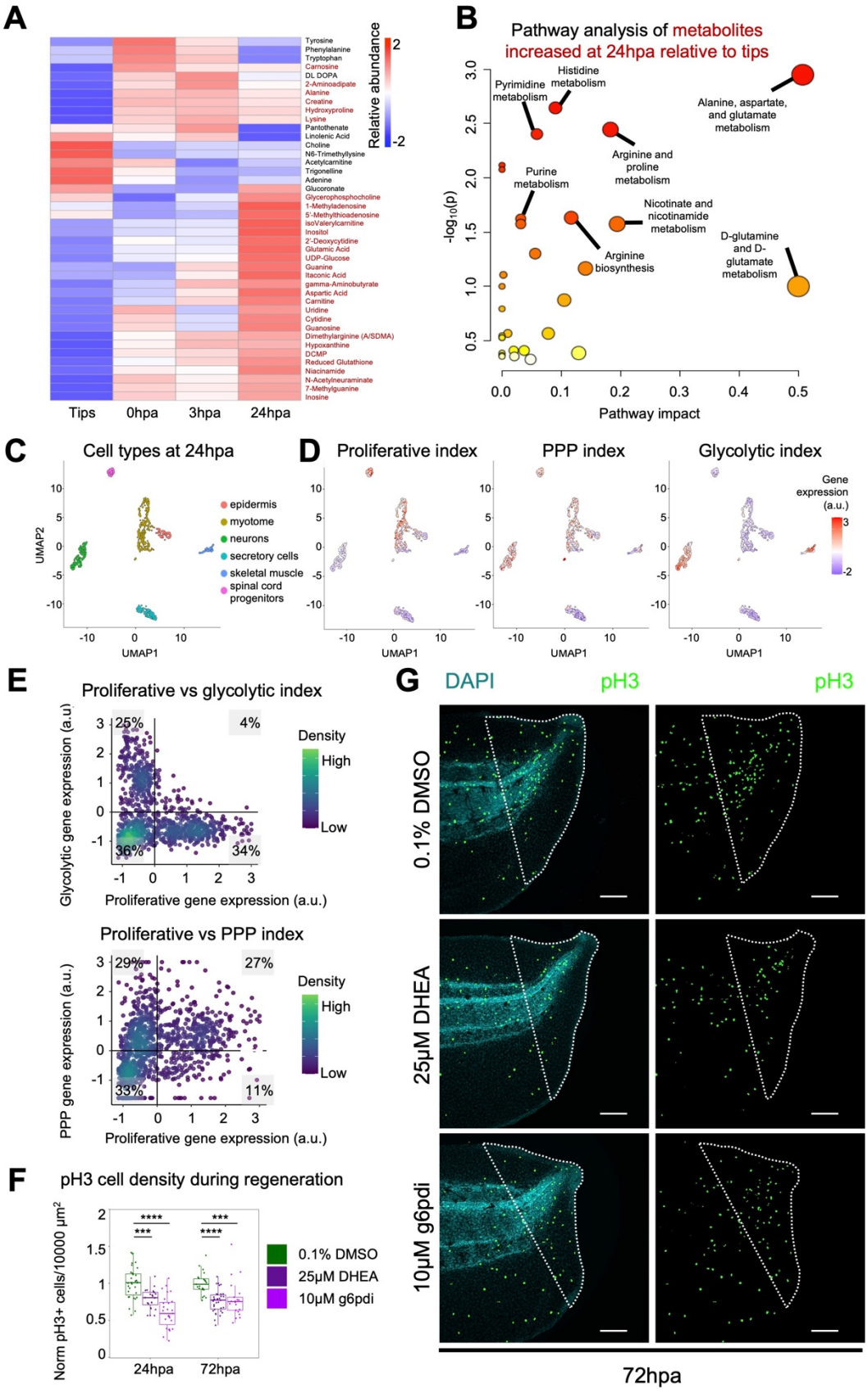
A
Tyrosine
Phenylalanine
Tryptophan
Carnosine
DL DOPA
2-Aminoadipate
Alanine
Creatine
Hydroxyproline
Lysine
Pantothenate
Linolenic Acid
Choline
N6-Trimethyllysine
Acetylcarnitine
Trigonelline
Adenine
Glucoronate
Glycerophosphocholine
1-Methyladenosine
5'-Methylthioadenosine
isoValerylcarnitine
Inositol
2'-Deoxycytidine
Glutamic Acid
UDP-Glucose
Guanine
Itaconic Acid
gamma-Aminobutyrate
Aspartic Acid
Carnitine
Uridine
Cytidine
Guanosine
Dimethylarginine (A/SDMA)
Hypoxanthine
DCMP
Reduced Glutathione
Niacinamide
N-Acetylneuraminate
7-Methylguanine
Inosine
Relative abundance
2
-2
Tips
0hpa
3hpa
24hpa
B
Pathway analysis of metabolites increased at 24hpa relative to tips
Pyrimidine metabolism
Histidine metabolism
Alanine, aspartate, and glutamate metabolism
Arginine and proline metabolism
Purine metabolism
Nicotinate and nicotinamide metabolism
Arginine biosynthesis
D-glutamine and D-glutamate metabolism
-log10(p)
Pathway impact
C
Cell types at 24hpa
epidermis
myotome
neurons
secretory cells
skeletal muscle
spinal cord progenitors
UMAP1
UMAP2
D
Proliferative index
PPP index
Glycolytic index
Gene expression (a.u.)
E
Proliferative vs glycolytic index
Glycolytic gene expression (a.u)
Proliferative gene expression (a.u.)
25%
4%
36%
34%
Density
High
Low
Proliferative vs PPP index
PPP gene expression (a.u.)
29%
27%
33%
11%
F
pH3 cell density during regeneration
Norm pH3+ cells/10000 µm2
0.1% DMSO
25µM DHEA
10µM g6pdi
24hpa
72hpa
G
DAPI
pH3
pH3
0.1% DMSO
25µM DHEA
10µM g6pdi
72hpa

Figure 3-6: **PPP activity is required for proliferation during regeneration**

A) Heatmap of differentially abundant metabolites determined by ANOVA. Post-hoc testing was performed with Fisher's LSD and metabolites significantly increased at 24hpa relative to uninjured tips are labeled red. B) Pathway analysis of 24hpa enriched metabolites. Labeled processes have $p<0.05$ and impact >0. C) UMAP projection of cells from 24hpa regenerating tissue with major cell type clusters. D) Expression of aggregated gene expression modules for proliferative, PPP, and glycolytic genes by cell. Red indicates higher aggregate expression. E) Correlation between proliferative and glycolytic (top) or PPP (bottom) gene expression from scRNA-seq at 24hpa. Each point is a cell colored by density with green representing more cells near that position. High values correlate to more proliferative gene expression (on x-axis) or more pathway expression (on y-axis). F-G) Assay for proliferation marker pH3 via IHC. F) pH3 cell density normalized to DMSO by experimental clutch for 24 and 72hpa. Statistical significance between groups was determined by ANOVA ($p=4.413\text{-}10$ for 24hpa and $p=8.25e\text{-}6$ for 72hpa) followed by Tukey's posttest. *** indicates $p<0.001$ and **** indicates $p<0.0001$. G) Representative 72hpa tails treated with 0.1% DMSO, 25μM DHEA, and 10μM g6pdi. Dashed white lines outline regenerating tissue.

3.3.5 *Regenerating tissues have a proliferative metabolic profile*

To identify metabolic processes prioritized during regeneration, specifically which metabolites the PPP could be supplying, we performed an unbiased analysis of our LC-MS data comparing developing tail tips and 3 regenerating timepoints: 0, 3, and 24hpa (Figure 3-2). We identified 42 metabolites which were differentially abundant across the timecourse (Figure 3-6 A, Figure 3-2, Table 3-1). We then performed a pathway enrichment analysis on metabolites increased at 24hpa relative to uninjured tips to identify metabolic processes likely increased during regeneration. The most impacted pathway was "alanine, aspartate, and glutamate metabolism," metabolites known to be enriched in proliferative cells in the zebrafish caudal fin (Figure 3-6 B) (Rabinowitz et al., 2017). More importantly, this analysis revealed clear links to the PPP. The PPP provides 2 principal resources for proliferation: NAPDH for fatty acid synthesis and R5P for nucleotide biosynthesis. Our LC-MS data showed significant enrichment for NADPH

intermediates via “nicotinate and nicotinamide metabolism” as well as nucleotide intermediates via “purine metabolism” and “pyrimidine metabolism” (Figure 3-6 B). This metabolic profile suggests a coupling of proliferation and PPP products (Figure 3-6 B).

3.3.6 *Increased PPP activity is required to sustain proliferation in regenerating tissues*

As LC-MS showed enrichment of proliferative metabolites and processes downstream of the PPP, we predicted that proliferative cells would have increased PPP activity. To test this, we analyzed published single-cell RNA-seq data of 24hpa regenerating tissue (Kakebeen et al., 2020). For each cell, we determined proliferative, glycolytic, and PPP gene expression indexes by aggregating relevant gene expression values (Figure 3-6 C-D, Figure 3-7, Table 3-2) (Cao et al., 2019). We found several cell types, notably spinal cord progenitors, with high proliferative and PPP indices but low glycolytic indices (Figure 3-6 C-D). Only 4% of cells have high proliferative and glycolytic gene expression; however, 27% of cells had high proliferative and PPP expression (Figure 3-6 E). This suggests that PPP activity may be elevated in proliferative cells during regeneration.

Because of the small size of DHEA and g6pdi treated regenerates, we predicted that PPP activity could be required for proliferation (Figure 3-4). We treated tadpoles with DHEA or g6pdi and stained for the proliferation marker pH3 at 24 and 72hpa. We found that inhibition of G6PD, and therefore the PPP, resulted in a significant decrease in proliferation rates within the new tissue at both timepoints (Figure 3-6 F-G). When we compared proliferation rates in regenerating vs anterior tail tissue, we found that G6PD

inhibition only reduced divisions on the regenerating side, demonstrating that the PPP is specifically required for proliferation in regenerating tissues (Figure 3-8).

Table 3-2: Genes used to calculate expression indexes

Proliferation Genes	Proliferation Genes	Glycolysis Genes	PPP Genes
dtl	tacc3	pgam5	hk2
msh2	slbp	aldoc	pgls
bub1	cks2	pdha1	taldo1
ttk	ung	ldhb	hk1
ect2	fam64a	hk2	pgd
gmnn	rpa2	pkm	g6pd
mcm6	clspn	pgam2	rpe
tyms	cdca8	gpi	tkt
mcm4	brip1	pfkp	
dscc1	rfc2	gapdh	
ncapd2	prim1	pgam1	
cdk1	hmmr	hk1	
kif11	cdc25c	eno1	
hells	tmpo	pgk1	
cenpa	gtse1	aldob	
ubr7	ccnb2	pdhb	
dlgap5	pcna		
g2e3	blm		
rad51	tipin		
nusap1	aurkb		
anp32e	fen1		
cdca7	usp1		
ube2c	ctcf		
hn1	gins2		
aurka	kif2c		
e2f8	nasp		
pold3	cdc20		
ndc80	nuf2		
tubb4b	rangap1		
cdc6	mcm2		
	cenpf		

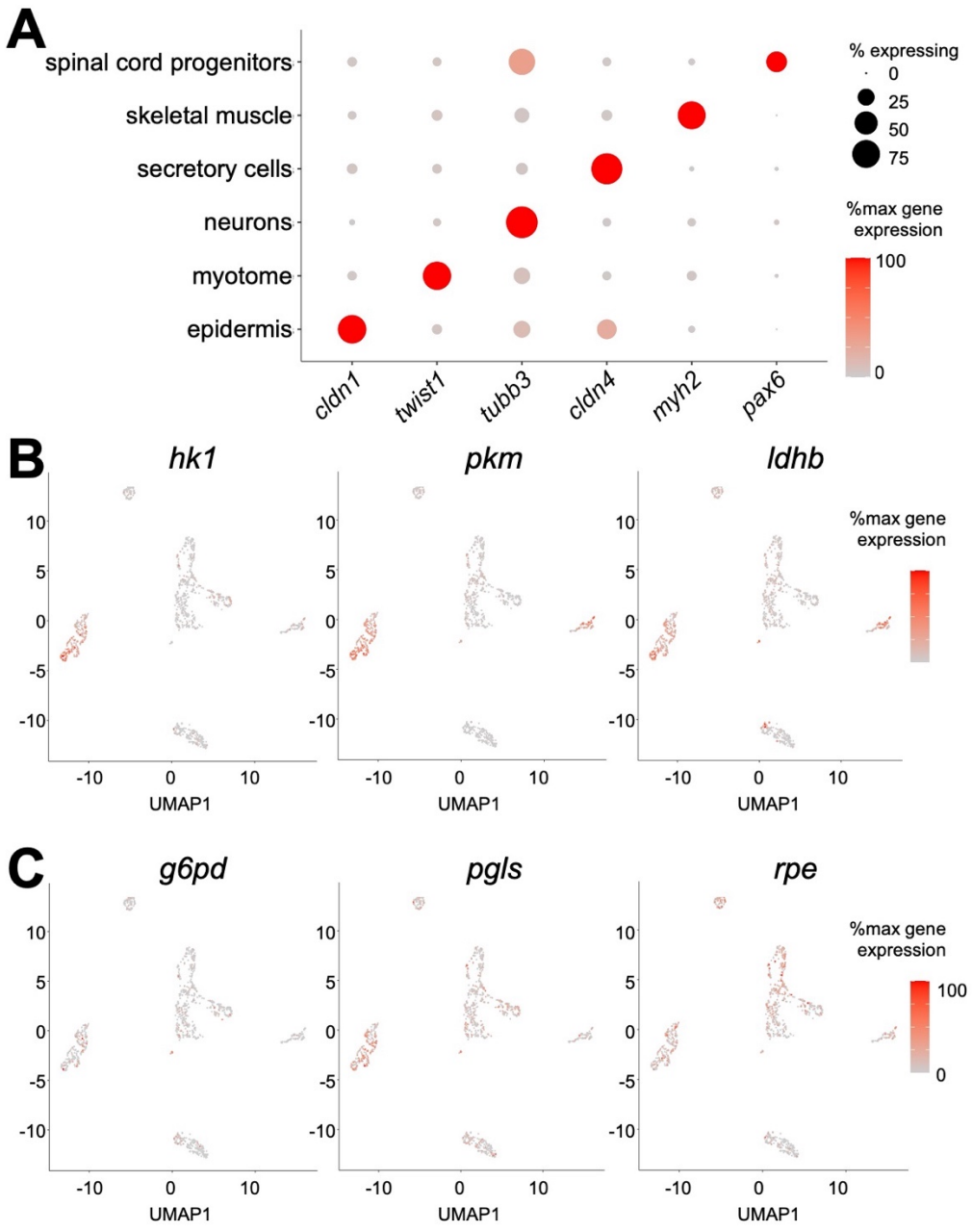

Figure 3-7: **Figure S3: Single cell analysis of 24hpa tissue**
A) Dot plot showing cell types and marker genes. B-C) UMAPs showing gene expression of individual glycolytic (B) and PPP (C) genes. Red indicates higher aggregate expression.

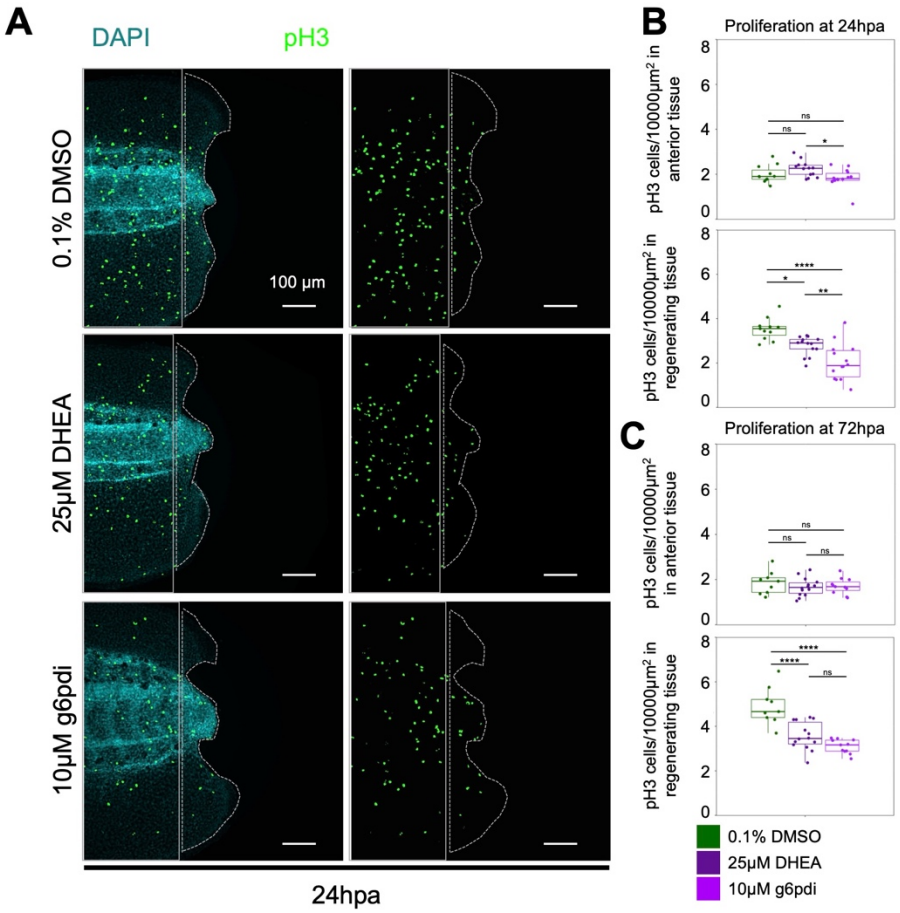

Figure 3-8: **Proliferation in tissue anterior to wound site is not sensitive to G6PD inhibition**
A) 24hpa pH3 stains under DMSO, DHEA, or g6pdi treatments noting regions quantified in proliferation assay. Anterior proliferation rate is indicated by the solid white line, 300µm from the amputation plane. Regenerating tissue outlined in dotted line. B-C) pH3 cell density 24 (B) and 72hpa (C) in anterior (top) and regenerating tissue (bottom). A subset of samples from Figure 4F-G were used in this analysis. Statistical significance between groups was determined by ANOVA followed by Tukey's posttest. * indicates $p<0.05$, ** indicates $p<0.01$, *** indicates $p<0.001$, **** indicates $p<0.0001$, ns indicates not significant.

3.4 Discussion

The metabolic changes driving regeneration are attractive targets for improving wound-healing outcomes in non-regenerative contexts. Here, we identify a critical increase in PPP activity downstream of increased glucose uptake in the regenerating

Xenopus tail. Further, we identify an increase in pro-proliferative metabolites during regeneration. In doing so, we uncover a link between increased PPP and proliferation in regenerating tissue.

3.4.1 *Glucose metabolism is a key regulator of signaling and growth*

Increased cell proliferation is a hallmark of tissue regeneration (Katsuyama et al., 2015; Lee et al., 2022; Williams et al., 2021). While signals that regulate cell cycle progression following injury are well known, fewer studies have focused on the metabolic demand that rapid proliferation places on tissues. It is well documented that highly proliferative cells – including cancers, embryonic stem cells, and proliferating parasites – utilize the Warburg effect to meet the demands of growth (Abdel-Haleem et al., 2017). In the Warburg effect, glucose uptake is prioritized but glycolysis is increased rather than oxidative phosphorylation. This means an increase in lactate production which can drive both biosynthesis and signaling via local changes in pH (de la Cruz-López et al., 2019). In mouse and chick presomitic mesoderm (PSM), it has been shown that glycolytic activity does not drive proliferation but is instead required for PSM differentiation (Bulusu et al., 2017; Oginuma et al., 2017). Based on this, glucose metabolism could play a role in generating biosynthetic fuel, maintaining necessary signaling intermediates, or a combination of these during regeneration.

3.4.2 *Different glucose metabolic fates direct regeneration in unique contexts*

How glucose metabolism contributes to complex appendage regeneration varies by context. Often, increased glucose is thought to coincide with increased activity in the glycolytic, PPP, and hexosamine biosynthetic pathways. However, in regeneration, this

is not the case. In planaria, glucose is driven through glycolysis while in zebrafish larval tail regeneration glucose is only required for hexosamine biosynthesis (Osuma et al., 2018; Sinclair et al., 2021). In the fish tail, this “modified” Warburg effect is used to increase glycosylation to establish the blastema. In *Xenopus* tail regeneration we see glucose uptake following injury and an increase in PPP enzyme transcription, as previously reported for *g6pd* (N. R. Love et al., 2011). However, 2DG treatment, which inhibits both the glycolytic and hexosamine branches of glucose metabolism, blocks regeneration in fish but not in *Xenopus* (Figure 3-1 H-J). Further, the PPP is only required for *Xenopus* regeneration, namely in proliferation of the new tissue, and appears dispensable in zebrafish (Sinclair et al., 2021). These different models suggest that glucose can be preferentially directed into branch pathways and the benefits of each pathway leveraged to meet unique biological needs.

Though multiple systems implicate glucose metabolism in regeneration, downstream requirements for glucose may be restricted by regenerative context. This highlights the value of investigation into how metabolites facilitate regeneration and emphasizes the diversity of functions metabolic intermediates can play. As in zebrafish tails and presomitic mesoderm of mice and chicks, glucose can be a driving force in cell signaling and fate regulation. As in tumors and *Xenopus* tail regeneration, glucose can fuel proliferation via a glycolytic Warburg effect or the PPP. The rapid generation of carbon intermediates by the Warburg effect seen in tumors may diverge in function from the value of increased PPP activity in a sustainable redox balanced tissue niche. While our study links glucose uptake to proliferation via increased PPP activity, it is tempting to consider signaling functions of intermediates such as NADPH or interactions with

metabolic pathways that may collectively balance the complex needs of regeneration. Building on our model of metabolic prioritization of glucose metabolism towards the PPP in regeneration has the potential to not only inform regenerative medicine, but also to evaluate divergent metabolic paradigms in complex and coordinated tissues.

3.5 METHODS

3.5.1 *Xenopus tropicalis husbandry and use*

Use of *Xenopus tropicalis* was carried out under the approval and oversight of the IACUC committee at UW, an AALAC-accredited institution, under animal protocol 4374-01. Ovulation of adult *Xenopus tropicalis* and generation of embryos by natural matings were performed according to published methods (Khokha et al., 2002; Sive et al., 2000). Embryos were reared as described in (Khokha et al., 2002). Staging was assessed by the Nieuwkoop and Faber (NF) staging series (Nieuwkoop & Faber, 1994).

3.5.2 *Xenopus tropicalis amputation assay*

NF stage 41 tadpoles were anesthetized with 0.05% MS-222 in 1/9x MR and tested for response to touch prior to amputation surgery. Once fully anesthetized, a sterilized scalpel was used to amputate the posterior third of the tail. Amputated tadpoles were removed from anesthetic media within 10 minutes of amputation into new 1/9x MR. Tadpoles were kept at a density of no more than 2.5 tadpoles per mL. Tadpoles were fixed for 1 hour in 1x MEM with 3.7% formaldehyde at room temperature at either 24 or 72hpa.

3.5.3 *2NBDG and 2DG tail vein injections*

Wild type tadpoles at stage 41 were anesthetized with MS-222 and moved from culture dish to a thickly coasted agarose dish in one drop of media. Excess media was removed. Using a microinjector, a pulled needle 2×2 nL of 5 mM 2NBDG (Invitrogen, N13195) or 1M 2DG and a labeled dextran (Sigma, D8375) were injected. Controls for 2DG experiments were injected with equal volumes of tracer. Embryos were returned to

fresh media and screened for 2NBDG or tracer fluorescence in the bloodstream. Injected tadpoles were amputated after 3 hours once signal could be seen throughout the body for 2NBDG. 2NBDG was imaged live. 2DG experiments were fixed at 72hpa for 1 hour in 1x MEM with 3.7% formaldehyde at room temperature and imaged as described below.

3.5.4 *Live imaging of 2NBDG*

Tadpoles were anesthetized with MS-222 and imaged on a Leica M205 FA with a color camera for whole animal imaging. For regeneration experiments, the tail was removed at the vent and mounted in 1/9X MR on a slide with a cover slip. Samples were assayed and imaged within 10 minutes using a Leica DM 5500 B microscope using a 10X objective and processed using FIJI image analysis software (Schindelin et al., 2012).

3.5.5 *Pharmacological inhibition*

Dihydroepiandrosterone (BioVision, 2172) was resuspended to a 1M stock in DMSO and g6pdi (Cayman Chemical Co., 31484) to a 10mM stock in DMSO. Uninjured and injured tadpoles were reared with 0.1% DMSO, 25μM DHEA or 10μM g6pdi diluted in 1/9x MR until collection at 24- or 72-hours following treatment. Other concentrations were used in establishing doses and are reported in *Figure 3-5*.

3.5.6 *Regeneration length measurement*

Stereoscope imaging was performed on a Leica M205 FA with a color camera. Fixed tadpoles were imaged in PBS on 1% agarose pads and measurements were recorded using the LAS software.

3.5.7 *Regeneration quality scoring*

Stereoscope imaging was performed on a Leica M205 FA with a color camera. Fixed tadpoles were imaged in PBS on a 1% agarose pads and each tail was assigned a regeneration score by binning tails into 4 categories: Complete (full tail

regeneration), strong (incomplete fin regeneration), poor (very little regeneration), or none (Beck, 2012).

3.5.8 *G6PD enzymatic rate assay*

Tadpoles were anesthetized with 0.05% ms-222 in 1/9x MR and tested for response to touch prior to tissue collection. For 1hpa samples, the posterior third of the tail was amputated followed by collection of tail tissue 250μm anterior to the initial wound. For 24hpa, 250μm of tissue, including the regenerating tissue, was collected at 23hpa. Sample preparation takes roughly 1 hour, so tissue was collected 1 hour before the reported timepoint (at 0hpa for 1hpa, at 23hpa for 24hpa). 3 biological replicates were collected per timepoint, with 25 tails isolated and immediate added to 100μL of lysis buffer from G6PD assay kit (BioVision K751) on ice. Samples were processed per kit recommendations. Note that in order to run the samples in parallel, some samples were kept on ice at least 10 but not more than 40 minutes. To account for this, 1 and 24hpa samples were collected as pairs within 5 minutes of each other to reduce impact of collection period. In brief, samples were lysed for ice for at least 10 minutes then centrifuged at 5 minutes at 10000g. Supernatant was removed and 25μL was utilized for a BCA assay to normalize by protein content. 50μL was diluted to 200μL in assay buffer and added to reaction buffer, made per kit instructions, in a 96-well, black bottom plate. The samples were immediately imaged on a plate reader. Rate of activity was assayed based on fluorometric changes across the linear phase of change and normalized to protein input by sample.

3.5.9 *Whole mount in situ hybridization*

Embryos and tadpoles were fixed overnight in 1x MEM with 3.7% formaldehyde at 4°C. *Xenopus tropicalis* multibasket *in situ* hybridization protocols were followed as described in (Khokha et al., 2002), with the notable change that pre-hybridization was always performed overnight. Isolated tails were mounted on slides in ProLong Gold (ThermoFisher P36930). Mounted tails and whole tadpoles were imaged on a Leica

M205 FA with a color camera. Probes were synthesized using the following primer pairs designed against a single exon of each mRNA:

g6pd (forward - GTGTCCCTTTCATTATGCGCT

, reverse - taatacgactcactatagggTCTGTTCCCATATGTTAAGTCAAGC

), *tkt* (forward - CGGCATTGGAGAAGCCGTG

, reverse - taatacgactcactataGGGTTATGAGAGCGGCGATG

).

3.5.10 *Immunohistochemistry*

Fixed tadpoles were permeabilized by washing 3x15 minutes in PBS + 0.01% Triton x-100 (PBT). Tadpoles were blocked for 1 hour at room temperature in 10% CAS-block (Invitrogen #00-8120) in PBT. Then, tadpoles were incubated in primary antibody [1:1000 mouse anti-Histone H3 (phospho S10), Abcam ab14955] diluted in 100% CAS-block overnight at 4°C. Tadpoles were then washed 3x10 minutes at room temperature in PBT and blocked for 30 minutes in 10% CAS-block in PBT. Secondary antibody (goat anti-mouse 488, ThermoFisher A11001) was diluted 1:500 in 100% CAS-block and incubated for 2 hours at room temperature. Tadpoles were then washed 3x10 minutes in PBT followed by a 10-minute incubation in 1:2000 DAPI (Sigma D9542) before being washed with 1xPBS for 10 more minutes. Isolated tails were mounted on slides in ProLong Gold (ThermoFisher P36930). Images were acquired using a Leica DM 5500 B microscope using a 10X objective and processed using FIJI image analysis software.

3.5.11 *Proliferation assay*

Images of pH3 stains were imported into FIJI. The amputation plane was identified, and the regenerating tissue area was measured. Then, the number of pH3 positive cells was counted. Density of pH3 cells was determined by dividing the number of cells by the total area. For each experiment, density was normalized to DMSO

controls of that timepoint so that data from multiple clutches could be analyzed in tandem.

3.5.12 *Metabolomics sample collection*

Tadpoles were anesthetized with 0.05% MS-222 in 1/9x MR and tested for response to touch prior to tissue collection. For uninjured tips, a sterilized scalpel was used to amputate 500μm of the posterior tip. For 0hpa samples, the posterior third of the tail was amputated followed by collection of tail tissue 250μm anterior to the initial wound. For 3 and 24hpa, 250μm of tissue, including the regenerating tissue, was collected. 10 replicates of 25 tails (8 replicates for the 24hpa timepoint) were collected. For each sample, media was removed, and samples were frozen on dry ice within 5-8 minutes from the first amputation. For 2DG experiments, injections of miniRuby or 2nmol of 2DG were performed as above and tails were not amputated. 10 whole animals were collected at 24 hours post treatment, media was removed, and samples were frozen on dry ice immediately.

3.5.13 *Metabolomics sample processing*

Aqueous metabolites for targeted LC-MS analysis were extracted using a protein precipitation method similar to the one described elsewhere (Mathon et al., 2019; Meador et al., 2020). Samples were first homogenized in 200 μL purified deionized water at 4 ˚C, and then 800 μL of methanol containing $6C_{13}$-glucose and $2C_{13}$-glutamate (reference internal standards) was added. Afterwards samples were vortexed, stored for 30 minutes at -20 ˚C, sonicated in an ice bath for 10 minutes, centrifuged for 15 min at 14,000 rpm and 4 ˚C, and then 600 μL of supernatant was collected from each sample. Lastly, recovered supernatants were dried on a SpeedVac and reconstituted in 1.0 mL of LC-matching solvent containing $2C_{13}$-tyrosine and $3C_{13}$-lactate (reference internal standards).

3.5.14 *LC-MS Assay*

Targeted LC-MS metabolite analysis was performed on a duplex-LC-MS system composed of two Shimadzu UPLC pumps, CTC Analytics PAL HTC-xt temperature-

controlled auto-sampler and AB Sciex 6500+ Triple Quadrupole MS equipped with ESI ionization source (Meador et al., 2020). UPLC pumps were connected to the auto-sampler in parallel and were able to perform two chromatography separations independently from each other. Each sample was injected twice on two identical analytical columns (Waters XBridge BEH Amide XP) performing separations in hydrophilic interaction liquid chromatography (HILIC) mode. While one column was performing separation and MS data acquisition in ESI+ ionization mode, the other column was getting equilibrated for sample injection, chromatography separation and MS data acquisition in ESI- mode. Each chromatography separation was 18 minutes (total analysis time per sample was 36 minutes). MS data acquisition was performed in multiple-reaction-monitoring (MRM) mode. LC-MS system was controlled using AB Sciex Analyst 1.6.3 software. Measured MS peaks were integrated using AB Sciex MultiQuant 3.0.3 software. The LC-MS assay was targeting 361 metabolites (plus 4 spiked reference internal standards). Metabolites and 4 reference standards were measured in the study samples. In the addition to the study samples, two sets of quality control (QC) samples were used to monitor the assay performance as well as data reproducibility. One QC [QC(I)] was a pooled human serum sample used to monitor system performance and the other QC [QC(S)] was pooled study samples and this QC was used to monitor data reproducibility. Each QC sample was injected per every 10 study samples. The data were well reproducible with a median CV under 5%. Generated MS data were normalized to the sum of all measured peaks per samples and subsequent analysis was performed with MetaboAnalyst 5.0 (Pang et al., 2021).

3.5.15 *Plotting and statistical analysis*

Boxplots and stacked bar plots were generated using the R package ggplot2 (Wickham, 2009). Length measurements were compared using T-tests or ANOVA and post hoc Tukey HSD to identify differences between groups. Chi-square analysis was used to compare distribution for regeneration scores. Statistical analysis was performed in R (R Core Team, 2020).

3.5.16 *Analysis of previously published datasets*

Published RNA-sequencing data (CPM and statistical analysis) was obtained from the NCBI Gene expression Omnibus (GEO) under accession number GSE174798 (Patel et al., 2022). The published single cell RNA-seq dataset was obtained from GEO under accession number GSE146836 (Kakebeen et al., 2020). Data from 24hpa cells were preprocessed and projected into UMAP space with Monocle 3 v1.2.7 (Cao et al., 2019). Module gene expression scores were calculated with the 'aggregate_gene_expression' function and genes contributing to each module are found in *Table 3-2*.

3.5.17 *Heatmap generation*

Heatmaps were generated by pheatmap (Kolde, 2019). Sum-normalized peak areas were averaged across replicates for plotting.

Chapter 4. HIF1α AND WNT ARE REQUIRED FOR POSTERIOR GENE EXPRESSION DURING *XENOPUS TROPICALIS* TAIL REGENERATION

Chapter 4 is adapted with minimal modification from

Patel, J.H., Schattinger, P.A., Takayoshi, E.E. and Wills, A.E., 2022. Hif1α and Wnt are required for posterior gene expression during Xenopus tropicalis tail regeneration. *Developmental Biology*. Dev Biol. 2022 Mar;483:157-168. PMID: 35065905. [link]

4.1 ABSTRACT

Regeneration of complex tissues is initiated by an injury-induced stress response, eventually leading to activation of developmental signaling pathways such as Wnt signaling. How early injury cues are interpreted and coupled to activation of these developmental signals and their targets is not well understood. Here, we show that Hif1α, a stress induced transcription factor, is required for tail regeneration in *Xenopus tropicalis*. We find that Hif1α is required for regeneration of differentiated axial tissues, including axons and muscle. Using RNA-sequencing, we find that Hif1α and Wnt converge on a broad set of genes required for posterior specification and differentiation, including the posterior *hox* genes. We further show that Hif1α is required for transcription via a Wnt-responsive element, a function that is conserved in both regeneration and early neural patterning. Our findings indicate that Hif1α has regulatory roles in Wnt target gene expression across multiple tissue contexts.

4.2 INTRODUCTION

Regeneration of complex tissues is initiated by an injury-induced stress response, eventually leading to activation of developmental signaling pathways such as Wnt signaling. How early injury cues are interpreted and coupled to activation of these developmental signals and their targets is not well understood. Here, we show that Hif1α, a stress induced transcription factor, is required for tail regeneration in *Xenopus tropicalis*. We find that Hif1α is required for regeneration of differentiated axial tissues, including axons and muscle. Using RNA-sequencing, we find that Hif1α and Wnt converge on a broad set of genes required for posterior specification and differentiation, including the posterior *hox* genes. We further show that Hif1α is required for transcription via a Wnt-responsive element, a function that is conserved in both regeneration and early neural patterning. Our findings indicate that Hif1α has regulatory roles in Wnt target gene expression across multiple tissue contexts.

4.3 METHODS

4.3.1 *Xenopus tropicalis husbandry and use*

Use of *Xenopus tropicalis* was carried out under the approval and oversight of the IACUC committee at UW, an AALAC-accredited institution, under animal protocol 4374-01. Ovulation of adult *Xenopus tropicalis* and generation of embryos by natural matings were performed according to published methods (Khokha et al., 2002; Sive et al., 2000). Embryos were reared as described in (Khokha et al., 2002). Staging was assessed by the Nieuwkoop and Faber (NF) staging series (Nieuwkoop & Faber, 1994).

4.3.2 *Xenopus tropicalis amputation assay*

NF stage 41 tadpoles were anesthetized with 0.05% ms-222 in 1/9x MR and tested for response to touch prior to amputation surgery. Once fully anesthetized, a sterilized scalpel was used to amputate the posterior third of the tail. Amputated tadpoles were removed from anesthetic media within 10 minutes of amputation into new 1/9x MR. Tadpoles were kept at a density of no more than 2.5 tadpoles per mL.

4.3.3 *Pharmacological inhibition*

2-methoxyestradiol (Sigma m6383-5mg) was resuspended to a 10mM stock in DMSO, Echinomycin (Calbiochem 512-64-1) to a 0.5mM stock in DMSO, and IWR (Sigma I0161) 10mM stock in DMSO. Uninjured and injured tadpoles were reared with 0.1% DMSO, 5μM 2ME, 0.5μM Echinomycin, or 10μM IWR diluted in 1/9x MR until collection at 24- or 72-hours following treatment. Other concentrations were used in establishing doses and are reported in *Figure 4-2*.

4.3.4 *Morpholino injections*

hif1α morpholino (MO) was ordered from GeneTools (sequence: CTCGCTACTACAGATCCCTCCATGC). Fertilized eggs from wild type and *pbin7:GFP* matings were de-jellied in 3% cysteine in H_2O for 10-15 minutes. 10ng of MO were injected into 1 cell at the 2-cell stage to generate unilateral morphants. Embryos were reared to NF stage 18 prior to fixation. 5 or 10ng of morpholino were injected at the 1 cell stage to generate uniform morphants which were reared to stage 41 for tail amputation assays.

4.3.5 *Morpholino tail vein injections*

hif1α vivo-morpholino (vMO) was ordered from GeneTools (sequence: CTCGCTACTACAGATCCCTCCATGC). Wild type tadpoles at stage 35-36 were anaesthetized with MS-222 and moved from culture dish to a thickly coasted agarose coated dish cover in one drop of media. Excess media was removed. Using a microinjector, a pulled needle containing vMO and labeled dextran tracer was inserted into the ventral tail vein in the tail and 2×2 nL (10 ng) or 4×2 nL injections were delivered (20 ng). Controls were injected with equal volumes of tracer. Embryos were returned to fresh media and screened for tracer fluorescence in the blood stream. Injected tadpoles were grown 24 hours to stage 41 and amputated. At 24hpa, tadpoles were re-injected into the tail vein as before and fixed for 1 hour in 1x MEM with 3.7% formaldehyde at room temperature.

4.3.6 *Regeneration length measurement*

Stereoscope imaging was performed on a Leica M205 FA with a color camera. Fixed tadpoles were imaged in PBS on a 1% agarose pads and measurements were recorded using the LAS software.

4.3.7 *Immunohistochemistry*

Xenopus tropicalis tadpoles were fixed for 1 hour in 1x MEM with 3.7% formaldehyde at room temperature. Tadpoles were permeabilized by washing 3x15 minutes in PBS + 0.01% Triton x-100 (PBT). Tadpoles were blocked for 1 hour at room temperature in 10% CAS-block (Invitrogen #00-8120) in PBT. Then tadpoles

were incubated in primary antibody [1:1 mouse anti-12/101, gift from Richard Harland (Kintner & Brockes, 1984); 1:50 mouse anti-neurofilament associated protein (DSHB 3A10) (Dodd & Jessell, 1988)] diluted in 100% CAS-block overnight at 4°C. Tadpoles were then washed 3x10 minutes at room temperature in PBT and blocked for 30 minutes in 10% CAS-block in PBT. Secondary antibody (goat anti-mouse 488, ThermoFisher A11001) were diluted 1:500 in 100% CAS-block and incubated for 2 hours at room temperature. Tadpoles were then washed 3x10 minutes in PBT followed by a 10-minute incubation in 1:2000 DAPI (Sigma D9542) before being washed with 1xPBS for 10 more minutes. Isolated tails were mounted on slides in ProLong Gold (ThermoFisher P36930). Images were acquired using a Leica DM 5500 B microscope using a 10X objective and processed using FIJI image analysis software (Schindelin et al., 2012).

4.3.8 *Whole mount in situ hybridization*

Embryos and tadpoles were fixed overnight in 1x MEM with 3.7% formaldehyde at 4°C. *Xenopus tropicalis* multibasket *in situ* hybridization protocols were followed as described in (Khokha et al., 2002), with the notable change that pre-hybridization was always performed overnight. Isolated tails were mounted on slides in ProLong Gold (ThermoFisher P36930). Mounted tails and whole tadpoles were imaged on a Leica M205 FA with a color camera. Plasmids for *sox2*, *otx2*, *en2*, *cdx4*, and *snai2* probes were gifted by the Harland lab. Other probes were synthesized using the following primer pairs designed against a single exon of each mRNA: *fgf20* (forward - CTTTTGGGGATTTTGGGACT, reverse - taatacgactcactatagggGGCAGTATCTGCAGGTGGA), *pbin7:GFP* (forward -

CACATGAAGCAGCACGACTT, reverse - taatacgactcactatagggTGCTCAGGTAGTGGTTGTCG), *hoxc9* (forward - CCAGCTACTGCCAGACCTTC, reverse - taatacgactcactatagggTCCAATTCCGACTTGTCCTC), *hoxc10* (forward - TCAATGGAGAAGACCCCAAG, reverse - taatacgactcactatagggTTGCTTCAGCGTCAGAATTG), *hoxd11* (forward - TGCTGTCCAAGCTCTCTTGA, reverse - taatacgactcactatagggCTCTGTGCATCACCTCCTCA).

4.3.9 *RNA extraction and sequencing*

All sequencing data associated with this manuscript can be found via GEO accession GSE174798.

Tadpoles were anesthetized with 0.05% ms-222 in 1/9x MR and tested for response to touch prior to tissue collection. For 0hpa collections, a sterilized scalpel was used to amputate the posterior third of the tail followed by amputation 250μm anterior to the wound. For 24hpa tails, 250μm of tissue, including the regenerating tissue, was collected. 25 tails were collected for each condition and experiments were carried out in triplicate. DNA/RNA were purified by lysing tissues followed by phenol:chloroform extraction with ethanol precipitation. DNAseI treatment (Invitrogen, 18068015) was used to remove DNA. Total RNA samples were quantified using Qubit 2.0 Fluorometer (Life Technologies) and RNA integrity was checked using Agilent TapeStation 4200 (Agilent Technologies). RNA sequencing libraries were prepared using the NEBNext Ultra RNA Library Prep Kit for Illumina following manufacturer's instructions (NEB). The sequencing libraries were validated on the Agilent TapeStation (Agilent Technologies),

and quantified by using Qubit 2.0 Fluorometer (Invitrogen) as well as by quantitative PCR (KAPA Biosystems). The sequencing libraries were clustered on a single lane of a flowcell. After clustering, the flowcell was loaded on the Illumina HiSeq instrument (4000 or equivalent) according to manufacturer's instructions. The samples were sequenced using a 2x150bp Paired End (PE) configuration. Image analysis and base calling were conducted by the HiSeq Control Software (HCS). Raw sequence data (.bcl files) generated from Illumina HiSeq was converted into fastq files and de-multiplexed using Illumina's bcl2fastq 2.17 software. One mismatch was allowed for index sequence identification.

4.3.10 *Trimming, alignment, and counts*

TrimGalore-0.6.5 was used to remove low quality reads (Phred33) and trim adapter sequences (http://www.bioinformatics.babraham.ac.uk/projects/trim_galore/). Pseudoalignment and count quantification was performed by Kallisto using an index built from the *Xenopus tropicalis* 9.1 transcriptome (Bray et al., 2016), returning .tsv files. These .tsv files were read into R, estimated counts for each gene were converted back to raw counts to generate a counts table suitable for processing with EdgeR.

4.3.11 *Multidimensional Scaling and differential expression analysis*

Analysis was performed using EdgeR (Robinson et al., 2010). The counts table was made into a DGEList object and filtered for transcripts with low counts and scaled with the calcNormFactors command. MDS plots were generated using plotMDS. Differential expression between 0hpa and DMSO (24hpa), and DMSO and each treatment group – 2ME, Ech, and IWR – were performed using glmQLFTest. To determine significance, p-

values for each gene generated for the DMSO vs 2ME, Ech, and IWR conditions were ordered and corrected using the Benjamini-Hochberg procedure to determine a false discovery rate (FDR). Genes considered differentially expressed between DMSO and each condition has FDR < 0.05 (as shown in *Supp. Figure 2*). Significantly downregulated genes were called using filters of FDR < 0.05 and $\log_2$FC < -0.2.

4.3.12 *Heatmap generation*

Heatmaps were generated by pheatmap (Kolde, 2019). Sequencing counts were converted to counts per million (cpm) and averaged across triplicates. The average cpm was normalized to DMSO to visualize fold change between DMSO and each treatment.

4.3.13 *PANTHER Gene Ontology*

Gene ontology was performed on the list of genes IDs called as significantly downregulated. This list was supplied to the PANTHER (Mi et al., 2019; Thomas, 2003) online portal using the reference genome for *Xenopus tropicalis* and a statistical overrepresentation test for GO biological processes was performed.

4.3.14 *Plotting and statistical analysis*

Boxplots and stacked bar plots were generated using the R package ggplot2 (Wickham, 2009). Venn diagrams were generated using eulerr (Larsson, 2020). Length measurements were compared using ANOVA and post hoc Tukey HSD to identify differences between groups. Difference in distribution of phenotypes across multiple treatments was assessed using a chi-square test. Statistical analysis was performed in R (R Core Team, 2020).

4.4 RESULTS

4.4.1 *Hif1α is necessary for muscle and axon regeneration in X. tropicalis*

Previously, Hif1α inhibition via Echinomycin (Ech), has been shown to reduce tail regeneration in *X. laevis* tadpoles (Ferreira et al., 2018; Kong et al., 2005). We first set out to determine if Hif1α antagonism inhibited tail regeneration in *X. tropicalis* tadpoles using Ech, which inhibits Hif1α binding to DNA, as well as 2-methoxyestradiol (2ME), which inhibits Hif1α nuclear localization and transcriptional activity (Mabjeesh et al., 2003). We identified effective doses of both inhibitors which reduced tail regeneration but did not cause lethality or impair health (Figure 4-1 A,B, Figure 4-2 A-D). Compared to DMSO treated tails, tails treated with 5μM 2ME or 0.5μM Ech had significantly reduced tail lengths compared to control clutchmates 72 hours post amputation (hpa) (Figure 4-1 C,D*)*. We scored regeneration by binning tails into 4 categories ranging from no regeneration to complete tail regeneration and found that Hif1α inhibited tails have significantly reduced regenerative outcomes relative to DMSO controls (Figure 4-1 C,E) (Beck, 2012). These data confirm that Hif1α is required for tail regeneration in *X. tropicalis*.

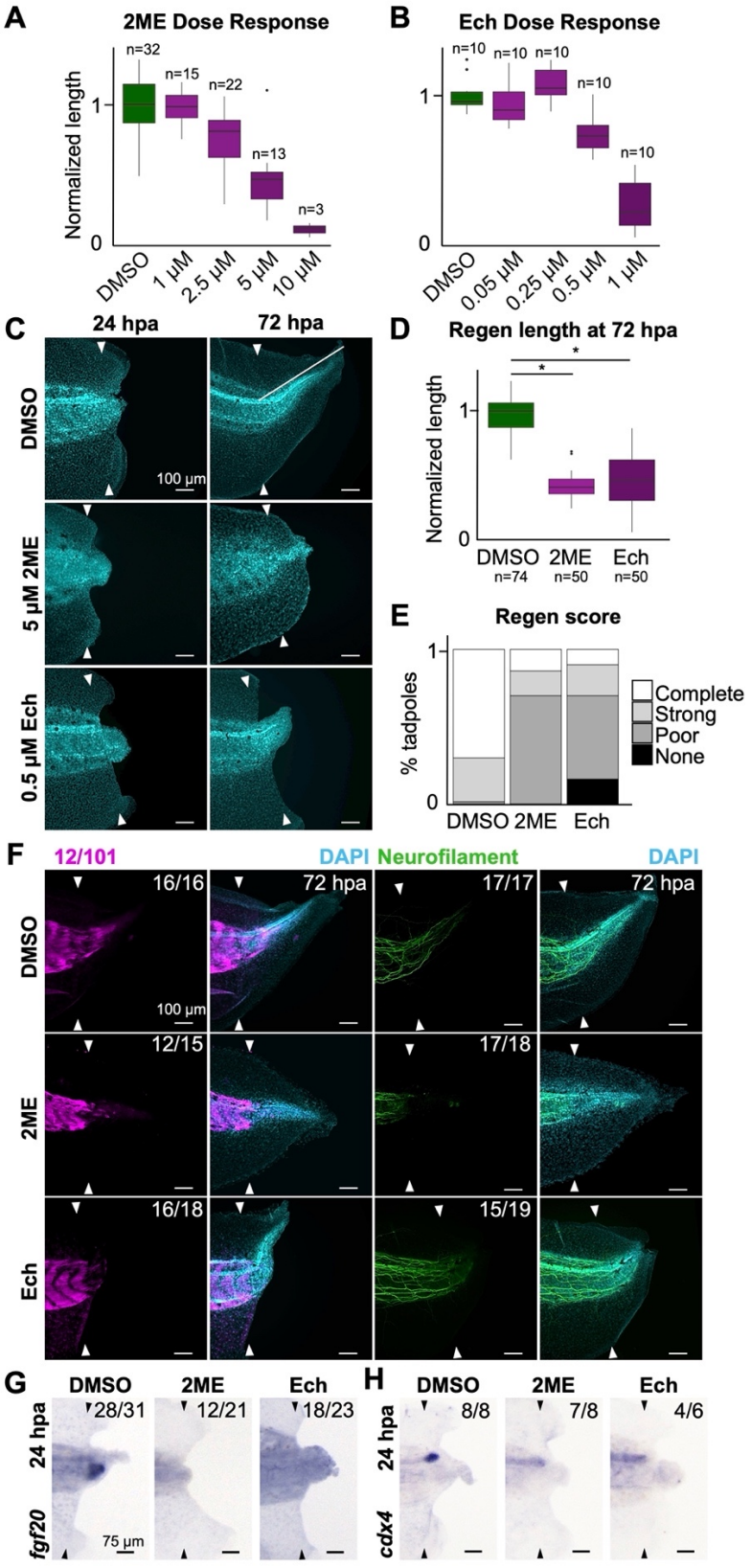

Figure 4-1: **Hif1α is required for regeneration of muscle and axons**

A-B) Quantification of regeneration length normalized to DMSO clutchmates across dose curves for 2ME (A) and Ech (B). C) Dapi counterstained tails at 24 and 72hpa following treatment with DMSO, 5μM 2ME, or 0.5μM Ech. D) Quantification of regeneration length normalized to DMSO clutchmates. Statistical significance between groups was determined by ANOVA ($p<2e-16$) followed by Tukey's posttest. * indicates $p < 0.001$. E) Regeneration scores binned to complete (full tail regeneration), strong (incomplete fin regeneration), poor (very little regeneration), or none. The treatments have statistically significant distribution of phenotypes (chi-square test, $p < 2.2e-16$). F) Immunohistochemical stains for 12/101 (muscle) and neurofilament (axons) at 72hpa after treatment with DMSO, 2ME, or Ech. G-H) *in situ* hybridization for *fgf20* (G) or *cdx4* (H) at 24hpa following DMSO, 2ME, or Ech treatment. Indicated numbers in F-H represent number of tails with prevented phenotype over total number assayed. Scale bars in C and F are 100μm, scale bars in G-H are 75μm. Arrowheads in C and F-H indicate amputation plane.

We next asked if axial tissues were specifically sensitive to loss of Hif1α function. Neither 2ME nor Ech completely abrogated regeneration in all treated tadpoles, but axial tissues always appeared to be reduced (Figure 4-1 E). The variation in regeneration outcomes could be attributed to differences in how much inhibitor each animals effectively gets from the media, though offers an opportunity to interrogate more nuanced consequences of Hif1α perturbation than completely abrogated regeneration would permit. To ask if axial tissues were specifically sensitive to loss of Hif1α function, we performed immunohistochemical staining for axons and muscle at 72hpa in tadpoles treated with DMSO, 2ME, or Ech from the time of amputation to collection and found that Hif1α antagonism resulted in tails with little to no muscle (12/101) or axon (neurofilament) regeneration, despite a large degree of fin regeneration (Figure 4-1 F). We then asked whether Hif1α was required for the activation of neural or mesodermal fate specification genes during regeneration. To this end, we performed *in situ* hybridization for *fgf20* and *cdx4*, posterior mesoderm and

neuronal markers, respectively (Lea et al., 2009; Northrop & Kimelman, 1994). We found that at 24hpa, both *fgf20* and *cdx4* are strongly induced in the regeneration bud in controls but not if Hif1α is inhibited (Figure 4-1 G,H). These results suggested that Hif1α might be specifically required for the activation of posterior fate genes during regeneration.

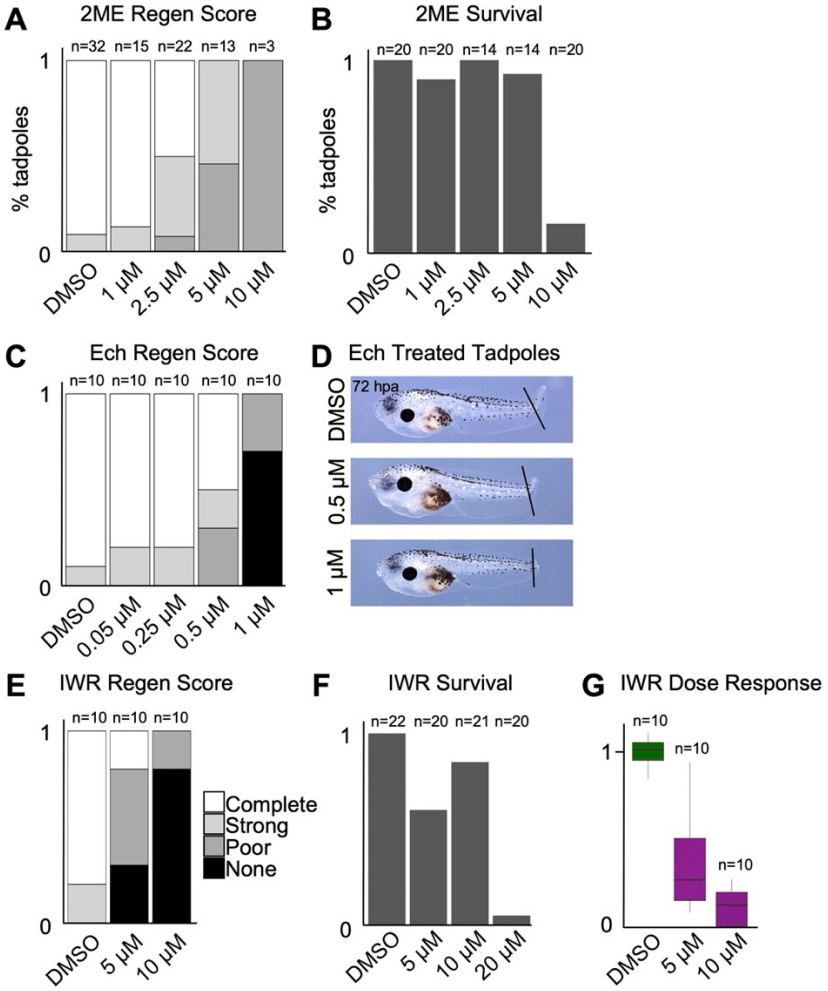

Figure 4-2: **Optimization of small molecule treatments for *Xenopus tropicalis* tail regeneration**

A,C,E) Regeneration scores binned to complete (full tail regeneration), strong (incomplete fin regeneration), poor (very little regeneration), or none across different concentrations of 2ME (A), Ech (C), and IWR (E). B,F) Percentage of tadpoles alive at

72hpa following treatment with different concentrations of 2ME (B) and IWR (F). D) Images of tadpoles at 72hpa following treatment with DMSO or Ech. The highest concentration of Ech tested results in curling of the fin epidermis and unhealthy tadpoles.G) Quantification of regeneration length normalized to DMSO clutchmates across dose curves for IWR.

4.4.2 *Hif1α and Wnt are necessary for expression of similar genes during regeneration*

Having found that Hif1α is required to activate *fgf20* and *cdx4*, known targets of canonical Wnt signaling, we hypothesized that Hif1α might broadly target the same genes as Wnt signaling (Chamorro et al., 2005; Haremaki et al., 2003). To test the requirement of Wnt signaling in regeneration, we used the Wnt inhibitor IWR-1 (IWR), which stabilizes the axin destruction complex (Borday et al., 2018; Chen et al., 2009). We find that treatment with 10μM IWR greatly reduces regeneration length and quality, in agreement with previous studies inhibiting Wnt in *Xenopus* tail regeneration (Figure 4-2 E-G) (G. Lin & Slack, 2008). We then performed RNA-sequencing to identify regeneration-induced changes in gene expression dependent on either Hif1α or Wnt. We collected tail tissue 250μm anterior to the amputation plane at either 0 or 24hpa following treatment with DMSO, 2ME, Ech, or IWR (Figure 4-3 A). RNA-Seq libraries were prepared and analyzed in triplicate. When multidimensional scaling (MDS) was applied to visualize the relationship between groups (Robinson et al., 2010) we found that biological replicate libraries clustered tightly together, demonstrating their reproducibility (Figure 4-3 B, Figure 4-4 A). We also found that 0hpa tails are largely distinct from all four 24hpa groups, suggesting that there is a gene expression signature

specific to the tissue following injury regardless of regenerative outcome (Figure 4-4 A). To visualize gene expression across treatments, we normalized all groups to DMSO and generated a heatmap. This revealed that the directionality of changes in expression relative to DMSO were largely shared following inhibition of Hif1α or Wnt (Figure 4-3 C). PANTHER Gene Ontology (GO) Enrichment analysis on genes differentially expressed by all three treatments called terms associated with several known Hif1α regulated processes, including erythrocyte cell homeostasis, as well as several not commonly associated with Hif1α, including macromolecule biosynthesis and mRNA splicing. Notably, developmental pattern specification terms which are not traditionally affiliated with Hif1α but are often associated with Wnt signaling, among other key developmental pathways, were enriched (Figure 4-4). We focused our downstream analysis on the 1443 genes downregulated by all treatments, as these represent genes which require Hif1α or Wnt for expression in this context (Figure 4-3 D). We then asked if the majority of these Hif1α and Wnt responsive genes were normally upregulated following injury or if they were normally downregulated. To this end, we analyzed only genes which increased from the 0hpa control to 24hpa DMSO, or injury-induced genes. We found that 1106 injury-induced genes fail to be upregulated when Hif1α or Wnt are inhibited, indicating that most of the 1443 Hif1α and Wnt regulated genes are normally upregulated during regeneration (Figure 4-4 C). These results suggest that Hif1α and Wnt direct similar gene expression programs during regeneration and identify those genes which are sensitive to perturbation of each pathway. GO analysis of genes downregulated in Hif1α and Wnt inhibited tadpoles found anterior/posterior pattern specification genes were enriched (Figure 4-3 E, Table 4-1). This result, together with

observed loss of posterior markers *fgf20* and *cdx4* (Figure 4-1 G,H), suggests that Hif1α may be a transcriptional activator of posterior patterning genes in the regenerating tail.

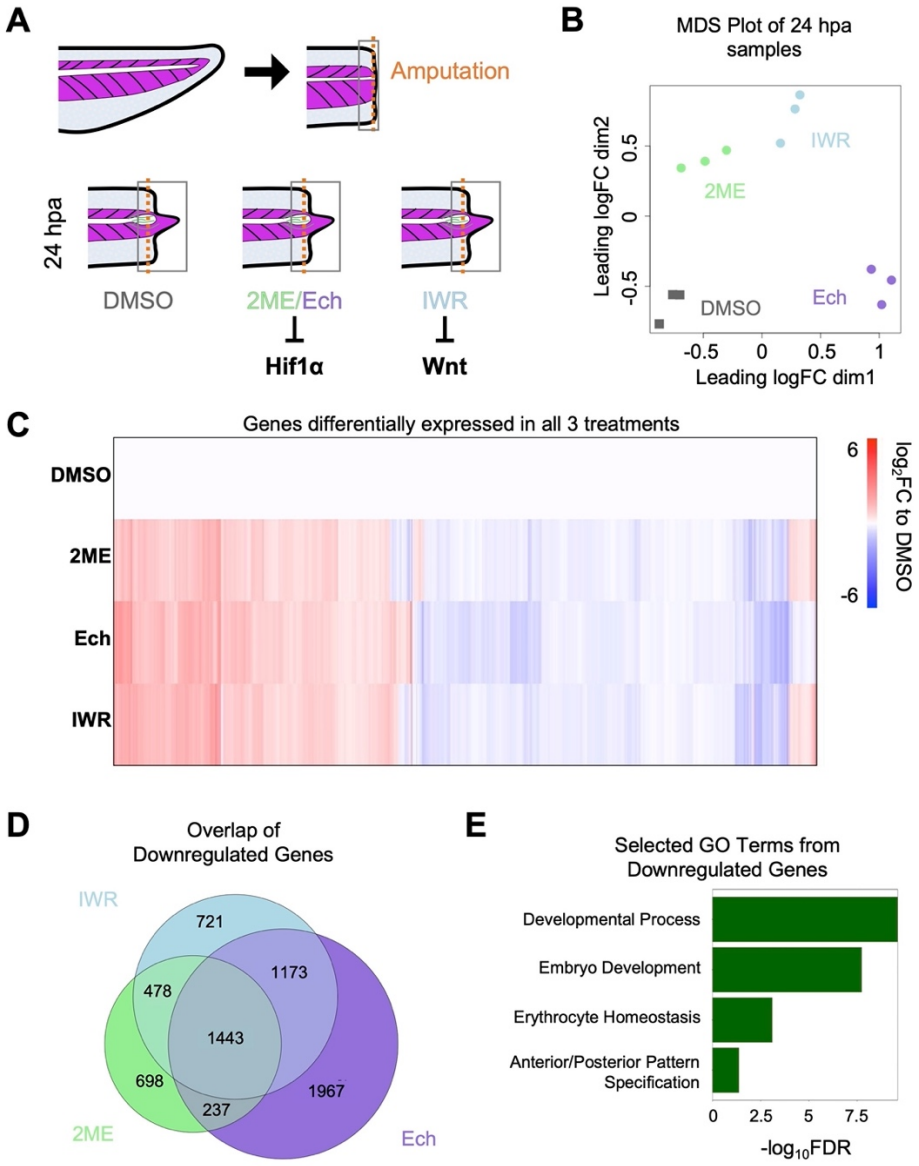

Figure 4-3: **RNA-sequencing reveals shared gene regulatory roles for Hif1α and Wnt**

A) Schematic depicting experimental setup for RNA-sequencing. Tails were amputated and treated with DMSO, 2ME, Ech, or IWR and collected at 0 or 24hpa for sequencing. Purple chevrons in tails represent somites, green line indicates spinal cord, and grey box marks tissues collected for sequencing. Amputation plane is marked with an orange dotted line. B) MDS plot depicting relationship between samples. C) Heatmap of gene

expression for genes differentially expressed in all 3 treatment groups as log_2FC relative to DMSO clustered by expression. *Lower bound of color scale represented values from -6 to -15. D) Venn diagram showing overlap in downregulated genes (FDR < 0.05 and log_2FC < -0.2). E) Selected GO terms from PANTHER gene ontology enrichment of 1443 downregulated genes plotted by -log_{10}FDR.

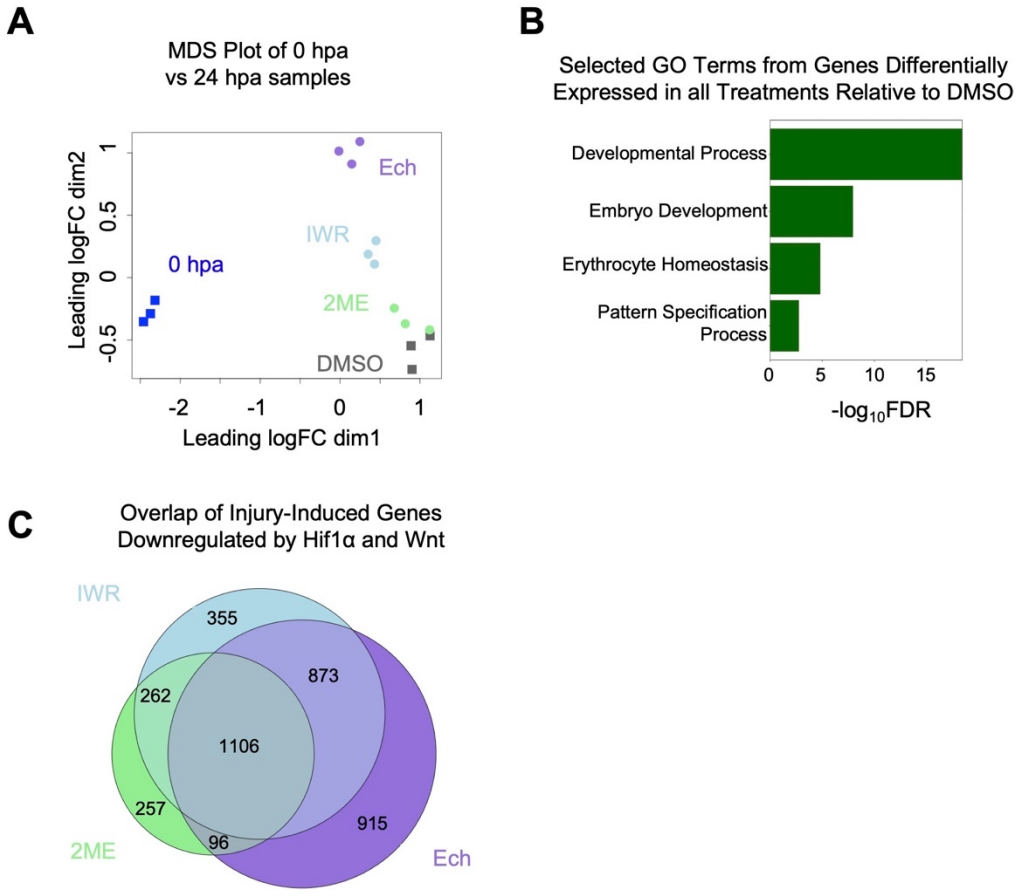

Figure 4-4: **RNA-seq reveals regeneration induced changes in gene expression and Hif1α and Wnt dependent genes**

A) MDS plot depicting relationship between samples including 0hpa. B) Selected GO terms from PANTHER gene ontology enrichment of all 3259 genes differentially expressed in all 3 treatments relative to DMSO, plotted by -log_{10}FDR. C) Venn diagram showing overlap in injury induced genes (log2FC(0hpa/ DMSO24hpa) < -0.2 and FDR < 0.05) downregulated by treatments (FDR < 0.05 and log_2FC < -0.2).

Table 4-1: GO Terms called by PANTHER from the intersection of genes downregulated by Hif1α and Wnt inhibition at 24hpa

GO	BackgroundN	TargetN	FoldEnrich	FDR
gene expression	1335	223	3.85857252	1.16E-59
peptide metabolic process	437	127	6.71313458	4.50E-54
translation	383	120	7.23744942	6.65E-54
peptide biosynthetic process	389	120	7.12581781	2.24E-53
cellular macromolecule biosynthetic process	1069	184	3.97597081	4.62E-50
macromolecule biosynthetic process	1084	185	3.94226229	6.15E-50
cellular nitrogen compound metabolic process	2486	290	2.69463498	6.43E-50
macromolecule metabolic process	5340	460	1.98984682	7.91E-50
amide biosynthetic process	467	123	6.08402935	9.09E-49
cellular process	12271	775	1.45889762	5.08E-48
metabolic process	7527	564	1.73085329	6.44E-47
cellular metabolic process	6313	501	1.83317956	6.03E-46
cellular amide metabolic process	618	135	5.04601298	6.55E-46
nitrogen compound metabolic process	5922	478	1.86450075	6.89E-45
primary metabolic process	6505	500	1.77552084	6.73E-42
organic substance metabolic process	6795	513	1.74393773	2.16E-41
cellular biosynthetic process	1775	220	2.86303985	5.04E-40
cellular nitrogen compound biosynthetic process	1028	162	3.64019769	1.41E-39
organonitrogen compound biosynthetic process	1127	170	3.48440056	1.57E-39
organic substance biosynthetic process	1831	221	2.78809135	1.20E-38
cellular macromolecule metabolic process	4161	366	2.03182565	1.24E-38
biosynthetic process	1875	222	2.73498389	1.24E-37
cellular protein metabolic process	3315	293	2.04167757	3.06E-29
protein metabolic process	4010	329	1.89519802	3.70E-28
organonitrogen compound metabolic process	4728	365	1.7832756	5.16E-27
nucleic acid metabolic process	1599	165	2.38362839	8.82E-21
cellular component organization or biogenesis	3196	254	1.83581966	1.64E-18
RNA metabolic process	1047	121	2.66957274	3.86E-18
ribonucleoprotein complex biogenesis	310	61	4.54539061	6.61E-18
heterocycle metabolic process	2098	188	2.06992893	7.14E-18
nucleobase-containing compound metabolic process	1995	180	2.08416777	3.53E-17
cellular aromatic compound metabolic process	2142	186	2.0058412	2.95E-16
RNA splicing	219	49	5.16838711	3.53E-16
cytoplasmic translation	55	28	11.7597587	3.57E-16
organic cyclic compound metabolic process	2247	192	1.97379128	3.60E-16
ribonucleoprotein complex assembly	123	37	6.94863792	1.78E-15
ribonucleoprotein complex subunit organization	127	37	6.72978319	4.17E-15
cellular component organization	3037	232	1.76459995	9.19E-15
mRNA metabolic process	380	61	3.70808182	2.82E-14
RNA splicing, via transesterification reactions	153	38	5.73713719	1.17E-13
RNA splicing, via transesterification reactions with bulged adenosine as nucleophile	153	38	5.73713719	1.20E-13
mRNA splicing, via spliceosome	153	38	5.73713719	1.22E-13
RNA processing	676	83	2.83618441	1.39E-13
mRNA processing	302	52	3.97740184	3.75E-13
regulation of macromolecule metabolic process	3111	229	1.70035084	7.56E-13
cellular protein-containing complex assembly	410	60	3.38041845	1.77E-12
multicellular organism development	1851	156	1.9467996	2.46E-12
anatomical structure development	2020	166	1.89827789	2.75E-12
cellular component biogenesis	1200	115	2.21370458	4.48E-12
organelle organization	2119	170	1.85319464	6.53E-12
regulation of metabolic process	3286	234	1.64494495	1.12E-11
developmental process	2201	172	1.80514243	3.80E-11
animal organ development	848	89	2.42436064	4.64E-11
regulation of nitrogen compound metabolic process	2891	209	1.66994153	7.77E-11
protein-containing complex subunit organization	590	70	2.74062174	9.68E-11
regulation of cellular metabolic process	3034	216	1.64452789	1.11E-10
regulation of primary metabolic process	2938	210	1.65108934	2.08E-10
protein-containing complex assembly	516	63	2.82029097	4.46E-10
ribosome biogenesis	225	39	4.00391785	7.70E-10
regulation of gene expression	2375	176	1.71179646	1.28E-09

system development	1498	123	1.89669006	9.27E-09
embryo development	359	48	3.08851602	1.06E-08
cellular component assembly	1024	92	2.07534805	5.28E-08
multicellular organismal process	2500	176	1.62620664	5.44E-08
ribosome assembly	42	16	8.79981945	1.30E-07
regulation of macromolecule biosynthetic process	2133	154	1.66775763	1.88E-07
biological regulation	8042	443	1.27245586	3.13E-07
regulation of cellular biosynthetic process	2157	154	1.64920121	3.24E-07
regulation of biosynthetic process	2165	154	1.64310717	4.56E-07
regulation of cellular macromolecule biosynthetic process	2078	149	1.65631828	4.64E-07
regulation of nucleobase-containing compound metabolic process	2127	152	1.65074187	4.69E-07
regulation of RNA metabolic process	2068	148	1.65315757	5.92E-07
regulation of biological process	7400	411	1.28296016	6.87E-07
negative regulation of macromolecule metabolic process	917	81	2.04041615	9.28E-07
ribosomal large subunit biogenesis	61	17	6.43757284	1.71E-06
negative regulation of metabolic process	952	82	1.98966506	2.60E-06
negative regulation of nitrogen compound metabolic process	782	70	2.06773251	6.23E-06
regulation of cellular process	7104	391	1.27138439	7.05E-06
chromosome organization	710	65	2.11474534	7.41E-06
negative regulation of cellular metabolic process	819	72	2.03072757	7.42E-06
anatomical structure morphogenesis	800	71	2.05008294	8.20E-06
translational initiation	89	19	4.9313595	9.05E-06
ribosomal small subunit biogenesis	53	15	6.53760172	9.08E-06
proteasomal ubiquitin-independent protein catabolic process	14	9	14.8496953	1.59E-05
cellular developmental process	1223	95	1.79432132	1.60E-05
cell differentiation	1211	94	1.7930268	2.02E-05
protein localization to endoplasmic reticulum	50	14	6.4678673	2.59E-05
macromolecule catabolic process	572	54	2.18072449	3.79E-05
negative regulation of macromolecule biosynthetic process	509	49	2.22372648	7.68E-05
cellular macromolecule catabolic process	538	51	2.18973203	8.09E-05
regulation of nucleic acid-templated transcription	1947	131	1.5542054	0.00011
regulation of RNA biosynthetic process	1947	131	1.5542054	0.00011118
negative regulation of cellular biosynthetic process	520	49	2.17668611	0.00015423
negative regulation of cellular process	1441	103	1.65111116	0.00015428
macromolecule localization	1279	94	1.69769777	0.00015461
negative regulation of biosynthetic process	521	49	2.17250821	0.00015516
regulation of mRNA metabolic process	113	19	3.88399111	0.00018744
ribosomal small subunit assembly	15	8	12.3197472	0.00019538
negative regulation of biological process	1634	113	1.59745805	0.00021858
myeloid cell homeostasis	45	12	6.15987362	0.00024513
hematopoietic or lymphoid organ development	164	23	3.23956768	0.00026302
regulation of transcription, DNA-templated	1893	126	1.53752788	0.00030292
regulation of protein metabolic process	882	70	1.83329572	0.0003187
embryonic morphogenesis	220	27	2.83494184	0.00036603
regulation of cellular protein metabolic process	857	68	1.83286788	0.00036813
negative regulation of nucleobase-containing compound metabolic process	493	46	2.15533103	0.00037344
embryo development ending in birth or egg hatching	157	22	3.23687626	0.000408
hemopoiesis	160	22	3.17618483	0.00053014
negative regulation of RNA metabolic process	458	43	2.1687328	0.00053056
immune system development	173	23	3.07103526	0.00053546
protein folding	124	19	3.53944351	0.0005455
animal organ morphogenesis	254	29	2.63734746	0.00054955
DNA replication	162	22	3.13697268	0.00060523
G protein-coupled receptor signaling pathway	1363	28	0.47453172	0.00061039
negative regulation of gene expression	601	52	1.99862788	0.00062077
cellular protein localization	758	61	1.85893284	0.00072617
erythrocyte differentiation	43	11	5.90918109	0.00075601
protein localization	1013	76	1.73303453	0.00076977
cytoskeleton organization	795	63	1.83052848	0.00077406
protein localization to organelle	271	30	2.55714311	0.00080214
spliceosomal snRNP assembly	20	8	9.23981043	0.00083684
erythrocyte homeostasis	44	11	5.77488152	0.00087316
positive regulation of cellular process	1660	111	1.54460686	0.0008983
establishment of protein localization to endoplasmic reticulum	36	10	6.41653502	0.0009683
protein targeting to ER	36	10	6.41653502	0.00097598

cellular macromolecule localization	762	61	1.84917466	0.0010207
intracellular transport	845	65	1.77688662	0.00127568
formation of cytoplasmic translation initiation complex	22	8	8.39982766	0.00138484
regulation of mRNA processing	77	14	4.19991383	0.00138516
negative regulation of cellular macromolecule biosynthetic process	464	42	2.09090538	0.00139562
regulation of mRNA splicing, via spliceosome	67	13	4.4819976	0.00146235
nitrogen compound transport	1057	77	1.68274693	0.00146942
peptide transport	831	64	1.77902487	0.00148066
regulation of translation	150	20	3.07993681	0.00161611
chordate embryonic development	150	20	3.07993681	0.00162791
regulation of actin filament-based process	203	24	2.73097845	0.00163978
pattern specification process	190	23	2.79625842	0.00167538
cytoplasmic translational initiation	31	9	6.70631402	0.00174969
protein transport	819	63	1.77688662	0.00180038
regulation of cellular amide metabolic process	153	20	3.01954589	0.00202414
negative regulation of nucleic acid-templated transcription	438	40	2.10954576	0.00204838
negative regulation of RNA biosynthetic process	438	40	2.10954576	0.0020627
proteolysis	1197	84	1.62101937	0.00207937
intracellular protein transport	573	48	1.93503883	0.00209291
morphogenesis of an epithelium	117	17	3.35634139	0.00227794
chromatin organization	476	42	2.03819348	0.00252
nervous system development	828	63	1.75757264	0.00271529
establishment of protein localization	830	63	1.75333752	0.00274392
homeostasis of number of cells	63	12	4.39990973	0.00307875
embryonic organ development	159	20	2.90560076	0.00307892
regulation of RNA splicing	85	14	3.80462782	0.00310277
positive regulation of cellular catabolic process	74	13	4.05802485	0.00313749
amide transport	855	64	1.72908733	0.00339179
regulation of cellular component size	202	23	2.63014406	0.00347615
ribosomal large subunit assembly	19	7	8.51035171	0.0034876
regulation of actin cytoskeleton organization	202	23	2.63014406	0.00349829
translational elongation	35	9	5.93987813	0.00350745
organelle assembly	393	36	2.11598712	0.00353761
oxidation-reduction process	1246	85	1.57581037	0.00364212
posttranscriptional regulation of gene expression	203	23	2.61718768	0.00365192
signal peptide processing	7	5	16.4996615	0.00376834
skeletal system development	125	17	3.14153555	0.00427087
regulation of actin filament organization	165	20	2.79994255	0.00450429
regulation of actin polymerization or depolymerization	152	19	2.88744076	0.00452861
positive regulation of cellular metabolic process	1104	77	1.61110825	0.0045404
regulation of actin filament length	152	19	2.88744076	0.00455556
protein catabolic process	432	38	2.03190276	0.0045793
epithelium development	234	25	2.46789808	0.00483924
central nervous system development	217	24	2.55478629	0.00507163
convergent extension	29	8	6.37228305	0.00533449
organic substance transport	1394	92	1.52450244	0.00582694
regulation of organelle organization	452	39	1.9931007	0.00597809
establishment of protein localization to organelle	184	21	2.63635895	0.00620152
proteasome-mediated ubiquitin-dependent protein catabolic process	171	20	2.70169896	0.00655178
cell redox homeostasis	49	10	4.71418899	0.00657146
tissue development	459	39	1.96270483	0.00692239
peptidyl-proline modification	60	11	4.23491311	0.0070672
DNA metabolic process	586	47	1.85269236	0.00711701
positive regulation of nitrogen compound metabolic process	1049	73	1.607498	0.00717052
actin nucleation	40	9	5.19739337	0.00723449
establishment of localization in cell	1017	71	1.61265128	0.0077755
Arp2/3 complex-mediated actin nucleation	23	7	7.03029054	0.00806707
rRNA processing	148	18	2.80940182	0.00838342
supramolecular fiber organization	319	30	2.17236922	0.00841224
regulation of actin filament polymerization	148	18	2.80940182	0.00842825
myeloid cell differentiation	62	11	4.09830301	0.00853589
regulation of transcription by RNA polymerase II	1226	82	1.54499277	0.00855386
brain development	135	17	2.90882921	0.0085689
localization	3591	201	1.29295593	0.0085975
regulation of cellular component biogenesis	277	27	2.25157835	0.00910911

cellular localization	1245	83	1.5399684	0.0092259
neurogenesis	582	46	1.82573574	0.00939834
mRNA transport	63	11	4.03325058	0.00940915
proteasomal protein catabolic process	178	20	2.59545237	0.00945969
regulation of supramolecular fiber organization	178	20	2.59545237	0.00950771
positive regulation of biological process	1902	117	1.42094876	0.00966393
tissue morphogenesis	151	18	2.75358589	0.00985665
regulation of cytoskeleton organization	280	27	2.2274543	0.00986826
head development	138	17	2.84559379	0.01014139
regulation of anatomical structure size	237	24	2.33919251	0.01036251
transcription, DNA-templated	180	20	2.56661401	0.01044132
nucleic acid-templated transcription	180	20	2.56661401	0.01049251
proteolysis involved in cellular protein catabolic process	409	35	1.97673206	0.01096071
regulation of protein polymerization	153	18	2.7175913	0.01101697
regulation of cellular component organization	639	49	1.77132516	0.01139987
rRNA metabolic process	154	18	2.69994461	0.01172411
protein peptidyl-prolyl isomerization	45	9	4.61990521	0.01348235
RNA catabolic process	103	14	3.13974141	0.01360046
RNA biosynthetic process	193	21	2.51341994	0.01361114
positive regulation of macromolecule metabolic process	1081	73	1.55991249	0.01368923
endoplasmic reticulum to Golgi vesicle-mediated transport	92	13	3.26406347	0.01551008
positive regulation of metabolic process	1156	77	1.53863625	0.01555516
cellular protein catabolic process	412	35	1.96233838	0.01599874
positive regulation of mRNA metabolic process	19	6	7.29458718	0.0169219
proteasome assembly	12	5	9.62480253	0.01850765
microtubule-based process	551	43	1.80268534	0.01869976
regulation of cell cycle	367	32	2.01412761	0.01873502
positive regulation of cell cycle G1/S phase transition	6	4	15.399684	0.018785
transcription by RNA polymerase II	82	12	3.38041845	0.01879238
regulation of protein-containing complex assembly	184	20	2.51081805	0.01880802
protein targeting	122	15	2.84010566	0.02104538
chromatin remodeling	96	13	3.12806082	0.02122068
modification-dependent protein catabolic process	376	32	1.96591711	0.02195866
tube development	232	23	2.29003922	0.02366568
cell cycle	579	44	1.7554044	0.02480657
modification-dependent macromolecule catabolic process	381	32	1.94011768	0.02481248
convergent extension involved in gastrulation	21	6	6.59986459	0.02485836
regulation of biological quality	1494	93	1.43792231	0.02494333
negative regulation of transcription, DNA-templated	393	33	1.93965486	0.02756358
ncRNA processing	315	28	2.05329121	0.02988466
SRP-dependent cotranslational protein targeting to membrane	22	6	6.29987075	0.03001523
Golgi vesicle transport	180	19	2.43828331	0.0300509
DNA repair	338	29	1.981912	0.03027246
electron transport chain	101	13	2.97320633	0.03062622
heterocycle biosynthetic process	604	45	1.72099118	0.03067496
organonitrogen compound catabolic process	641	47	1.693725	0.03074695
nucleobase-containing compound transport	143	16	2.58456236	0.03290539
intracellular protein transmembrane transport	42	8	4.39990973	0.03301533
nucleobase-containing compound biosynthetic process	541	41	1.75061103	0.03408306
actin filament organization	201	20	2.29846031	0.03421244
gastrulation	77	11	3.2999323	0.03433747
nucleic acid transport	90	12	3.07993681	0.03486704
cotranslational protein targeting to membrane	23	6	6.02596332	0.03488968
RNA transport	90	12	3.07993681	0.0350082
establishment of RNA localization	90	12	3.07993681	0.03515051
positive regulation of epithelial cell proliferation	15	5	7.69984202	0.03660045
cellular catabolic process	1053	69	1.51364416	0.03999743
organic substance catabolic process	1057	69	1.50791608	0.04094459
alpha-amino acid biosynthetic process	67	10	3.44769046	0.04116287
cellular response to DNA damage stimulus	395	32	1.87135401	0.04182937
regulation of mitotic cell cycle	134	15	2.58576784	0.04416155
cartilage development	56	9	3.71242383	0.04445371
anterior/posterior pattern specification	81	11	3.13697268	0.04712359
RNA localization	94	12	2.94887567	0.0471419
regulation of programmed cell death	238	22	2.13525031	0.04729127

regulation of nuclear-transcribed mRNA catabolic process, deadenylation-dependent decay	9	4	10.266456	0.04875189
connective tissue development	57	9	3.64729359	0.04884522
positive regulation of macromolecule biosynthetic process	663	47	1.63752296	0.04902847

4.4.3 *Posterior hox gene expression in the regeneration bud requires Hif1α and Wnt*

Because Hif1α and Wnt inhibition resulted in a downregulation of genes involved in patterning, we examined the genes under these GO terms and noticed that more than half of all *hox* genes were downregulated under all 3 treatments (Figure 4-5 A,B). To determine the normal expression for relevant *hox* genes during development, we examined *in situ* expression patterns at stages 30-35 on Xenbase for *hox* genes that were differentially expressed in all 3 of our treatment groups to determine the normal expression of this family of patterning related genes (Bowes et al., 2010). Notably, all but one of the *hox* genes that were downregulated following Hif1α and Wnt inhibition are expressed in the most posterior region of tailbud stage tadpoles. The only gene that was upregulated in each group was *hoxb4*, which we noted had a distinct domain in the anterior of the tadpole (Figure 4-5 C, Table 4-2). Using previously published RNA-sequencing data over a regeneration timecourse in *X. tropicalis* (Chang et al., 2017), we queried the normal expression dynamics of the *hox* genes were across a regenerative timecourse. Relative to uninjured tadpoles, the expression of most *hox* genes decreased at 0 and 6hpa but then increased by 15 and 24hpa (Figure 4-5 D). Of those genes that were activated during regeneration, most failed to increase in expression when Hif1α and Wnt were inhibited (Figure 4-5 E). Examining expression of several representatives of this trend (*hoxc9*, *hoxc10*, and *hoxd11*), we found that at 24hpa these transcripts are normally abundant in the regenerating axial tissue but that they fail to be

induced when tadpoles are treated with 2ME, Ech, or IWR (Figure 4-5 F). These results suggest that *hox* genes are activated in response to injury and that this activation depends on both Hif1α and Wnt.

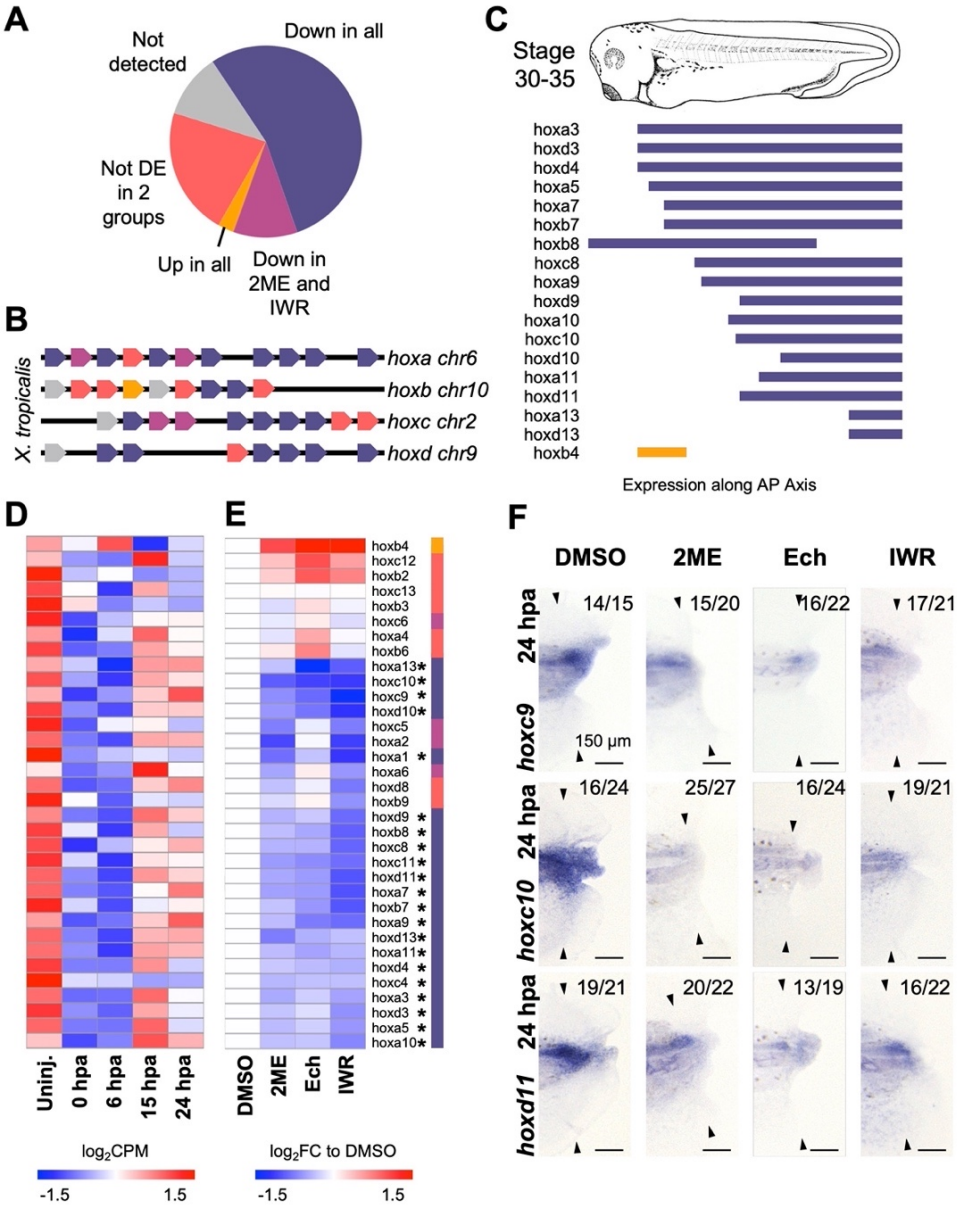

Figure 4-5: **Posterior *hox* gene expression in regeneration requires Hif1α and Wnt**

A) Pie chart of *hox* gene expression changes following 2ME, Ech, or IWR treatment. B) Schematic representation of *hox* gene organization in *Xenopus*. Color coding is as in (A). C) Schematic depicting *hox* gene expression in tailbud stage tadpoles. Color coding

is as in (A). Boundaries were determined by lining up *in situ* expression patterns from Xenbase at the noted stages and using structural landmarks to determine the anterior and posterior domains. D) Heatmap displaying all detected *hox* genes across a regeneration timecourse. E) Heatmap displaying all detected *hox* genes clustered by expression. Genes significantly differentially expressed in all treatments are indicated by *. F) *in situ* hybridization for selected *hox* genes at 24hpa following treatment with DMSO, 2ME, Ech, or IWR. Arrowheads indicate amputation plane. Scale bars in E are 150μm.

Table 4-2: Links to *hox* gene ISH images used for Figure 4-5 C

Gene	Xenbase Image Number	Link
hoxa3	86758	https://www.xenbase.org/common/ViewImageActionNonAdmin.do?imageId=86758
hoxd3	140200	https://www.xenbase.org/common/ViewImageActionNonAdmin.do?imageId=140200
hoxd4	142167	https://www.xenbase.org/common/ViewImageActionNonAdmin.do?imageId=142167
hoxa5	140669	https://www.xenbase.org/common/ViewImageActionNonAdmin.do?imageId=140669
hoxa7	156276	https://www.xenbase.org/common/ViewImageActionNonAdmin.do?imageId=156276
hoxb7	156246	https://www.xenbase.org/common/ViewImageActionNonAdmin.do?imageId=156246
hoxb8	156239	https://www.xenbase.org/common/ViewImageActionNonAdmin.do?imageId=156239
hoxc8	156198	https://www.xenbase.org/common/ViewImageActionNonAdmin.do?imageId=156198
hoxa9	156268	https://www.xenbase.org/common/ViewImageActionNonAdmin.do?imageId=156268
hoxd9	156118	https://www.xenbase.org/common/ViewImageActionNonAdmin.do?imageId=156118
hoxa10	142483	https://www.xenbase.org/common/ViewImageActionNonAdmin.do?imageId=142483
hoxc10	141346	https://www.xenbase.org/common/ViewImageActionNonAdmin.do?imageId=141346
hoxd10	37498	https://www.xenbase.org/common/ViewImageActionNonAdmin.do?imageId=37498
hoxa11	141894	https://www.xenbase.org/common/ViewImageActionNonAdmin.do?imageId=141894
hoxd11	156260	https://www.xenbase.org/common/ViewImageActionNonAdmin.do?imageId=156260
hoxa13	81826	https://www.xenbase.org/common/ViewImageActionNonAdmin.do?imageId=81826
hoxd13	44767	https://www.xenbase.org/common/ViewImageActionNonAdmin.do?imageId=44767
hoxb4	37488	https://www.xenbase.org/common/ViewImageActionNonAdmin.do?imageId=37488

4.4.4 *Most Wnt signaling ligands and receptors are not regulated by Hif1α*

Because the expression of posterior patterning genes was decreased if either Hif1α or Wnt signaling was blocked, we asked if Hif1α might be acting upstream of Wnt

signaling, such that inhibition of Hif1α caused an indirect downregulation of Wnt target genes. Specifically, we asked whether inhibition of Hif1α resulted in downregulation of Wnt ligands or receptors. To test this, we examined expression of Wnt ligands and receptors and found that the majority were not differentially expressed following Hif1α or Wnt inhibition, several had an increase in expression under these treatments, and only *wnt5a* and *wnt5b* are weakly downregulated (Figure 4-6 A). This suggested that it is unlikely that the primary role of Hif1α in patterning is to transcriptionally upregulate Wnt ligands or receptors. We also considered that Hif1α might be required to repress expression of components of the β-catenin degradation complex, but found that *dsh2* and *axin2* expression are decreased upon Hif1α inhibition, while other components are not significantly affected (Figure 4-6 A). These results suggest that the sensitivity of Wnt target genes to Hif1α perturbation is not likely due to Hif1α being a direct activator of Wnt signaling components or repressor of factors that destabilize β-catenin. The upregulation of several Wnt signaling components that we observed following 2ME, Ech, and IWR treatments does suggest that there may be compensatory upregulation of these factors when Wnt or Hif1α is inhibited, but it is not clear whether this regulation is direct.

4.4.5 *Hif1α is required for expression of Wnt responsive elements and direct target genes of canonical Wnt signaling*

Our data to this point suggested that Hif1α is required for expression of many of the same patterning genes targeted by canonical Wnt signaling, but that it is not likely to act by directly upregulating Wnt ligands or receptors. We next asked more specifically whether Hif1α acts on Wnt-dependent gene expression by determining if Hif1α

perturbation affects transcription via Wnt-responsive promoter elements (WREs). To visualize when and where WRE-dependent transcription is active during regeneration, we utilized the *pbin7:GFP* transgenic line, in which GFP expression serves as a readout of Wnt activity via WREs (Tran & Vleminckx, 2014). Although GFP fluorescence in the regenerating tail was relatively faint and variable, by using *in situ* hybridization to visualize GFP transcripts directly, we found *pbin7:GFP* transcripts throughout the axial tissues in uninjured tails which appeared to be strongly upregulated at the posterior extreme of the tail (Figure 4-6 B, Figure 4-7). Following amputation, we find GFP transcript localized to regenerating tissue 24hpa and find that this transcription is sustained until 72hpa while signal anterior to the wound site is reduced (Figure 4-6 B). To confirm that *pbin7:GFP* transcripts are a reliable readout of Wnt activity, we treated regenerating tadpoles from this line with IWR, and found that IWR treatment reduced GFP expression at 24hpa (Figure 4-6 C). Inhibition of Hif1α with either 2ME or Ech also reduced GFP expression at 24hpa, at a comparable degree to IWR (Figure 4-6 C). As an independent test of whether Hif1α is required for Wnt-dependent gene expression, we examined expression of established direct target genes of canonical Wnt signaling established at gastrula and neurula stages (Kjolby & Harland, 2017; Young et al., 2014). We find that, while not all of these targets are sensitive to Wnt inhibition in regeneration, those that are downregulated by IWR, including well-established targets such as *axin2, cdx2, cdx4, prickle, sall1* and *sall4*, are also downregulated by Hif1α inhibition (Figure 4-6 D). These results suggest that Hif1α is acting upstream of the activation of regeneration specific Wnt targets and WRE-mediated transcription, though they do not distinguish between a direct or indirect interaction at WREs.

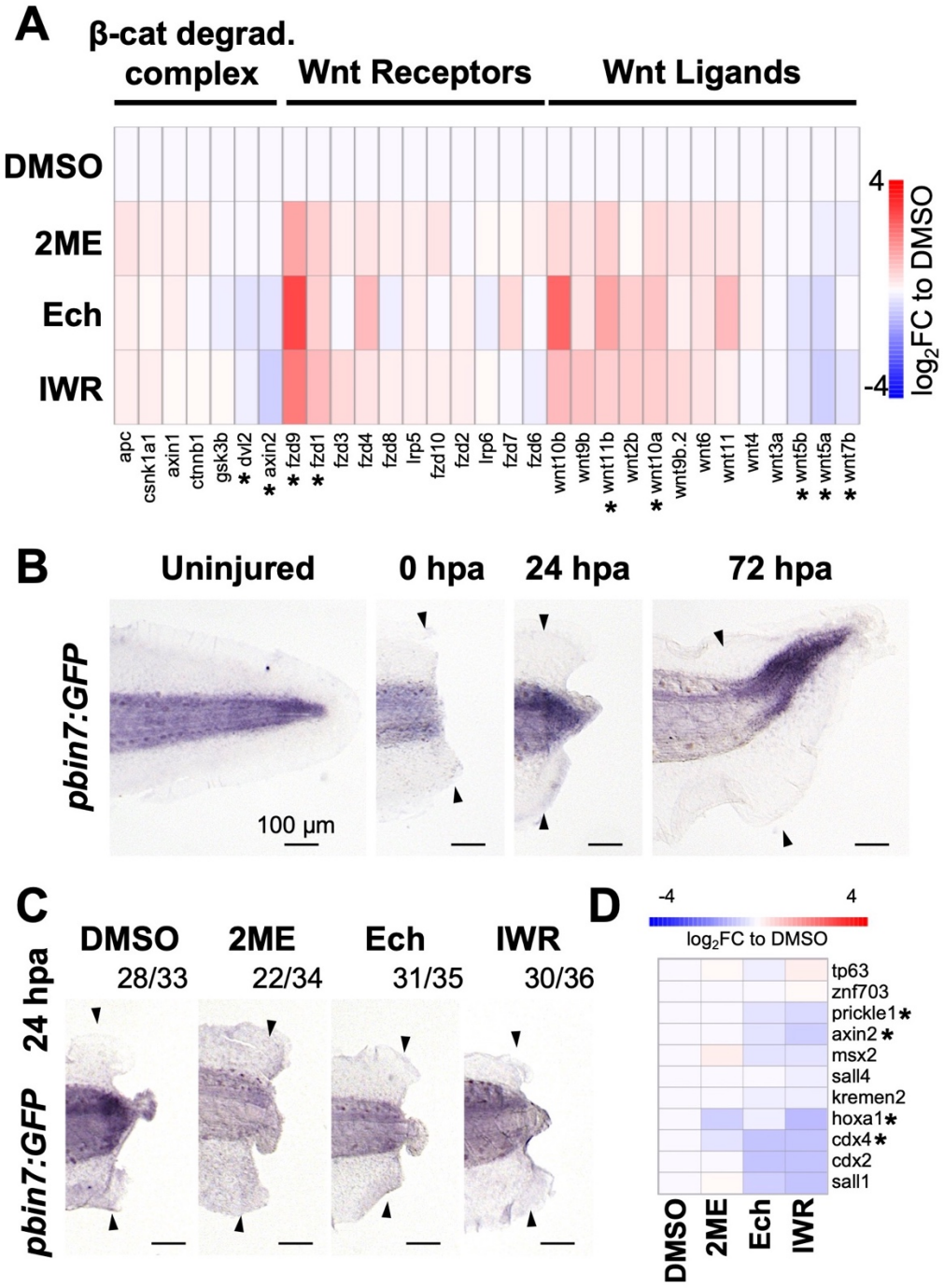

Figure 4-6: **Hif1α directs WRE activity in regeneration**

A) Heatmap displaying genes of the Wnt signaling pathway ordered by expression in IWR and sorted by position in pathway. Genes differentially expressed in all treatments are indicated by *. B) Timecourse of WRE-driven GFP transcript in *pbin7:GFP* tadpoles via *in situ hybridization*. C) Visualization of GFP transcripts at 24hpa following treatment

with DMSO, 2ME, Ech, or IWR. D) Heatmap displaying posterior neural patterning Wnt target genes. Genes differentially expressed in all treatments are indicated by *. Indicated numbers in C represent number of tails with prevented phenotype over total number assayed. Scale bars in B-C are 150μm. Arrowheads indicate amputation plane.

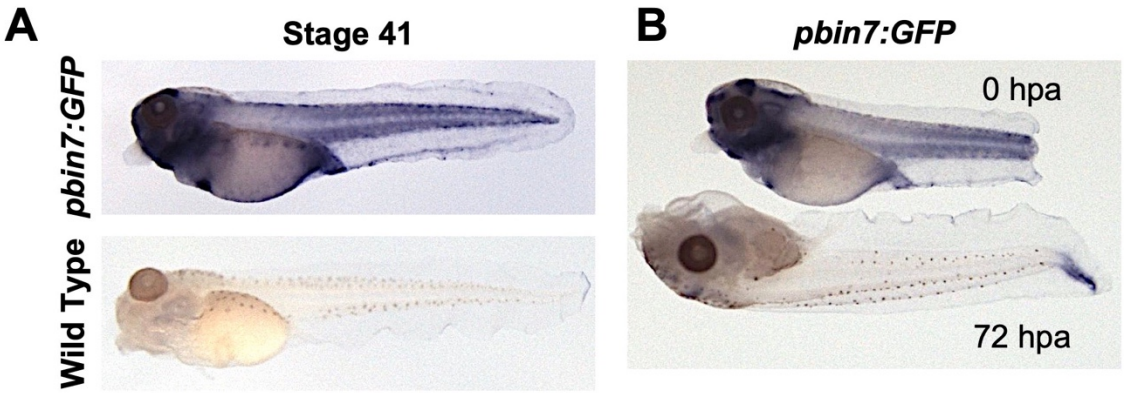

Figure 4-7: **pbin7:GFP transcripts are uniquely detected in transgenic animals and axial expression declines over regenerative time**

A) *In situ* hybridization for *pbin7:GFP* in WT and transgenic tadpoles. There is no detected transcript in the WT while the transgenic have patterns of expression as previously described. B) Expression in the whole tadpole from 0 to 72hpa. Axial staining declines broadly while staining in the regenerating tissue is prominently seen at 72hpa. Staining in the anterior tail tissue declines in the time between amputation (stage 41) and 72hpa (equivalent to stage 46). All transgenic tadpoles can be identified at NF stage 41 by staining in the brain.

4.4.6 *Hif1α regulates anteroposterior patterning during neurula stages*

Having seen that Hif1α is required during regeneration to activate expression of posterior neural Wnt targets, we asked if Hif1α modulated Wnt-mediated gene expression in other contexts. First, we confirmed that inhibiting translation of Hif1α resulted in the same inhibition of regeneration as pharmacological Hif1α inhibition. To do this, we first examined regeneration in tadpoles that were injected with a *hif1α*

translation blocking morpholino (MO). Using a unilateral injection strategy, we confirmed that our MO caused the same developmental effects as previously reported for Hif1α, specifically a reduction in the migration of cranial neural crest on the injected side relative to the contralateral control (Figure 4-8A) (Barriga et al., 2013). At stage 41, amputation of the tail resulted in minimal regeneration compared to controls (Figure 4-8B, D, E). We noted Hif1α morphants had shortened anterior-posterior axes at tailbud and tadpole stages. To bypass the significant early developmental effects of Hif1α depletion, we blocked Hif1α translation using tail vein injection of a vivo-morpholino (vivo-*hif1α* MO), which we utilized to inhibit Hif1α during regeneration while circumventing any developmental consequences (Kakebeen et al., 2020; Y. Liu et al., 2012). This method of Hif1α inhibition also reduced regeneration length and score (Figure 4-8C, F, G).

Because Hif1α morphants had shortened axes, we hypothesized that Hif1α might be required for proper anterior-posterior patterning in the early embryo, and specifically, might modulate Wnt-dependent gene expression in this context, as in regeneration. We therefore used unilaterally-injected Hif1α morphants to assay *pbin7:GFP* expression during embryonic neural patterning. GFP expression at stage 18 spans the posterior of the neural folds with a clear anterior boundary in agreement with previous descriptions and with the well-known function of Wnt signaling in posteriorization of the neural tube (Figure 4-8H) (Borday et al., 2018; Kiecker & Niehrs, 2001). Embryos in which *hif1α* MO was injected unilaterally showed posteriorly-shifted *pbin7:GFP* expression on the injected side. This reflects an anteriorization of that side, as would be expected for loss of Wnt-dependent transcriptional activation. To confirm this, we assayed expression of

regional neural tube markers (*sox2*, *otx2*, and *en2*) in unilaterally injected Hif1α morphants at stage 20 (Figure 4-8 H) (Brivanlou & Harland, 1989; Mancilla & Mayor, 1996; Pannese et al., 1995). *Sox2*, a pan-neural marker, is largely unaffected by *hif1α* MO, suggesting that Hif1α is not required for neural induction. However, the forebrain marker *otx2* has an expanded domain on the MO injected side, while the hindbrain marker *en2* shifted towards the posterior following *hif1α* MO injection. Both these outcomes are consistent with an anteriorization of the neural plate on the injected side. These results suggest that Hif1α is necessary for establishing posterior identity of the embryo during neurulation as well as during tail regeneration.

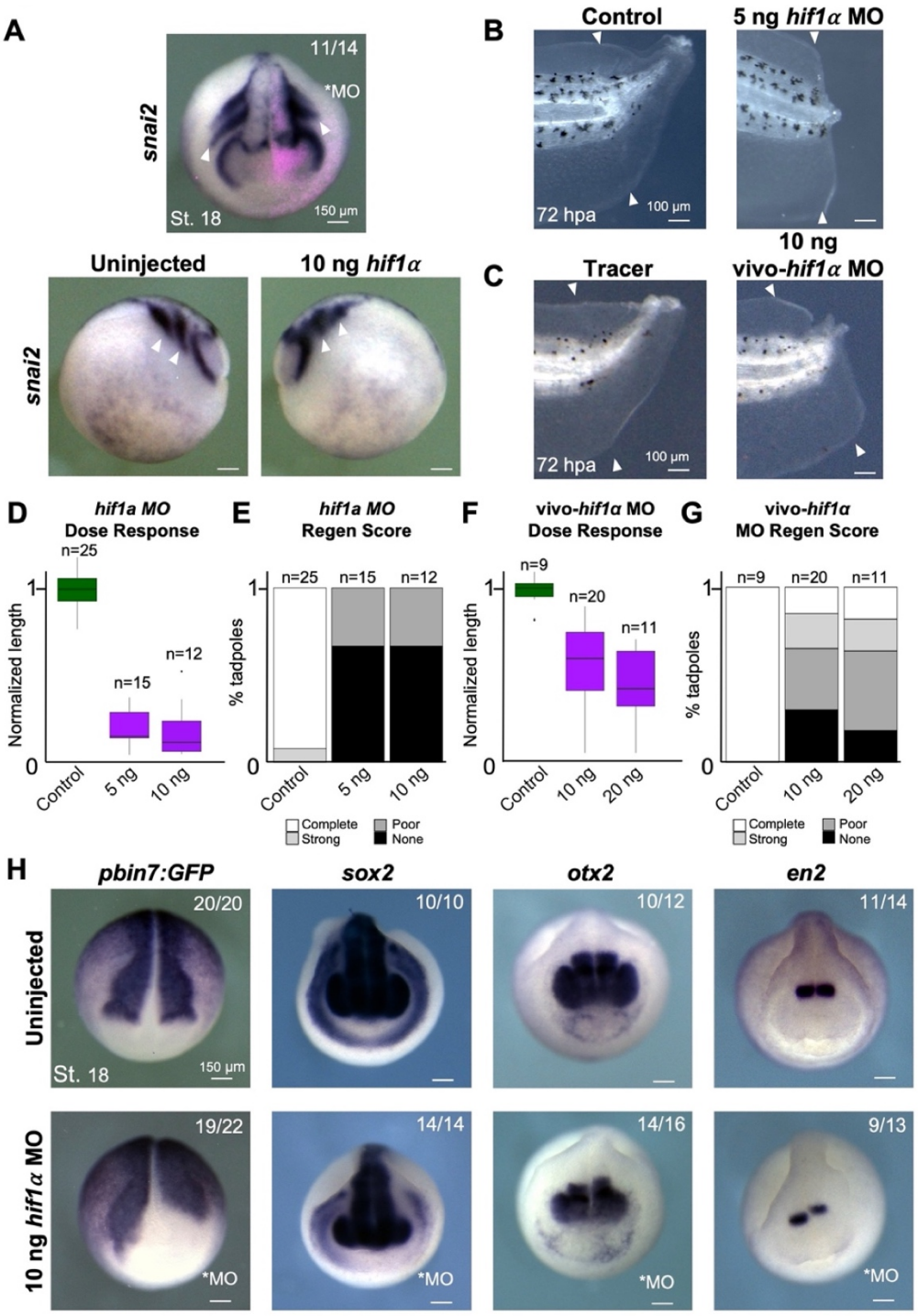

Figure 4-8: **Hif1α regulates WRE expression and AP patterning at neurula stages**

A) Dorsal and lateral views of *in situ* hybridization for *snai2* in a stage 23 embryo injected unilaterally with *hif1α* morpholino. Miniruby fluorescent tracer was used to identify the injected side (dorsal view). *snai2* expression in the migrating neural crest

streams is reduced on the injected side, noted with white arrowheads. B) Control and 5ng *hif1α* morpholino injected tails at 72hpa. C) Tracer and 10ng vivo-*hif1α* morpholino injected tails at 72hpa. D) Length of regenerated tissue normalized to average control length in control, 5ng, and 10ng *hif1α* morpholino injected tails at 72hpa. E) Regeneration score for control, 5ng, and 10ng *hif1α* morpholino injected tails at 72hpa. F) Length of regenerated tissue normalized to average tracer-only length in tracer and 10ng vivo-*hif1α* morpholino injected tails at 72hpa. G) Regeneration score for tracer-only and 10ng vivo-*hif1α* morpholino injected tails at 72hpa. Legend as in (E). H) Dorsal views of *in situ* hybridization for *pbin7:GFP*, *sox2*, *otx2*, and *en2* in stage 18-20 embryos. Uninjected controls (upper panels) and stage matched, unilaterally injected Hif1α morphants (lower panels) are shown. Morpholino injected side is marked with * in each lower panel. Scale bars in A, H are 150μm and in C,D are 100μm.

4.5 DISCUSSION

Regenerative healing requires that initial wounding signals of injury be coupled not to scarring, but to growth and patterning of new tissues. Injury-induced stresses, including ROS, bioelectrical signals, and innate immune cell recruitment, are critical to regeneration across taxa (Kakebeen & Wills, 2019; Tseng & Levin, 2008). Similarly, developmental patterning signals including Wnt, FGF, BMP, and TGF-β are required for full tail regeneration in *Xenopus* (Beck et al., 2003; Christen et al., 2003; G. Lin & Slack, 2008). In some cases, injury stresses are known to act upstream of specific growth factor pathways, as in the case of ROS, which acts upstream of FGF in *X. laevis* tail regeneration (N. R. Love et al., 2013). Still, the mechanistic link between these aspects of regeneration is not clear. Recent work has shown that Hif1α is required for regeneration in *X. laevis*, acting in the first hour after injury and responding to injury-induced hypoxia and, at least indirectly, ROS (Ferreira et al., 2018). Here we propose that Hif1α bridges injury to transcriptional remodeling during regeneration by activating a

broad suite of posterior patterning factors and regulatory elements that are also targeted by Wnt signaling.

Interactions between Hif1α and Wnt signaling have been described in several *in vitro* or *ex vivo* models. In prostate cancer cell lines and embryoid bodies, Hif1α has been shown to increase β-catenin target gene expression to drive differentiation (Luo et al., 2018; Večeřa et al., 2017). Hif1α has also been reported to be essential for transcription via Wnt-responsive elements in colon cancer cell lines (Rohwer et al., 2019). An *in vivo* model of murine muscle regeneration found that Hif1α actually represses Wnt signaling to inhibit regeneration (Majmundar et al., 2015). Our study demonstrates that Hif1α is upstream of Wnt target gene expression during both axial regeneration and early embryonic patterning.

One of the principal findings of our analysis is that the majority of *hox* genes transcriptionally upregulated during regeneration, and that this expression is reduced when either Hif1α or Wnt signaling are inhibited. Of note, *hox* gene expression in *Xenopus* does not follow typical temporal co-linearity (Kondo et al., 2017) and we find that posterior *hox* expression domains are largely overlapping in the tail (Figure 4-5 E). Previous work has found that several *hox* genes, including *hoxc10* and *hoxd13*, are activated in regenerating limbs and tails in *Xenopus,* and Hoxc13 orthologs are also required for regeneration in the zebrafish tail fin (Thummel et al., 2007). It has also been proposed that ectopic *hox* gene expression many contribute to homeotic transformation of regenerating tails into limbs in *Rana temporaria* via retinyl palmitate (Christen et al., 2003; Maden, 1993). These observations could point to a mechanism in which regenerating tissues re-establish positional identity through *hox* gene expression, and

our results suggest that Hif1α and Wnt are both required for this positional mapping in the regenerating tail. Our data further support that Hif1α activates other posteriorizing genes in regeneration, including FGF, *cdx*, and *sal* family members, which are known to be regulated by Wnt signaling. We also find that Hif1α depletion anteriorizes the neural tube, suggesting that tail regeneration could be recapitulating the developmental gene expression programs used during embryonic regionalization. Our study does not preclude the possibility that other developmental pathways, such as FGF and retinoic acid signaling, are also involved in establishing posterior identify, but we propose that interactions between Hif1α and Wnt signaling help drive this process.

The specific mechanism by which Hif1α and Wnt signaling converge on shared gene targets is not yet clear, and our work is consistent with several possibilities. While our RNASeq data suggest that Hif1α inhibition does not lead to transcriptional downregulation of most Wnt ligands, receptors, or effector proteins, it remains possible that Hif1α could be contributing to Wnt target regulation through alterations in the stability, localization, or longevity of any of these components. Our finding that Hif1α is required for TCF/LEF reporter expression suggests that Hif1α does have a specific effect on transcriptional regulation at Wnt reporter elements. However, this could be mediated by direct binding of Hif1α at these sites, as is the case in colon cancer (Rohwer et al., 2019), or by Hif1α forming a complex with β-catenin or TCF, or by indirectly enhancing the ability of β-catenin to activate these sites. We are eager to pursue these possibilities further.

Our study expands the range of processes and genes known to be targeted by Hif1α in *Xenopus*, where it was previously known to regulate heart development, neural

crest migration, and redox balance after injury (Barriga et al., 2013; Ferreira et al., 2018; Nagao et al., 2008). That Hif1α is capable of interacting with Wnt signaling is not a new premise, but here we show that Hif1α can activate canonically Wnt-dependent gene expression during vertebrate regeneration as well as embryonic neural pattering. Further, we demonstrate that Hif1α is essential for establishing muscle and neural tissue in the regenerating tail. Finally, our work introduces the possibility that other Wnt dependent processes may be coregulated by Hif1α, providing another level of regulation to the establishment of embryonic gradients and cell fate branches.

4.6 Acknowledgements

We thank members of the Wills lab and Dana Miller (University of Washington) for thoughtful discussion throughout the course of this work. We thank Mustafa Khokha's group for gifting the *pbin7:GFP* transgenics used in this work and Richard Harland's group for 12/101 antibody and plasmids for *in situ* probes. We acknowledge Xenbase (www.xenbase.org) for staging, gene expression resources, and genomic reference material consulted throughout this work. JHP was supported by the Cellular and Molecular Biology Training Grant PHS NRSA T32GM007270 from NIGMS as well as National Science Foundation Graduate Research Fellowship under Grant No. DGE-1762114. This work was supported by R01NS099124 from NINDS to AEW.

Chapter 5. CONCLUSIONS

Thus far, I have described my efforts to identify key steps in injury response which guide regenerative outcomes in *X. tropicalis* tail regeneration. My initial interest in this work stemmed from a traditional developmental biology perspective: how does an injured tissue determine what cell and tissue types need to be made and how does it make them. This was driven by a focus on transcriptional regulation, though 2 of the 3 experimental chapters of this work notably lack a focus on gene expression. Over the course of my work, my questions and methodology shifted from this question of differentiation towards a more fundamental question: how a tissue knows if it can and should attempt to regenerate. In my work I have been able to highlight 3 key steps in injury response that are required to start a regenerative response. First, the presence of sufficient nutrient stores to fuel growth must be evaluated at the time of injury to initiate regeneration. Then, tissue growth must be supported with a required metabolic shift of glucose towards the PPP to generate building blocks for proliferation. Finally, early injury cues must be transduced through Hif1α to reestablish posterior positional identity to regenerate the tail. These findings are substantial not only in their relevance to regeneration, but also reveal mechanisms which are broadly relevant to developmental and cell biological processes. Here, I will place the major findings of my work into a broader context and describe new avenues of study that stem from these discoveries.

5.1 THE REFRACTORY PERIOD: CAUTIONS FOR USE OF A POWERFUL SYSTEM

As explored in Chapter 2, *Xenopus tropicalis* have a regenerative refractory period, or a brief window of development in which they lose regenerative potential

before regaining it. This was among the first questions I set out to address when I began my thesis work. This feature of *Xenopus laevis* regenerative capacity was a huge lure in that it allowed prior studies to not only have a rapid model to break regeneration, but by waiting just 2-3 days, it was possible to identify factors which were sufficient to restore regeneration (Barker & Beck, 2009; Beck et al., 2003; Fukazawa et al., 2009). Anecdotally, we had seen similar results in our own lab, but careful characterization of a similar phenomenon was a critical first step. We expected similar results between the relatives, *X. laevis* and *X. tropicalis*, and were quite surprised by our findings. Unlike in *X. laevis*, we find that *X. tropicalis* have a gradual loss of regenerative potential rather than the more stark loss seen in *X. laevis* (Beck et al., 2003; Wang & Shi, 2021).

This result has actually been somewhat contentious however, as another group recently published a study describing the absence of a refractory period in *X. tropicalis* (Wang & Shi, 2021). For use as an experimental tool, we must understand what the origin of this discrepancy is. In correspondence with Dr. Shi at the NIH, we identified a major difference in husbandry practices. In Dr. Shi's lab, tadpoles are immediately fed starting at stage 45, a practice that is not common in our lab. In fact, feeding tadpoles at stage 45 in our hands often leads to death so we carefully designed a feeding regimen that allowed us to test the impacts of eating on our refractory period. This experiment revealed that feeding prior to injury at stage 47 (at stage 46) was sufficient to enable regeneration, but not when feeding was initiated after (Figure 2-11 B-C). These series of experiments in tandem highlight several key points:

1. In *X. laevis*, feeding is not sufficient to cause regeneration. In the study by Wang and Shi, *X. laevis* did not regenerate while *X. tropicalis* did under

presumably similar husbandry conditions. This suggests that our findings about nutrient sensing in *X. tropicalis* may not hold in both species, though this remains to be tested.

2. The specifics of the experiments done in our study and the other both agree that regeneration is possible in *X. tropicalis* under what we identify as refractory conditions, specifically with the constraint that feeding is abundant prior to injury.

3. Husbandry conditions are an important component of experimental systems and should be well documented in studies. This also highlights that the use of proper controls and interpreting results in the context of known biological variables is vital, as both of these studies draw appropriate conclusions from their respective experiments.

4. To reiterate the importance of husbandry conditions, I would like to highlight 2 recent studies in *X. laevis* that examine the contributions of the microbiome to the refractory period. In these studies, it was found that the absence of antibiotics *X. laevis* tadpoles actually regenerate relatively well (Beck et al., 2003; Bishop & Beck, 2021; Chapman et al., 2022). This is just another example of how a change in rearing can have dramatic effects on phenotypes and why we must be diligent in including these details for reproducibility.

Some of this remains speculation, of course, as we would need to compare results of refractory experiments between labs using multiple husbandry conditions. This experiment, provided it was well controlled, would be a valuable addition to the field and help to generate a standard refractory period that could be leveraged for powerful

rescue assays. I will note here, that prior studies which make use of the refractory period to identify factors sufficient for regeneration usually include controls (refractory tadpoles that fail to regenerate). By restoring regeneration under non-regenerative conditions, we can determine pathways able to rescue regeneration despite potential caveats in rearing conditions, though a field standard for the refractory period would be incredibly helpful to cementing this tool in *Xenopus* regeneration research.

5.2 WNT IS HAPPENING: HIF1α'S UNIQUE FUNCTIONS IN DEVELOPMENT

As part of my characterization of Hif1α in regeneration presented in Chapter 4, I initially began by inhibiting Hif1α with a translation blocking morpholino (MO). Previous work had identified some requirements for Hif1α in neural crest migration as well as in cardiac development in *X. laevis* (Barriga et al., 2013; Nagao et al., 2008). These studies did not describe major developmental consequences of Hif1α inhibition outside of their cell types of interest; however, my own experiments in *X. tropicalis* revealed major axis specification phenotypes. As described in Chapter 4, Hif1α inhibition results in anteriorization of embryos, consistent with loss of Wnt phenotypes (Figure 4-8 H). While this phenotype, and similar regulation of posterior fates in regeneration, is discussed in this text, the ability of Hif1α to direct fate is not among its most well-known functions (Masoud & Li, 2015). This leads to the important question: if Hif1α is capable of regulating Wnt targets during these 2 developmental contexts, is this interaction used in other instances? In brief, the answer is yes. In collaboration with Mustafa Khokha's Lab at Yale, I have helped to identify a novel role for Hif1α in dorsoventral patterning. To highlight my contribution to this work, currently being reviewed for publication, I was able to show that activation of Hif1α is able to drive an increase in dorsal organizer gene

expression. In these experiments, I adapted a hypoxic chamber system to be compatible with aquatic organisms and exposed embryos to 0.5% O_2 from the 8-cell stage to gastrula (stage 10.5) (Fawcett et al., 2012). This treatment serves to activate Hif1α and I found that this leads to an expansion of the dorsal organizer, a phenotype usually associated with increased Wnt activity (Figure 5-1). Further, when Wnt signaling is blocked using a *β-catenin* MO, organizer gene expression is lost confirming that the organizer genes, *goosecoid* (*gsc*) and *chordin* (*chr*), are β-catenin targets. Of note, exposure to hypoxia is sufficient to rescue expression of these targets in β-catenin morphants, further supporting the model that Hif1α is capable of regulating β-catenin targets in diverse developmental contexts.

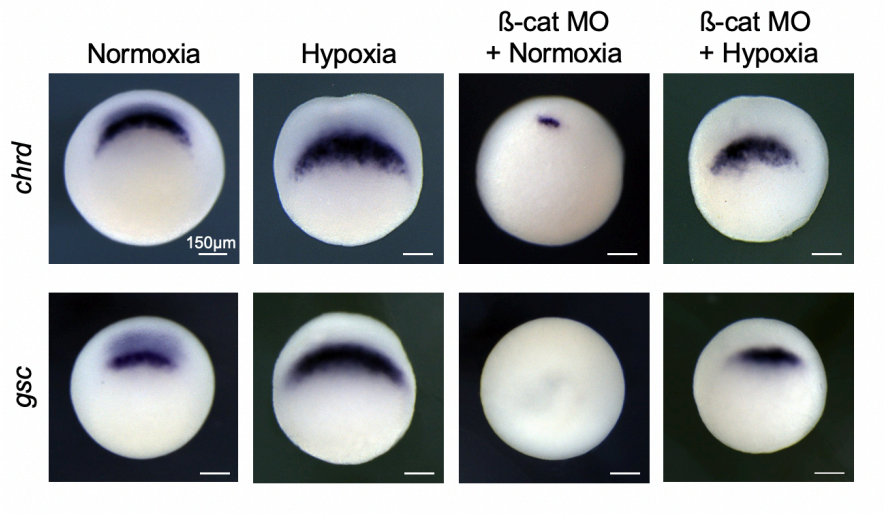

Figure 5-1: **Hypoxia is capable of activating dorsal organizer gene expression in the absence of β-catenin**
Expression of dorsal organizer genes (*chrd* and *gsc*) in stage 10.5 embryos following normoxic or hypoxic exposure starting at the 8-cell stage. Embryos were either uninjected or injected with 20 ng of *β-catenin* (*β-cat*) MO (tttcaaccgtttccaaagaaccagg).

As Wnt signaling via β-catenin is a key player in many other developmental processes, one standing question is how different Wnt target genes get activated in

different contexts. As β-catenin is a major transcriptional regulator of Wnt signaling, prior work has aimed to identify Wnt targets by looking for β-catenin binding (Kjolby & Harland, 2017; Nakamura et al., 2016). One could imagine that regulation of Wnt targets is facilitated by a combination of β-catenin binding and access to these occupancy sites via differences in chromatin accessibility in different cell types. However, recent evidence suggests that occupancy alone is not sufficient to explain transcriptional output, so further fine tuning must occur downstream (Nakamura et al., 2016). Attractive options for this downstream regulation are secondary transcriptional regulators, either co-factors in the β-catenin/TCF/LEF complex or other transcription factors with unique binding elements that can attenuate target transcription. My work presents Hif1α as a potential candidate to modulate Wnt signaling in a context dependent manner.

To determine this, we must first determine which specific developmental processes Hif1α is capable of modulating Wnt target genes and if there are specific instances where this regulation model does not hold. For instance, both Hif1α and Wnt signaling are required for neural crest migration, but it is not clear if they are required to activate shared or distinct transcriptional targets (Barriga et al., 2013; Maj et al., 2016). Additionally, Hif1α has specifically been shown to inhibit, rather than promote, Wnt signaling in skeletal muscle myogenesis, though if this is a direct link between the two has not yet been explored (Majmundar et al., 2015). Using these different developmental processes, we can start to interrogate the mechanism of Wnt/Hif1α interaction more closely. Specifically, it would be highly informative to query direct binding of Hif1α to TCF/LEF and β-catenin during processes where we can functionally

confirm shared targets to see if Hif1α is a cofactor in the complex. This is a particularly important experiment in light of my gastrula experiments, which suggest that Hif1α is capable of activating β-catenin targets in the absence of β-catenin, suggesting that these targets either have Hif1α responsive promoters or that Hif1α is activating the TCF/LEF complex. Prior studies have shown that Hif1α is capable of binding to TCF4 in competition with β-catenin in colorectal cancers while Hif1α instead promotes β-catenin nuclear import in prostate cancers, leaving binding of Hif1α to either component an attractive model for gene regulation (Kaidi et al., 2007; Luo et al., 2018). Using healthy, developmental models to determine the extent to which these different modes of Wnt modulation by Hif1α could be implemented and if these are dictated by physiological stresses (hypoxia, mitochondrial stress, etc.) would help add a new layer to our understanding of how development is fine-tuned and how a limited number of signaling pathways are robustly utilized to give rise to complex organisms.

5.3 METABOLIC REGULATION BY HIF1α IN DEVELOPMENT AND REGENERATION

Hif1α is generally considered to be a key component of stress response and regulation of tissue homeostasis; described functions of this transcription factor include modulation of proliferation and apoptosis, angiogenesis and vascularization, inflammatory signaling, and energy metabolism (Masoud & Li, 2015). As these processes are vital in a regenerative response, we expect that Hif1α may serve both to regulate tissue homeostasis and posterior gene expression in the regenerating *Xenopus* tail. In other contexts, such as pancreatic cancer cell lines and hematopoetic cells, Hif1α specifically regulates expression of *Idha* to increase glucose consumption and leads to a Warburg-like metabolic state (Cui et al., 2017; Lum et al., 2007). Preliminary

exploration of glycolytic genes during regeneration, however, does not show a clear reduction after inhibition of Hif1α (see Figure 5-2). Most notably, *ldha*, which was among the first glycolytic genes shown to be directly activated by Hif1α, shows no change in either of the 2 inhibitors treatments (Semenza et al., 1996). These findings suggest that while Hif1α is required in regeneration, it may actually have a stronger impact on fate regulation, as discussed in Chapter 4, than on homeostasis. This result is somewhat confounded by the major premise of Chapter 3, that glycolytic metabolism is not prioritized during regeneration. As glycolytic gene expression largely does not seem to be increased at 24hpa in our regeneration model, it is difficult to say if Hif1α could regulate glucose metabolism in other regenerative contexts in *Xenopus*. For instance, in limb regeneration or regeneration post-refractory period, when tadpoles are feeding and nutrient state is highly different than the stages discussed here, it is possible that Hif1α serves a dual role in patterning and metabolic regulation. In either case, this would be interesting for not only a greater understanding of the unique role of Hif1α in regeneration but also as we consider how metabolic changes are facilitated in regeneration.

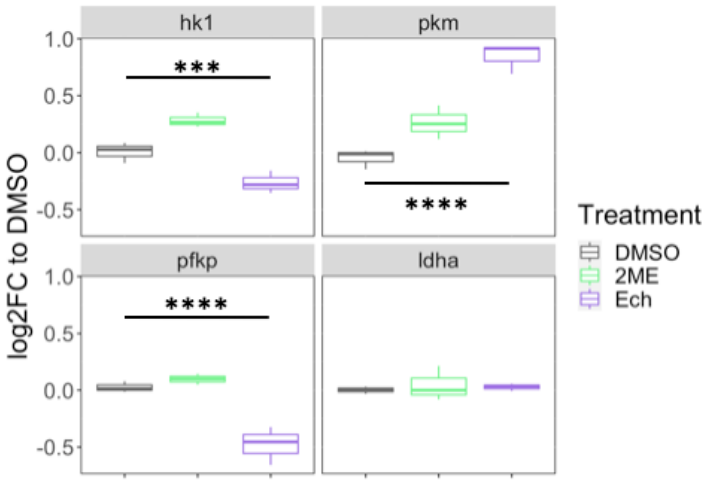

Figure 5-2: **Hif1α inhibition does not reduce glycolytic gene expression in regeneration**
Expression of glycolytic genes at 24hpa following treatment with 0.1% DMSO, 5μM 2ME, or 0.5μM echinomycin. log_2FC relative to 0hpa mean. Statistical significance was determined using EdgeR. *** indicates p<0.001; **** indicates p<0.0001.

5.4 METABOLIC REGULATION BY NON-TRANSCRIPTIONAL MECHANISMS

As I have viewed metabolic regulation largely through the lens of transcription in the preceding section, I find it prudent to note that metabolic changes are often regulated at the reaction level. While prior transcriptomic studies in *Xenopus* have suggested there are metabolic shifts that occur following injury based on changes in gene expression, there are some processes which would not become apparent by these strategies (Chang et al., 2017; N. R. Love et al., 2011, 2014). For instance, pyruvate kinase (PKM) is a major glycolytic enzyme with 2 isoforms. PKM1 is often associated with progression of glycolysis; however, PKM2 modulation at the protein level impacts the rate of glycolysis (Dayton et al., 2016; Zhang et al., 2019). By modulating PKM2 activity, metabolic changes in the cell can be used to rapidly address physiological stresses. Reactive oxygen species (ROS), which are induced by injury and

mitochondrial stress, are known to inhibit PKM2, leading to a diversion of glucose into the PPP (Anastasiou et al., 2011). Increased PPP activity allows for an increase in reducing agents needs to suppress ROS, thereby creating a highly responsive regulatory loop for control of ROS levels in cells via metabolic regulation of PKM. This particular mechanism is a compelling target for regeneration as induction and maintenance of ROS are required for regeneration in multiple systems (Ferreira et al., 2018; N. R. Love et al., 2013; Pirotte et al., 2015; M. M. G. Romero et al., 2018), but unchecked ROS damage membranes, DNA, and protein homeostasis (Schieber & Chandel, 2014). Perhaps the ROS induced by injury inhibit PKM2 activity driving a shift towards the PPP as described in Chapter 3. This could then help to maintain an instructive but non-toxic level of ROS through regeneration by generating reducing potential and also driving increased proliferation via nucleotide and fatty acid precursor generation. To really tease this apart, we would need to be able to delineate if NAPDH, a primary product of the PPP, is serving to reduce glutathione or if it is fueling ROS synthesis via NADPH oxidase activity (Bhowmick & Sarkar, 2020). If metabolic shifts in regeneration are regulated by available metabolites and cellular stressors, it is possible that these variables can be treated following injury to promote regeneration in non-regenerative systems.

The findings of my thesis work highlight that regenerative outcomes are largely dictated by programs initiated at injury. By understanding checkpoints that enable regeneration, we can start to think about generating regenerative permissive environments in scar-forming injury models. *Xenopus tropicalis* is a system which is amenable to new techniques and assays which make it a powerful model for these

types of studies moving forward, and the datasets generated in this body of work can be leveraged to generate new hypothesis for testing. While many questions remain thinking about processes that drive regeneration, I am particularly excited about future work that considers transcription-independent mechanisms for wound healing and those at the intersection of gene regulation and physiology.

Chapter 6. BIBLIOGRAPHY

Abdel-Haleem, A. M., Lewis, N. E., Jamshidi, N., Mineta, K., Gao, X., & Gojobori, T. (2017). The Emerging Facets of Non-Cancerous Warburg Effect. *Frontiers in Endocrinology*, *8*, 279. https://doi.org/10.3389/fendo.2017.00279

Adams, D. S., Masi, A., & Levin, M. (2007). H+ pump-dependent changes in membrane voltage are an early mechanism necessary and sufficient to induce *Xenopus* tail regeneration. *Development*, *134*(7), 1323–1335. https://doi.org/10.1242/dev.02812

Agathocleous, M., Love, N. K., Randlett, O., Harris, J. J., Liu, J., Murray, A. J., & Harris, W. A. (2012). Metabolic differentiation in the embryonic retina. *Nature Cell Biology*, *14*(8), 859–864. https://doi.org/10.1038/ncb2531

Anastasiou, D., Poulogiannis, G., Asara, J. M., Boxer, M. B., Jiang, J., Shen, M., Bellinger, G., Sasaki, A. T., Locasale, J. W., Auld, D. S., Thomas, C. J., Vander Heiden, M. G., & Cantley, L. C. (2011). Inhibition of Pyruvate Kinase M2 by Reactive Oxygen Species Contributes to Cellular Antioxidant Responses. *Science*, *334*(6060), 1278–1283. https://doi.org/10.1126/science.1211485

Aztekin, C., Hiscock, T. W., Butler, R., De Jesús Andino, F., Roberts, J., Gurdon, J. B., & Jullien, J. (2020). The myeloid lineage is required for the emergence of a regeneration permissive environment following *Xenopus* tail amputation. *Development*, dev.185496. https://doi.org/10.1242/dev.185496

Aztekin, C., Hiscock, T. W., Marioni, J. C., Gurdon, J. B., Simons, B. D., & Jullien, J. (2019). Identification of a regeneration-organizing cell in the *Xenopus* tail. *Science*, *364*(6441), 653–658. https://doi.org/10.1126/science.aav9996

Barker, D. M., & Beck, C. W. (2009). Overexpression of the transcription factor Msx1 is insufficient to drive complete regeneration of refractory stage *Xenopus laevis* hindlimbs. *Developmental Dynamics*, *238*(6), 1366–1378. https://doi.org/10.1002/dvdy.21923

Barriga, E. H., Maxwell, P. H., Reyes, A. E., & Mayor, R. (2013). The hypoxia factor Hif-1α controls neural crest chemotaxis and epithelial to mesenchymal transition. *The Journal of Cell Biology*, *201*(5), 759–776. https://doi.org/10.1083/jcb.201212100

Beck, C. W. (2012). Studying Regeneration in Xenopus. In S. Hoppler & P. D. Vize (Eds.), *Xenopus Protocols* (Vol. 917, pp. 525–539). Humana Press. https://doi.org/10.1007/978-1-61779-992-1_30

Beck, C. W., Belmonte, J. C. I., & Christen, B. (2009). Beyond early development: Xenopus as an emerging model for the study of regenerative mechanisms. *Developmental Dynamics*, *238*(6), 1226–1248. https://doi.org/10.1002/dvdy.21890

Beck, C. W., Christen, B., & Slack, J. M. W. (2003). Molecular Pathways Needed for Regeneration of Spinal Cord and Muscle in a Vertebrate. *Developmental Cell*, *5*(3), 429–439. https://doi.org/10.1016/S1534-5807(03)00233-8

Beck, C. W., Whitman, M., & Slack, J. M. W. (2001). The Role of BMP Signaling in Outgrowth and Patterning of the Xenopus Tail Bud. *Developmental Biology*, *238*(2), 303–314. https://doi.org/10.1006/dbio.2001.0407

Bender, M. C., Sifuentes, C. J., & Denver, R. J. (2017). Leptin Induces Mitosis and Activates the Canonical Wnt/β-Catenin Signaling Pathway in Neurogenic Regions of Xenopus Tadpole Brain. *Frontiers in Endocrinology*, *8*, 99. https://doi.org/10.3389/fendo.2017.00099

Bhowmick, R., & Sarkar, R. R. (2020). Differential suitability of reactive oxygen species and the role of glutathione in regulating paradoxical behavior in gliomas: A mathematical perspective. *PLOS ONE*, *15*(6), e0235204. https://doi.org/10.1371/journal.pone.0235204

Bishop, T. F., & Beck, C. W. (2021). Bacterial lipopolysaccharides can initiate regeneration of the Xenopus tadpole tail. *IScience*, *24*(11), 103281. https://doi.org/10.1016/j.isci.2021.103281

Borday, C., Parain, K., Thi Tran, H., Vleminckx, K., Perron, M., & Monsoro-Burq, A. H. (2018). An atlas of Wnt activity during embryogenesis in Xenopus tropicalis. *PLOS ONE*, *13*(4), e0193606. https://doi.org/10.1371/journal.pone.0193606

Bowes, J. B., Snyder, K. A., Segerdell, E., Jarabek, C. J., Azam, K., Zorn, A. M., & Vize, P. D. (2010). Xenbase: Gene expression and improved integration. *Nucleic Acids Research*, *38*(Database issue), D607-612. https://doi.org/10.1093/nar/gkp953

Bray, N. L., Pimentel, H., Melsted, P., & Pachter, L. (2016). Near-optimal probabilistic RNA-seq quantification. *Nature Biotechnology*, *34*(5), 525–527. https://doi.org/10.1038/nbt.3519

Brivanlou, A. H., & Harland, R. M. (1989). Expression of an engrailed-related protein is induced in the anterior neural ectoderm of early Xenopus embryos. *Development (Cambridge, England)*, *106*(3), 611–617.

Bulusu, V., Prior, N., Snaebjornsson, M. T., Kuehne, A., Sonnen, K. F., Kress, J., Stein, F., Schultz, C., Sauer, U., & Aulehla, A. (2017). Spatiotemporal Analysis of a Glycolytic Activity Gradient Linked to Mouse Embryo Mesoderm Development. *Developmental Cell*, *40*(4), 331-341.e4. https://doi.org/10.1016/j.devcel.2017.01.015

Cao, J., Spielmann, M., Qiu, X., Huang, X., Ibrahim, D. M., Hill, A. J., Zhang, F., Mundlos, S., Christiansen, L., Steemers, F. J., Trapnell, C., & Shendure, J. (2019). The single-cell

transcriptional landscape of mammalian organogenesis. *Nature*, *566*(7745), 496–502. https://doi.org/10.1038/s41586-019-0969-x

Carro, E., Señaris, R., Considine, R. V., Casanueva, F. F., & Dieguez, C. (1997). Regulation of in vivo growth hormone secretion by leptin. *Endocrinology*, *138*(5), 2203–2206. https://doi.org/10.1210/endo.138.5.5238

Carron, C., & Shi, D. (2016). Specification of anteroposterior axis by combinatorial signaling during *Xenopus* development. *WIREs Developmental Biology*, *5*(2), 150–168. https://doi.org/10.1002/wdev.217

Chamorro, M. N., Schwartz, D. R., Vonica, A., Brivanlou, A. H., Cho, K. R., & Varmus, H. E. (2005). FGF-20 and DKK1 are transcriptional targets of β-catenin and FGF-20 is implicated in cancer and development. *The EMBO Journal*, *24*(1), 73–84. https://doi.org/10.1038/sj.emboj.7600460

Chang, J., Baker, J., & Wills, A. (2017). Transcriptional dynamics of tail regeneration in *Xenopus tropicalis*: CHANG et al. *Genesis*, *55*(1–2), e23015. https://doi.org/10.1002/dvg.23015

Chantranupong, L., Wolfson, R. L., & Sabatini, D. M. (2015). Nutrient-Sensing Mechanisms across Evolution. *Cell*, *161*(1), 67–83. https://doi.org/10.1016/j.cell.2015.02.041

Chapman, P. A., Gilbert, C. B., Devine, T. J., Hudson, D. T., Ward, J., Morgan, X. C., & Beck, C. W. (2022). Manipulating the microbiome alters regenerative outcomes in *Xenopus laevis* tadpoles via lipopolysaccharide signalling. *Wound Repair and Regeneration*, wrr.13003. https://doi.org/10.1111/wrr.13003

Chen, B., Dodge, M. E., Tang, W., Lu, J., Ma, Z., Fan, C.-W., Wei, S., Hao, W., Kilgore, J., Williams, N. S., Roth, M. G., Amatruda, J. F., Chen, C., & Lum, L. (2009). Small

molecule–mediated disruption of Wnt-dependent signaling in tissue regeneration and cancer. *Nature Chemical Biology*, *5*(2), 100–107. https://doi.org/10.1038/nchembio.137

Chen, E. Y., Fujinaga, M., & Giaccia, A. J. (1999). Hypoxic microenvironment within an embryo induces apoptosis and is essential for proper morphological development. *Teratology*, *60*(4), 215–225. https://doi.org/10.1002/(SICI)1096-9926(199910)60:4<215::AID-TERA6>3.0.CO;2-2

Child, C. M. (1913). Studies on the dynamics of morphogenesis and inheritance in experimental reproduction. V. The relation between resistance to depressing agents and rate of metabolism in Planaria dorotocephala and its value as a method of investigation. *Journal of Experimental Zoology*, *14*(2), 153–206. https://doi.org/10.1002/jez.1400140202

Chou, Y.-Y., Gao, J.-I., Chang, S.-F., Chang, P.-Y., & Lu, S.-C. (2011). Rapamycin inhibits lipopolysaccharide induction of granulocyte-colony stimulating factor and inducible nitric oxide synthase expression in macrophages by reducing the levels of octamer-binding factor-2: Rapamycin inhibits LPS-induced G-CSF and iNOS expression. *FEBS Journal*, *278*(1), 85–96. https://doi.org/10.1111/j.1742-4658.2010.07929.x

Christen, B., Beck, C. W., Lombardo, A., & Slack, J. M. W. (2003). Regeneration-specific expression pattern of three posterior Hox genes. *Developmental Dynamics: An Official Publication of the American Association of Anatomists*, *226*(2), 349–355. https://doi.org/10.1002/dvdy.10231

Crespi, E. J., & Denver, R. J. (2006). Leptin (ob gene) of the South African clawed frog Xenopus laevis. *Proceedings of the National Academy of Sciences of the United States of America*, *103*(26), 10092–10097. https://doi.org/10.1073/pnas.0507519103

Cui, X.-G., Han, Z.-T., He, S.-H., Wu, X., Chen, T.-R., Shao, C.-H., Chen, D.-L., Su, N., Chen, Y.-M., Wang, T., Wang, J., Song, D.-W., Yan, W.-J., Yang, X.-H., Liu, T., Wei, H.-F., & Xiao, J. (2017). HIF1/2α mediates hypoxia-induced LDHA expression in human pancreatic cancer cells. *Oncotarget*, *8*(15), 24840–24852. https://doi.org/10.18632/oncotarget.15266

Dai, W., Meng, X., Mo, S., Xiang, W., Xu, Y., Zhang, L., Wang, R., Li, Q., & Cai, G. (2020). FOXE1 represses cell proliferation and Warburg effect by inhibiting HK2 in colorectal cancer. *Cell Communication and Signaling*, *18*(1), 7. https://doi.org/10.1186/s12964-019-0502-8

Davies, M. R., Liu, X., Lee, L., Laron, D., Ning, A. Y., Kim, H. T., & Feeley, B. T. (2016). TGF-β Small Molecule Inhibitor SB431542 Reduces Rotator Cuff Muscle Fibrosis and Fatty Infiltration By Promoting Fibro/Adipogenic Progenitor Apoptosis. *PLOS ONE*, *11*(5), e0155486. https://doi.org/10.1371/journal.pone.0155486

Dayton, T. L., Jacks, T., & Vander Heiden, M. G. (2016). PKM2, cancer metabolism, and the road ahead. *EMBO Reports*, *17*(12), 1721–1730. https://doi.org/10.15252/embr.201643300

de la Cruz-López, K. G., Castro-Muñoz, L. J., Reyes-Hernández, D. O., García-Carrancá, A., & Manzo-Merino, J. (2019). Lactate in the Regulation of Tumor Microenvironment and Therapeutic Approaches. *Frontiers in Oncology*, *9*, 1143. https://doi.org/10.3389/fonc.2019.01143

De Bock, K., Georgiadou, M., Schoors, S., Kuchnio, A., Wong, B. W., Cantelmo, A. R., Quaegebeur, A., Ghesquière, B., Cauwenberghs, S., Eelen, G., Phng, L.-K., Betz, I., Tembuyser, B., Brepoels, K., Welti, J., Geudens, I., Segura, I., Cruys, B., Bifari, F., …

Carmeliet, P. (2013). Role of PFKFB3-Driven Glycolysis in Vessel Sprouting. *Cell*, *154*(3), 651–663. https://doi.org/10.1016/j.cell.2013.06.037

Dickinson, A. J. G., & Sive, H. (2006). Development of the primary mouth in Xenopus laevis. *Developmental Biology*, *295*(2), 700–713. https://doi.org/10.1016/j.ydbio.2006.03.054

Dodd, J., & Jessell, T. (1988). Axon guidance and the patterning of neuronal projections in vertebrates. *Science*, *242*(4879), 692–699. https://doi.org/10.1126/science.3055291

Erickson, J. R., & Echeverri, K. (2018). Learning from regeneration research organisms: The circuitous road to scar free wound healing. *Developmental Biology*, *433*(2), 144–154. https://doi.org/10.1016/j.ydbio.2017.09.025

Espeillac, C., Mitchell, C., Celton-Morizur, S., Chauvin, C., Koka, V., Gillet, C., Albrecht, J. H., Desdouets, C., & Pende, M. (2011). S6 kinase 1 is required for rapamycin-sensitive liver proliferation after mouse hepatectomy. *The Journal of Clinical Investigation*, *121*(7), 2821–2832. https://doi.org/10.1172/JCI44203

Fawcett, E. M., Horsman, J. W., & Miller, D. L. (2012). Creating defined gaseous environments to study the effects of hypoxia on C. elegans. *Journal of Visualized Experiments: JoVE*, *65*, e4088. https://doi.org/10.3791/4088

Ferreira, F., Raghunathan, V., Luxardi, G., Zhu, K., & Zhao, M. (2018). Early redox activities modulate Xenopus tail regeneration. *Nature Communications*, *9*(1), 4296. https://doi.org/10.1038/s41467-018-06614-2

Filoni, S., & Bosco, L. (1981). Comparative analysis of the regenerative capacity of caudal spinal cord in larvae of serveral Anuran amphibian species. *Acta Embryologiae Et Morphologiae Experimentalis ("Halocynthia" Association")*, *2*(3), 199–226.

Fingar, D. C., & Blenis, J. (2004). Target of rapamycin (TOR): An integrator of nutrient and growth factor signals and coordinator of cell growth and cell cycle progression. *Oncogene*, *23*(18), 3151–3171. https://doi.org/10.1038/sj.onc.1207542

Finnson, K. W., McLean, S., Di Guglielmo, G. M., & Philip, A. (2013). Dynamics of Transforming Growth Factor Beta Signaling in Wound Healing and Scarring. *Advances in Wound Care*, *2*(5), 195–214. https://doi.org/10.1089/wound.2013.0429

Fukazawa, T., Naora, Y., Kunieda, T., & Kubo, T. (2009). Suppression of the immune response potentiates tadpole tail regeneration during the refractory period. *Development*, *136*(14), 2323–2327. https://doi.org/10.1242/dev.033985

Galliot, B., & Ghila, L. (2010). Cell plasticity in homeostasis and regeneration. *Molecular Reproduction and Development*, *77*(10), 837–855. https://doi.org/10.1002/mrd.21206

Gat-Yablonski, G., & Phillip, M. (2015). Nutritionally-induced catch-up growth. *Nutrients*, *7*(1), 517–551. https://doi.org/10.3390/nu7010517

Gat-Yablonski, G., Shtaif, B., Abraham, E., & Phillip, M. (2008). Nutrition-induced catch-up growth at the growth plate. *Journal of Pediatric Endocrinology & Metabolism: JPEM*, *21*(9), 879–893. https://doi.org/10.1515/jpem.2008.21.9.879

Ge, Y., Wu, A.-L., Warnes, C., Liu, J., Zhang, C., Kawasome, H., Terada, N., Boppart, M. D., Schoenherr, C. J., & Chen, J. (2009). MTOR regulates skeletal muscle regeneration in vivo through kinase-dependent and kinase-independent mechanisms. *American Journal of Physiology - Cell Physiology*, *297*(6), C1434–C1444. https://doi.org/10.1152/ajpcell.00248.2009

Ghanem, N., El-Baba, C., Araji, K., El-Khoury, R., Usta, J., & Darwiche, N. (2021). The Pentose Phosphate Pathway in Cancer: Regulation and Therapeutic Opportunities. *Chemotherapy*, *66*(5–6), 179–191. https://doi.org/10.1159/000519784

Ghergurovich, J. M., García-Cañaveras, J. C., Wang, J., Schmidt, E., Zhang, Z., TeSlaa, T., Patel, H., Chen, L., Britt, E. C., Piqueras-Nebot, M., Gomez-Cabrera, M. C., Lahoz, A., Fan, J., Beier, U. H., Kim, H., & Rabinowitz, J. D. (2020). A small molecule G6PD inhibitor reveals immune dependence on pentose phosphate pathway. *Nature Chemical Biology*, *16*(7), 731–739. https://doi.org/10.1038/s41589-020-0533-x

Giguère, V. (2018). Canonical signaling and nuclear activity of mTOR-a teamwork effort to regulate metabolism and cell growth. *The FEBS Journal*, *285*(9), 1572–1588. https://doi.org/10.1111/febs.14384

Godwin, J. W., Pinto, A. R., & Rosenthal, N. A. (2013). Macrophages are required for adult salamander limb regeneration. *Proceedings of the National Academy of Sciences*, *110*(23), 9415–9420. https://doi.org/10.1073/pnas.1300290110

González-Estévez, C., Felix, D. A., Rodríguez-Esteban, G., & Aboobaker, A. A. (2012). Decreased neoblast progeny and increased cell death during starvation-induced planarian degrowth. *The International Journal of Developmental Biology*, *56*(1–3), 83–91. https://doi.org/10.1387/ijdb.113452cg

González-Estévez, C., Felix, D. A., Smith, M. D., Paps, J., Morley, S. J., James, V., Sharp, T. V., & Aboobaker, A. A. (2012). SMG-1 and mTORC1 act antagonistically to regulate response to injury and growth in planarians. *PLoS Genetics*, *8*(3), e1002619. https://doi.org/10.1371/journal.pgen.1002619

Haissaguerre, M., Saucisse, N., & Cota, D. (2014). Influence of mTOR in energy and metabolic homeostasis. *Molecular and Cellular Endocrinology*, *397*(1–2), 67–77. https://doi.org/10.1016/j.mce.2014.07.015

Haremaki, T., Tanaka, Y., Hongo, I., Yuge, M., & Okamoto, H. (2003). Integration of multiple signal transducing pathways on Fgf response elements of the Xenopus caudal homologue Xcad3. *Development*, *130*(20), 4907–4917. https://doi.org/10.1242/dev.00718

Harland, R. M., & Grainger, R. M. (2011). Xenopus research: Metamorphosed by genetics and genomics. *Trends in Genetics: TIG*, *27*(12), 507–515. https://doi.org/10.1016/j.tig.2011.08.003

Hirose, K., Shiomi, T., Hozumi, S., & Kikuchi, Y. (2014). Mechanistic target of rapamycin complex 1 signaling regulates cell proliferation, cell survival, and differentiation in regenerating zebrafish fins. *BMC Developmental Biology*, *14*(1), 42. https://doi.org/10.1186/s12861-014-0042-9

Ho, D. M., & Whitman, M. (2008). TGF-β signaling is required for multiple processes during Xenopus tail regeneration. *Developmental Biology*, *315*(1), 203–216. https://doi.org/10.1016/j.ydbio.2007.12.031

Hu, F., Xu, Y., & Liu, F. (2016). Hypothalamic roles of mTOR complex I: Integration of nutrient and hormone signals to regulate energy homeostasis. *American Journal of Physiology. Endocrinology and Metabolism*, *310*(11), E994–E1002. https://doi.org/10.1152/ajpendo.00121.2016

Hyman, L. H. (1921). THE METABOLIC GRADIENTS OF VERTEBRATE EMBRYOS. I. TELEOST EMBRYOS. *The Biological Bulletin*, *40*(1), 32–72. https://doi.org/10.2307/1536713

Hyman, L. H. (1927a). THE METABOLIC GRADIENTS OF VERTEBRATE EMBRYOS. III. THE CHICK. *The Biological Bulletin*, *52*(1), 1–38. https://doi.org/10.2307/1536828

Hyman, L. H. (1927b). THE METABOLIC GRADIENTS OF VERTEBRATE EMBRYOS. IV. THE HEART. *The Biological Bulletin*, *52*(1), 39–50. https://doi.org/10.2307/1536829

Ivankovic, M., Haneckova, R., Thommen, A., Grohme, M. A., Vila-Farré, M., Werner, S., & Rink, J. C. (2019). Model systems for regeneration: Planarians. *Development*, *146*(17), dev167684. https://doi.org/10.1242/dev.167684

Iyer, N. V., Kotch, L. E., Agani, F., Leung, S. W., Laughner, E., Wenger, R. H., Gassmann, M., Gearhart, J. D., Lawler, A. M., Yu, A. Y., & Semenza, G. L. (1998). Cellular and developmental control of O2 homeostasis by hypoxia-inducible factor 1alpha. *Genes & Development*, *12*(2), 149–162. https://doi.org/10.1101/gad.12.2.149

Jansen, H. J., Wacker, S. A., Bardine, N., & Durston, A. J. (2007). The role of the Spemann organizer in anterior–posterior patterning of the trunk. *Mechanisms of Development*, *124*(9–10), 668–681. https://doi.org/10.1016/j.mod.2007.07.004

Jiang, P., Du, W., & Yang, X. (2013). A critical role of glucose-6-phosphate dehydrogenase in TAp73-mediated cell proliferation. *Cell Cycle*, *12*(24), 3720–3726. https://doi.org/10.4161/cc.27267

Jorgensen, P., Steen, J. A. J., Steen, H., & Kirschner, M. W. (2009). The mechanism and pattern of yolk consumption provide insight into embryonic nutrition in Xenopus. *Development*, *136*(9), 1539–1548. https://doi.org/10.1242/dev.032425

Kaidi, A., Williams, A. C., & Paraskeva, C. (2007). Interaction between β-catenin and HIF-1 promotes cellular adaptation to hypoxia. *Nature Cell Biology*, *9*(2), 210–217. https://doi.org/10.1038/ncb1534

Kakanj, P., Moussian, B., Grönke, S., Bustos, V., Eming, S. A., Partridge, L., & Leptin, M. (2016). Insulin and TOR signal in parallel through FOXO and S6K to promote epithelial wound healing. *Nature Communications*, *7*(1), 1–16. https://doi.org/10.1038/ncomms12972

Kakebeen, A. D., Chitsazan, A. D., Williams, M. C., Saunders, L. M., & Wills, A. E. (2020). Chromatin accessibility dynamics and single cell RNA-Seq reveal new regulators of regeneration in neural progenitors. *ELife*, *9*. https://doi.org/10.7554/eLife.52648

Kakebeen, A. D., & Wills, A. E. (2019). More Than Just a Bandage: Closing the Gap Between Injury and Appendage Regeneration. *Frontiers in Physiology*, *10*. https://doi.org/10.3389/fphys.2019.00081

Kang, J., Hu, J., Karra, R., Dickson, A. L., Tornini, V. A., Nachtrab, G., Gemberling, M., Goldman, J. A., Black, B. L., & Poss, K. D. (2016). Modulation of tissue repair by regeneration enhancer elements. *Nature*, *532*(7598), 201–206. https://doi.org/10.1038/nature17644

Katare, R., Oikawa, A., Cesselli, D., Beltrami, A. P., Avolio, E., Muthukrishnan, D., Munasinghe, P. E., Angelini, G., Emanueli, C., & Madeddu, P. (2013). Boosting the pentose phosphate pathway restores cardiac progenitor cell availability in diabetes. *Cardiovascular Research*, *97*(1), 55–65. https://doi.org/10.1093/cvr/cvs291

Katsuyama, T., Comoglio, F., Seimiya, M., Cabuy, E., & Paro, R. (2015). During *Drosophila* disc regeneration, JAK/STAT coordinates cell proliferation with Dilp8-mediated developmental delay. *Proceedings of the National Academy of Sciences*, *112*(18). https://doi.org/10.1073/pnas.1423074112

Khokha, M. K., Chung, C., Bustamante, E. L., Gaw, L. W. K., Trott, K. A., Yeh, J., Lim, N., Lin, J. C. Y., Taverner, N., Amaya, E., Papalopulu, N., Smith, J. C., Zorn, A. M., Harland, R. M., & Grammer, T. C. (2002). Techniques and probes for the study of Xenopus tropicalis development. *Developmental Dynamics: An Official Publication of the American Association of Anatomists*, *225*(4), 499–510. https://doi.org/10.1002/dvdy.10184

Kiecker, C., & Niehrs, C. (2001). A morphogen gradient of Wnt/beta-catenin signalling regulates anteroposterior neural patterning in Xenopus. *Development (Cambridge, England)*, *128*(21), 4189–4201.

Kintner, C. R., & Brockes, J. P. (1984). Monoclonal antibodies identify blastemal cells derived from dedifferentiating muscle in newt limb regeneration. *Nature*, *308*(5954), 67–69. https://doi.org/10.1038/308067a0

Kjolby, R. A. S., & Harland, R. M. (2017). Genome-wide identification of Wnt/β-catenin transcriptional targets during Xenopus gastrulation. *Developmental Biology*, *426*(2), 165–175. https://doi.org/10.1016/j.ydbio.2016.03.021

Koch, C. J. (2008). Importance of Antibody Concentration in the Assessment of Cellular Hypoxia by Flow Cytometry: EF5 [1] and Pimonidazole. *Radiation Research*, *169*(6), 677–688. https://doi.org/10.1667/RR1305.1

Kolde, R. (2019). *pheatmap: Pretty Heatmaps* (R package version 1.0.12) [R]. https://CRAN.R-project.org/package=pheatmap

Kondo, M., Yamamoto, T., Takahashi, S., & Taira, M. (2017). Comprehensive analyses of *hox* gene expression in *Xenopus laevis* embryos and adult tissues. *Development, Growth & Differentiation*, *59*(6), 526–539. https://doi.org/10.1111/dgd.12382

Kong, D., Park, E. J., Stephen, A. G., Calvani, M., Cardellina, J. H., Monks, A., Fisher, R. J., Shoemaker, R. H., & Melillo, G. (2005). Echinomycin, a Small-Molecule Inhibitor of Hypoxia-Inducible Factor-1 DNA-Binding Activity. *Cancer Research*, *65*(19), 9047–9055. https://doi.org/10.1158/0008-5472.CAN-05-1235

Larsson, J. (2020). *_eulerr: Area-Proportional Euler and Venn Diagrams with Ellipses_* (R package version 6.1.0) [R]. https://cran.r-project.org/package=eulerr

Lea, R., Papalopulu, N., Amaya, E., & Dorey, K. (2009). Temporal and spatial expression of FGF ligands and receptors during Xenopus development. *Developmental Dynamics: An Official Publication of the American Association of Anatomists*, *238*(6), 1467–1479. https://doi.org/10.1002/dvdy.21913

Leclercq, I. A., Field, J., & Farrell, G. C. (2003). Leptin-specific mechanisms for impaired liver regeneration in ob/ob mice after toxic injury. *Gastroenterology*, *124*(5), 1451–1464. https://doi.org/10.1016/S0016-5085(03)00270-1

Lee, H., Hikasa, K., Umesono, Y., Hayashi, T., Agata, K., & Shibata, N. (2022). Loss of *plac8* expression rapidly leads pluripotent stem cells to enter active state during planarian regeneration. *Development*, *149*(3), dev199449. https://doi.org/10.1242/dev.199449

Li, Q., Yang, H., & Zhong, T. P. (2015). Regeneration across Metazoan Phylogeny: Lessons from Model Organisms. *Journal of Genetics and Genomics*, *42*(2), 57–70. https://doi.org/10.1016/j.jgg.2014.12.002

Lim, S.-O., Li, C.-W., Xia, W., Lee, H.-H., Chang, S.-S., Shen, J., Hsu, J. L., Raftery, D., Djukovic, D., Gu, H., Chang, W.-C., Wang, H.-L., Chen, M.-L., Huo, L., Chen, C.-H., Wu, Y., Sahin, A., Hanash, S. M., Hortobagyi, G. N., & Hung, M.-C. (2016). EGFR Signaling Enhances Aerobic Glycolysis in Triple-Negative Breast Cancer Cells to

Promote Tumor Growth and Immune Escape. *Cancer Research*, *76*(5), 1284–1296. https://doi.org/10.1158/0008-5472.CAN-15-2478

Lin, G., & Slack, J. M. W. (2008). Requirement for Wnt and FGF signaling in Xenopus tadpole tail regeneration. *Developmental Biology*, *316*(2), 323–335. https://doi.org/10.1016/j.ydbio.2008.01.032

Lin, T.-Y., Gerber, T., Taniguchi-Sugiura, Y., Murawala, P., Hermann, S., Grosser, L., Shibata, E., Treutlein, B., & Tanaka, E. M. (2021). Fibroblast dedifferentiation as a determinant of successful regeneration. *Developmental Cell*, *56*(10), 1541-1551.e6. https://doi.org/10.1016/j.devcel.2021.04.016

Liu, T., & Yin, H. (2017). PDK1 promotes tumor cell proliferation and migration by enhancing the Warburg effect in non-small cell lung cancer. *Oncology Reports*, *37*(1), 193–200. https://doi.org/10.3892/or.2016.5253

Liu, Y., Yu, H., Deaton, S. K., & Szaro, B. G. (2012). Heterogeneous Nuclear Ribonucleoprotein K, an RNA-Binding Protein, Is Required for Optic Axon Regeneration in Xenopus laevis. *Journal of Neuroscience*, *32*(10), 3563–3574. https://doi.org/10.1523/JNEUROSCI.5197-11.2012

Love, N. K., Keshavan, N., Lewis, R., Harris, W. A., & Agathocleous, M. (2014). A nutrient-sensitive restriction point is active during retinal progenitor cell differentiation. *Development*, *141*(3), 697–706. https://doi.org/10.1242/dev.103978

Love, N. R., Chen, Y., Bonev, B., Gilchrist, M. J., Fairclough, L., Lea, R., Mohun, T. J., Paredes, R., Zeef, L. A., & Amaya, E. (2011). Genome-wide analysis of gene expression during Xenopus tropicalis tadpole tail regeneration. *BMC Developmental Biology*, *11*(1), 70. https://doi.org/10.1186/1471-213X-11-70

Love, N. R., Chen, Y., Ishibashi, S., Kritsiligkou, P., Lea, R., Koh, Y., Gallop, J. L., Dorey, K., & Amaya, E. (2013). Amputation-induced reactive oxygen species are required for successful Xenopus tadpole tail regeneration. *Nature Cell Biology*, *15*(2), 222–228. https://doi.org/10.1038/ncb2659

Love, N. R., Ziegler, M., Chen, Y., & Amaya, E. (2014). Carbohydrate metabolism during vertebrate appendage regeneration: What is its role? How is it regulated?: A postulation that regenerating vertebrate appendages facilitate glycolytic and pentose phosphate pathways to fuel macromolecule biosynthesis. *BioEssays*, *36*(1), 27–33. https://doi.org/10.1002/bies.201300110

Lum, J. J., Bui, T., Gruber, M., Gordan, J. D., DeBerardinis, R. J., Covello, K. L., Simon, M. C., & Thompson, C. B. (2007). The transcription factor HIF-1α plays a critical role in the growth factor-dependent regulation of both aerobic and anaerobic glycolysis. *Genes & Development*, *21*(9), 1037–1049. https://doi.org/10.1101/gad.1529107

Luo, Y., Li, M., Zuo, X., Basourakos, S., Zhang, J., Zhao, J., Han, Y., Lin, Y., Wang, Y., Jiang, Y., & Lan, L. (2018). B-catenin nuclear translocation induced by HIF-1α overexpression leads to the radioresistance of prostate cancer. *International Journal of Oncology*. https://doi.org/10.3892/ijo.2018.4368

Mabjeesh, N. J., Escuin, D., LaVallee, T. M., Pribluda, V. S., Swartz, G. M., Johnson, M. S., Willard, M. T., Zhong, H., Simons, J. W., & Giannakakou, P. (2003). 2ME2 inhibits tumor growth and angiogenesis by disrupting microtubules and dysregulating HIF. *Cancer Cell*, *3*(4), 363–375. https://doi.org/10.1016/S1535-6108(03)00077-1

Maden, M. (1993). The Homeotic Transformation of Tails into Limbs in Rana temporaria by Retinoids. *Developmental Biology*, *159*(2), 379–391. https://doi.org/10.1006/dbio.1993.1249

Maj, E., Künneke, L., Loresch, E., Grund, A., Melchert, J., Pieler, T., Aspelmeier, T., & Borchers, A. (2016). Controlled levels of canonical Wnt signaling are required for neural crest migration. *Developmental Biology*, *417*(1), 77–90. https://doi.org/10.1016/j.ydbio.2016.06.022

Majmundar, A. J., Lee, D. S. M., Skuli, N., Mesquita, R. C., Kim, M. N., Yodh, A. G., Nguyen-McCarty, M., Li, B., & Simon, M. C. (2015). HIF modulation of Wnt signaling regulates skeletal myogenesis in vivo. *Development (Cambridge, England)*, *142*(14), 2405–2412. https://doi.org/10.1242/dev.123026

Mancilla, A., & Mayor, R. (1996). Neural crest formation in Xenopus laevis: Mechanisms of Xslug induction. *Developmental Biology*, *177*(2), 580–589. https://doi.org/10.1006/dbio.1996.0187

Marques, I. J., Lupi, E., & Mercader, N. (2019). Model systems for regeneration: Zebrafish. *Development*, *146*(18). https://doi.org/10.1242/dev.167692

Martínez, M. S., García, A., Luzardo, E., Chávez-Castillo, M., Olivar, L. C., Salazar, J., Velasco, M., Quintero, J. J. R., & Bermúdez, V. (2017). Energetic metabolism in cardiomyocytes: Molecular basis of heart ischemia and arrhythmogenesis. *Vessel Plus*, *1*(12). https://doi.org/10.20517/2574-1209.2017.34

Mas-Bargues, C., Sanz-Ros, J., Román-Domínguez, A., Inglés, M., Gimeno-Mallench, L., El Alami, M., Viña-Almunia, J., Gambini, J., Viña, J., & Borrás, C. (2019). Relevance of

Oxygen Concentration in Stem Cell Culture for Regenerative Medicine. *International Journal of Molecular Sciences*, *20*(5), E1195. https://doi.org/10.3390/ijms20051195

Masoud, G. N., & Li, W. (2015). HIF-1α pathway: Role, regulation and intervention for cancer therapy. *Acta Pharmaceutica Sinica B*, *5*(5), 378–389. https://doi.org/10.1016/j.apsb.2015.05.007

Mathon, C., Bovard, D., Dutertre, Q., Sendyk, S., Bentley, M., Hoeng, J., & Knorr, A. (2019). Impact of sample preparation upon intracellular metabolite measurements in 3D cell culture systems. *Metabolomics*, *15*(6), 92. https://doi.org/10.1007/s11306-019-1551-0

McCusker, C., Bryant, S. V., & Gardiner, D. M. (2015). The axolotl limb blastema: Cellular and molecular mechanisms driving blastema formation and limb regeneration in tetrapods: The Axolotl Limb Blastema. *Regeneration*, *2*(2), 54–71. https://doi.org/10.1002/reg2.32

McKeown, C. R., & Cline, H. T. (2019). Nutrient restriction causes reversible G2 arrest in Xenopus neural progenitors. *Development*, *146*(20). https://doi.org/10.1242/dev.178871

McKeown, C. R., Thompson, C. K., & Cline, Hollis. T. (2017). Reversible developmental stasis in response to nutrient availability in the Xenopus laevis central nervous system. *The Journal of Experimental Biology*, *220*(3), 358–368. https://doi.org/10.1242/jeb.151043

McNamara, S., Wlizla, M., & Horb, M. E. (2018). Husbandry, general care, and transportation of Xenopus laevis and Xenopus tropicalis. *Methods in Molecular Biology (Clifton, N.J.)*, *1865*, 1–17. https://doi.org/10.1007/978-1-4939-8784-9_1

Meador, J. P., Bettcher, L. F., Ellenberger, M. C., & Senn, T. D. (2020). Metabolomic profiling for juvenile Chinook salmon exposed to contaminants of emerging concern. *Science of The Total Environment*, *747*, 141097. https://doi.org/10.1016/j.scitotenv.2020.141097

Mi, H., Muruganujan, A., Ebert, D., Huang, X., & Thomas, P. D. (2019). PANTHER version 14: More genomes, a new PANTHER GO-slim and improvements in enrichment analysis tools. *Nucleic Acids Research*, *47*(D1), D419–D426. https://doi.org/10.1093/nar/gky1038

Millman, J. R., Tan, J. H., & Colton, C. K. (2009). The effects of low oxygen on self-renewal and differentiation of embryonic stem cells. *Current Opinion in Organ Transplantation*, *14*(6), 694–700. https://doi.org/10.1097/MOT.0b013e3283329d53

Mondragon-Teran, P., Lye, G. J., & Veraitch, F. S. (2009). Lowering oxygen tension enhances the differentiation of mouse embryonic stem cells into neuronal cells. *Biotechnology Progress*, *25*(5), 1480–1488. https://doi.org/10.1002/btpr.248

Morgan, T. H. (1901a). *Regeneration* (Vol. 3). The Macmillan Company.

Nagao, K., Taniyama, Y., Kietzmann, T., Doi, T., Komuro, I., & Morishita, R. (2008). HIF-1α Signaling Upstream of NKX2.5 Is Required for Cardiac Development in *Xenopus*. *Journal of Biological Chemistry*, *283*(17), 11841–11849. https://doi.org/10.1074/jbc.M702563200

Nakamura, Y., de Paiva Alves, E., Veenstra, G. J. C., & Hoppler, S. (2016). Tissue- and stage-specific Wnt target gene expression is controlled subsequent to β-catenin recruitment to cis-regulatory modules. *Development*, *143*(11), 1914–1925. https://doi.org/10.1242/dev.131664

Ng, S. K., Wood, J. P., Chidlow, G., Han, G., Kittipassorn, T., Peet, D. J., & Casson, R. J. (2015). Cancer-like metabolism of the mammalian retina: Mammalian retina metabolism. *Clinical & Experimental Ophthalmology*, *43*(4), 367–376. https://doi.org/10.1111/ceo.12462

Nieuwkoop, P. D., & Faber, J. (1994). *Normal Table of Xenopus laevis (Daudin): A Systematical and Chronological Survey of the Development from the Fertilized Egg Till the End of Metamorphosis*. Garland Pub.

Northrop, J. L., & Kimelman, D. (1994). Dorsal-ventral differences in Xcad-3 expression in response to FGF-mediated induction in Xenopus. *Developmental Biology*, *161*(2), 490–503. https://doi.org/10.1006/dbio.1994.1047

Oginuma, M., Moncuquet, P., Xiong, F., Karoly, E., Chal, J., Guevorkian, K., & Pourquié, O. (2017). A Gradient of Glycolytic Activity Coordinates FGF and Wnt Signaling during Elongation of the Body Axis in Amniote Embryos. *Developmental Cell*, *40*(4), 342-353.e10. https://doi.org/10.1016/j.devcel.2017.02.001

Osuma, E. A., Riggs, D. W., Gibb, A. A., & Hill, B. G. (2018). High throughput measurement of metabolism in planarians reveals activation of glycolysis during regeneration. *Regeneration*, *5*(1), 78–86. https://doi.org/10.1002/reg2.95

Pang, Z., Chong, J., Zhou, G., de Lima Morais, D. A., Chang, L., Barrette, M., Gauthier, C., Jacques, P.-É., Li, S., & Xia, J. (2021). MetaboAnalyst 5.0: Narrowing the gap between raw spectra and functional insights. *Nucleic Acids Research*, *49*(W1), W388–W396. https://doi.org/10.1093/nar/gkab382

Pannese, M., Polo, C., Andreazzoli, M., Vignali, R., Kablar, B., Barsacchi, G., & Boncinelli, E. (1995). The Xenopus homologue of Otx2 is a maternal homeobox gene that demarcates and specifies anterior body regions. *Development (Cambridge, England)*, *121*(3), 707–720.

Parker, G. H. (1929). The Metabolic Gradient and its Applications. *Journal of Experimental Biology*, *6*(4), 412–426. https://doi.org/10.1242/jeb.6.4.412

Patel, J. H., Schattinger, P. A., Takayoshi, E. E., & Wills, A. E. (2022). Hif1α and Wnt are required for posterior gene expression during Xenopus tropicalis tail regeneration. *Developmental Biology*, *483*, 157–168. https://doi.org/10.1016/j.ydbio.2022.01.007

Patel, J. H., & Wills, A. E. (2022). Gradient expectations: Revisiting Charles Manning Child's theory of metabolic regionalisation in developmental patterning and regeneration. *Wound Repair and Regeneration: Official Publication of the Wound Healing Society [and] the European Tissue Repair Society*. https://doi.org/10.1111/wrr.12998

Pelzer, D., Phipps, L. S., Thuret, R., Gallardo-Dodd, C. J., Baker, S. M., & Dorey, K. (2021). Foxm1 regulates neural progenitor fate during spinal cord regeneration. *EMBO Reports*, *22*(9). https://doi.org/10.15252/embr.202050932

Pirotte, N., Stevens, A.-S., Fraguas, S., Plusquin, M., Van Roten, A., Van Belleghem, F., Paesen, R., Ameloot, M., Cebrià, F., Artois, T., & Smeets, K. (2015). Reactive Oxygen Species in Planarian Regeneration: An Upstream Necessity for Correct Patterning and Brain Formation. *Oxidative Medicine and Cellular Longevity*, *2015*, 1–19. https://doi.org/10.1155/2015/392476

R Core Team. (2020). *R: A language and environment for statistical computing*. R Foundation for Statistical Computing. http://www.r-project.org/

Rabinowitz, J. S., Robitaille, A. M., Wang, Y., Ray, C. A., Thummel, R., Gu, H., Djukovic, D., Raftery, D., Berndt, J. D., & Moon, R. T. (2017). Transcriptomic, proteomic, and metabolomic landscape of positional memory in the caudal fin of zebrafish. *Proceedings of the National Academy of Sciences*, *114*(5). https://doi.org/10.1073/pnas.1620755114

Raineri, R. R., & Levy, H. R. (1970). Specificity of steroid interaction with mammary glucose 6-phosphate dehydrogenase. *Biochemistry*, *9*(11), 2233–2243. https://doi.org/10.1021/bi00813a003

Rajala, R. V. S. (2020). Aerobic Glycolysis in the Retina: Functional Roles of Pyruvate Kinase Isoforms. *Frontiers in Cell and Developmental Biology*, *8*, 266. https://doi.org/10.3389/fcell.2020.00266

Reddy, P. C., Gungi, A., & Unni, M. (2019). Cellular and Molecular Mechanisms of Hydra Regeneration. *Results and Problems in Cell Differentiation*, *68*, 259–290. https://doi.org/10.1007/978-3-030-23459-1_12

Robinson, M. D., McCarthy, D. J., & Smyth, G. K. (2010). edgeR: A Bioconductor package for differential expression analysis of digital gene expression data. *Bioinformatics*, *26*(1), 139–140. https://doi.org/10.1093/bioinformatics/btp616

Rohwer, N., Jumpertz, S., Erdem, M., Egners, A., Warzecha, K. T., Fragoulis, A., Kühl, A. A., Kramann, R., Neuss, S., Rudolph, I., Endermann, T., Zasada, C., Apostolova, I., Gerling, M., Kempa, S., Hughes, R., Lewis, C. E., Brenner, W., Malinowski, M. B., … Cramer, T. (2019). Non-canonical HIF-1 stabilization contributes to intestinal tumorigenesis. *Oncogene*, *38*(28), 5670–5685. https://doi.org/10.1038/s41388-019-0816-4

Romero, M. M. G., McCathie, G., Jankun, P., & Roehl, H. H. (2018). Damage-induced reactive oxygen species enable zebrafish tail regeneration by repositioning of Hedgehog expressing cells. *Nature Communications*, *9*(1), 4010. https://doi.org/10.1038/s41467-018-06460-2

Romero, R., & Baguñà, J. (1991). Quantitative cellular analysis of growth and reproduction in freshwater planarians (Turbellaria; Tricladida). I. A cellular description of the intact

organism. *Invertebrate Reproduction & Development*, *19*(2), 157–165. https://doi.org/10.1080/07924259.1991.9672170

Sabatini, D. M. (2017). Twenty-five years of mTOR: Uncovering the link from nutrients to growth. *Proceedings of the National Academy of Sciences of the United States of America*, *114*(45), 11818–11825. https://doi.org/10.1073/pnas.1716173114

Schieber, M., & Chandel, N. S. (2014). ROS Function in Redox Signaling and Oxidative Stress. *Current Biology*, *24*(10), R453–R462. https://doi.org/10.1016/j.cub.2014.03.034

Schindelin, J., Arganda-Carreras, I., Frise, E., Kaynig, V., Longair, M., Pietzsch, T., Preibisch, S., Rueden, C., Saalfeld, S., Schmid, B., Tinevez, J.-Y., White, D. J., Hartenstein, V., Eliceiri, K., Tomancak, P., & Cardona, A. (2012). Fiji: An open-source platform for biological-image analysis. *Nature Methods*, *9*(7), 676–682. https://doi.org/10.1038/nmeth.2019

Selman, G. G., & Pawsey, G. J. (1965). The utilization of yolk platelets by tissues of Xenopus embryos studied by a safranin staining method. *Development*, *14*(2), 191–212.

Semenza, G. L., Jiang, B.-H., Leung, S. W., Passantino, R., Concordet, J.-P., Maire, P., & Giallongo, A. (1996). Hypoxia Response Elements in the Aldolase A, Enolase 1, and Lactate Dehydrogenase A Gene Promoters Contain Essential Binding Sites for Hypoxia-inducible Factor 1. *Journal of Biological Chemistry*, *271*(51), 32529–32537. https://doi.org/10.1074/jbc.271.51.32529

Simkin, J., Gawriluk, T. R., Gensel, J. C., & Seifert, A. W. (2017). Macrophages are necessary for epimorphic regeneration in African spiny mice. *ELife*, *6*, e24623. https://doi.org/10.7554/eLife.24623

Sinclair, J. W., Hoying, D. R., Bresciani, E., Nogare, D. D., Needle, C. D., Berger, A., Wu, W., Bishop, K., Elkahloun, A. G., Chitnis, A., Liu, P., & Burgess, S. M. (2021). The Warburg effect is necessary to promote glycosylation in the blastema during zebrafish tail regeneration. *NPJ Regenerative Medicine*, *6*(1), 55. https://doi.org/10.1038/s41536-021-00163-x

Sive, H. L., Grainger, R. M., & Harland, R. M. (2000). *Early Development of Xenopus Laevis: A Laboratory Manual*. CSHL Press.

Slack, J. M. W., Beck, C. W., Gargioli, C., & Christen, B. (2004). Cellular and molecular mechanisms of regeneration in *Xenopus*. *Philosophical Transactions of the Royal Society of London. Series B: Biological Sciences*, *359*(1445), 745–751. https://doi.org/10.1098/rstb.2004.1463

Slack, J. M. W., Lin, G., & Chen, Y. (2008). Molecular and Cellular Basis of Regeneration and Tissue Repair: The Xenopus tadpole: a new model for regeneration research. *Cellular and Molecular Life Sciences*, *65*(1), 54–63. https://doi.org/10.1007/s00018-007-7431-1

Squarize, C. H., Castilho, R. M., Bugge, T. H., & Gutkind, J. S. (2010). Accelerated wound healing by mTOR activation in genetically defined mouse models. *PloS One*, *5*(5), e10643. https://doi.org/10.1371/journal.pone.0010643

Tabler, J. M., Bolger, T. G., Wallingford, J., & Liu, K. J. (2014). Hedgehog activity controls opening of the primary mouth. *Developmental Biology*, *396*(1), 1–7. https://doi.org/10.1016/j.ydbio.2014.09.029

Tadokoro, S., Ide, S., Tokuyama, R., Umeki, H., Tatehara, S., Kataoka, S., & Satomura, K. (2015). Leptin promotes wound healing in the skin. *PloS One*, *10*(3), e0121242. https://doi.org/10.1371/journal.pone.0121242

Tanaka, E. M. (2016). The Molecular and Cellular Choreography of Appendage Regeneration. *Cell*, *165*(7), 1598–1608. https://doi.org/10.1016/j.cell.2016.05.038

Thomas, P. D. (2003). PANTHER: A Library of Protein Families and Subfamilies Indexed by Function. *Genome Research*, *13*(9), 2129–2141. https://doi.org/10.1101/gr.772403

Thoreen, C. C., Kang, S. A., Chang, J. W., Liu, Q., Zhang, J., Gao, Y., Reichling, L. J., Sim, T., Sabatini, D. M., & Gray, N. S. (2009). An ATP-competitive Mammalian Target of Rapamycin Inhibitor Reveals Rapamycin-resistant Functions of mTORC1. *Journal of Biological Chemistry*, *284*(12), 8023–8032. https://doi.org/10.1074/jbc.M900301200

Thummel, R., Ju, M., Sarras, M. P., & Godwin, A. R. (2007). Both Hoxc13 orthologs are functionally important for zebrafish tail fin regeneration. *Development Genes and Evolution*, *217*(6), 413–420. https://doi.org/10.1007/s00427-007-0154-3

Tran, H. T., & Vleminckx, K. (2014). Design and use of transgenic reporter strains for detecting activity of signaling pathways in Xenopus. *Methods*, *66*(3), 422–432. https://doi.org/10.1016/j.ymeth.2013.06.028

Tseng, A.-S., & Levin, M. (2008). Tail Regeneration in *Xenopus laevis* as a Model for Understanding Tissue Repair. *Journal of Dental Research*, *87*(9), 806–816. https://doi.org/10.1177/154405910808700909

Vander Heiden, M. G., Cantley, L. C., & Thompson, C. B. (2009). Understanding the Warburg effect: The metabolic requirements of cell proliferation. *Science (New York, N.Y.)*, *324*(5930), 1029–1033. https://doi.org/10.1126/science.1160809

Večeřa, J., Kudová, J., Kučera, J., Kubala, L., & Pacherník, J. (2017). Neural Differentiation Is Inhibited through HIF1 α / β -Catenin Signaling in Embryoid Bodies. *Stem Cells International*, *2017*, 1–12. https://doi.org/10.1155/2017/8715798

Wamelink, M. M. C., Struys, E. A., & Jakobs, C. (2008). The biochemistry, metabolism and inherited defects of the pentose phosphate pathway: A review. *Journal of Inherited Metabolic Disease*, *31*(6), 703–717. https://doi.org/10.1007/s10545-008-1015-6

Wang, S., & Shi, Y.-B. (2021). Evolutionary divergence in tail regeneration between Xenopus laevis and Xenopus tropicalis. *Cell & Bioscience*, *11*(1), 71. https://doi.org/10.1186/s13578-021-00582-9

Wick, A. N., Drury, D. R., Nakada, H. I., & Wolfe, J. B. (1957). Localization of the primary metabolic block produced by 2-deoxyglucose. *The Journal of Biological Chemistry*, *224*(2), 963–969.

Wickham, H. (2009). *ggplot2: Elegant Graphics for Data Analysis*. Springer-Verlag. https://doi.org/10.1007/978-0-387-98141-3

Williams, M. C., Patel, J. H., Kakebeen, A. D., & Wills, A. E. (2021). Nutrient availability contributes to a graded refractory period for regeneration in Xenopus tropicalis. *Developmental Biology*, *473*, 59–70. https://doi.org/10.1016/j.ydbio.2021.01.005

Young, J. J., Kjolby, R. A. S., Kong, N. R., Monica, S. D., & Harland, R. M. (2014). Spalt-like 4 promotes posterior neural fates via repression of pou5f3 family members in Xenopus. *Development*, *141*(8), 1683–1693. https://doi.org/10.1242/dev.099374

Yuan, H.-X., Xiong, Y., & Guan, K.-L. (2013). Nutrient Sensing, Metabolism, and Cell Growth Control. *Molecular Cell*, *49*(3), 379–387. https://doi.org/10.1016/j.molcel.2013.01.019

Zhang, Z., Deng, X., Liu, Y., Liu, Y., Sun, L., & Chen, F. (2019). PKM2, function and expression and regulation. *Cell & Bioscience*, *9*(1), 52. https://doi.org/10.1186/s13578-019-0317-8

Zhao, X.-F., Wan, J., Powell, C., Ramachandran, R., Myers, M. G., & Goldman, D. (2014). Leptin and IL-6 Family Cytokines Synergize to Stimulate Müller Glia Reprogramming and Retina Regeneration. *Cell Reports*, *9*(1), 272–284. https://doi.org/10.1016/j.celrep.2014.08.047

Zou, C., Wang, Y., & Shen, Z. (2005). 2-NBDG as a fluorescent indicator for direct glucose uptake measurement. *Journal of Biochemical and Biophysical Methods*, *64*(3), 207–215. https://doi.org/10.1016/j.jbbm.2005.08.001

APPENDIX A: METABOLOMICS PROCESSING AND R CODE

This code can be used to process metabolomics data if the input sheet has metabolites as rows and samples as columns. For statistical analysis and Pathway Impact, MetaboAnalyst 5.0 can be used. Statistical Analysis [one factor] can be used to run ANOVA with FisherLSD by running your input table. Pathway Analysis (targeted) can be used by inputting a list of metabolites of interest (for instance, differentially accessible ones).

```
library(ggplot2)
library(reshape2)

# Set working directory *****This should be where you will pull files from
setwd("~/Documents/Wills Lab/Metabolism/Metabolomics/Timecourse/")

#### Import Data ####
metab <- read.csv("MassSpecTimeCourse211202.csv", check.names = FALSE,
stringsAsFactors = FALSE)

nalist  <- metab[metab$`1` == "N/A",]
metab <- metab[!metab$`1` == "N/A",]

#### Normalize to peaks ####
# Convert matrix to numeric and normalize to peak sum
metabnorm <- t(matrix(as.numeric(as.matrix(metab[1:104,2:39])), nrow = nrow(metab)-
3))
metabnorm[is.na(metabnorm)] <- 0
for (i in 1:nrow(metabnorm)) {
  rowav <- sum(metabnorm[i,])
  metabnorm[i,] <- metabnorm[i,]/rowav
}
```

```
# Make normalized table and change column names to make it easier to sort later
(based on timepoint and replicate)
metabnorm <- t(metabnorm)
metab2 <- metab[1:104,]
metab2[1:104,2:39] <- metabnorm
metab2[105,] <- paste(metab[106,], metab[107,], sep = ".")
colnames(metab2) <- metab2[105,]
metab2 <- metab2[1:104,]
idlist <- colnames(metab2)
idlist <- idlist[2:39]

# Replace NA with rowmin/100 to prevent 0s for log transformation
metab3 <- matrix(as.numeric(as.matrix(metab2[2:39])), ncol = 38)
for(i in 2:ncol(metab3)) {
  colc <- as.numeric(metab3[,i])
  rowmin <- max(colc, na.rm = TRUE)
  colc[is.na(colc)] <- rowmin/100
  metab3[,i] <- colc
}

rownames(metab3) <- metab2$Time.Rep
colnames(metab3) <- idlist

#### Convert to long for plotting ####
metablong <- melt(metab3, measure.vars = idlist)
colnames(metablong) <- c("compound", "sample", "value")
metablong$Time <- gsub("\\..*", "", metablong$sample)
metablong$Rep <- gsub("^.*\\.", "", metablong$sample)
metablong$value <- as.numeric(metablong$value)
```

```
# Factor plotting variables
metablong$Time <- factor(metablong$Time, levels = c("T", "0", "3", "24"))
metablong$Rep <- factor(metablong$Rep)

# Make box plot
ggplot(metablong[metablong$compound %in% c("Glucose", "Pyruvate", "Lactate"),],
aes(color = Time, x = compound, y = value)) + geom_boxplot(outlier.shape = NA) +
geom_point(aes(color = Time), position = position_jitterdodge()) + theme(axis.text.x =
element_text(vjust = 0.5, angle = 45), panel.background = element_rect(fill = "white",
colour = "black"), panel.border = element_rect(linetype = "solid", fill = NA), text =
element_text(size = 20))

# ANOVA for individual metabolites (NOTE: bulk statistics are done with MetaboAnalyst
web app)
apyr <- aov(value~Time, metablong[metablong$compound %in% c("Pyriuvate"),])
summary(apyr)
TukeyHSD(apyr)

#### Heatmaps (import ANOVA stats from MetaboAnalyst in this section) ####
# Convert to wide for heatmaps
metabav <- aggregate(value~compound+Time, metablong, mean)
metabavshort <- dcast(metabav, compound~Time)

library(pheatmap)
# Log transform data for all metabolites
logheat <- log(metabavshort[,2:5],2)
rownames(logheat) <- metabavshort[,1]

# Seq function goes seq(from, to, by)
myBreaks <- c(seq(-max(logheat), 0, length.out=ceiling(500/2) + 1),
          seq(max(logheat)/500, max(logheat), length.out=floor(500/2)))
```

```
myColor <- colorRampPalette(c("blue", "white", "red"))(500)

# Import ANOVA stats from Metaboanalyst (from Statistical Analysis, export ANOVA table)
metabstats <- read.csv("anova_posthocsumnorm.csv", check.names = FALSE, stringsAsFactors = FALSE)
colnames(metabstats) <- c("metabolite", "fval", "pval", "fdr", "fisherLSD")

# Create a dataframe for significant vs not significant metabolites
issig <- as.data.frame(rownames(logheat) %in% metabstats$metabolite)
issig[issig == TRUE] <- "sig"
issig[issig == FALSE] <- "notsig"
rownames(issig) <- rownames(logheat)
colnames(issig) <- c("sigq")

annotcolor <- list(
  sigq = c(sig = "red", notsig = "black")
)

pheatmap(logheat, cluster_rows = TRUE, cluster_cols = FALSE, show_rownames = FALSE, breaks = myBreaks, color = myColor, scale = "row", annotation_row = issig, annotation_colors = annotcolor)

#### Heatmap for only significantly changed metabolites ####
metabstats$u24o3 <- grepl("24 - 3", metabstats$fisherLSD)
metabstats$u24o0 <- grepl("24 - 0", metabstats$fisherLSD)
metabstats$u24oT <- grepl("24 - T", metabstats$fisherLSD)

# Annotation Table
annots <- metabstats[,6:8]
rownames(annots) <- metabstats$metabolite
```

```
annots[annots == TRUE] <- "Sig"
annots[annots == FALSE] <- "Not"

# Log transform for only significantly changed metabolites
logheat <- log(metabavshort[metabavshort$compound %in% metabstats$metabolite,
2:5],2)
rownames(logheat) <- metabavshort[metabavshort$compound %in%
metabstats$metabolite, 1]

# Seq function goes seq(from, to, by) for color scale
myBreaks <- c(seq(-max(logheat), 0, length.out=ceiling(500/2) + 1),
              seq(max(logheat)/500, max(logheat), length.out=floor(500/2)))
myColor <- colorRampPalette(c("blue", "white", "red"))(500)
annotcolor <- list(
  u24oT = c(Sig = "red", Not = "black"),
  u24o0 = c(Sig = "red", Not = "black"),
  u24o3 = c(Sig = "red", Not = "black")
)

# Plot heatmap
pheatmap(logheat, cluster_rows = TRUE, cluster_cols = FALSE, show_rownames =
TRUE, breaks = myBreaks, color = myColor, scale = "row", annotation_row = annots,
annotation_colors = annotcolor)
```

VITA

Jeet H. Patel grew up in the Carolinas, spending most of his childhood in Monroe, NC. His science background began in the Biotechnology academic track at Central Academy of Technology and Arts and his interest in systems approaches to biology was fostered through the online program through North Carolina School of Science and Mathematics (NCSSM) online program. He completed his undergraduate work at the University of North Carolina at Chapel Hill with a B.S. in Quantitative Biology. He achieved highest honors for his thesis Dr. Scott Williams' where he studied the development and maintenance of the oral mucosa, with a focus on the palate and was awarded the Stephen Brantley Award for Excellence in Research in Molecular, Cellular, and Developmental Biology. At UNC, he also discovered a passion for developmental biology and education, earning the Lawrence Gilbert Undergraduate Teaching Award for his efforts as a supplemental instructor in cell and developmental biology courses. During a summer internship with Nicolas Chevrier at Harvard, he developed a strong interest in sequencing approaches and molecular biology. For his Ph.D. he joined the lab of Dr. Andrea Wills, implementing techniques in molecular biology and biochemistry to investigate how patterning and growth are regulated during development and if these mechanisms are reimplemented during regeneration. Outside of lab, Jeet enjoys playing video games, reading novels, rock climbing, and trying new foods.